

AD-A131 469

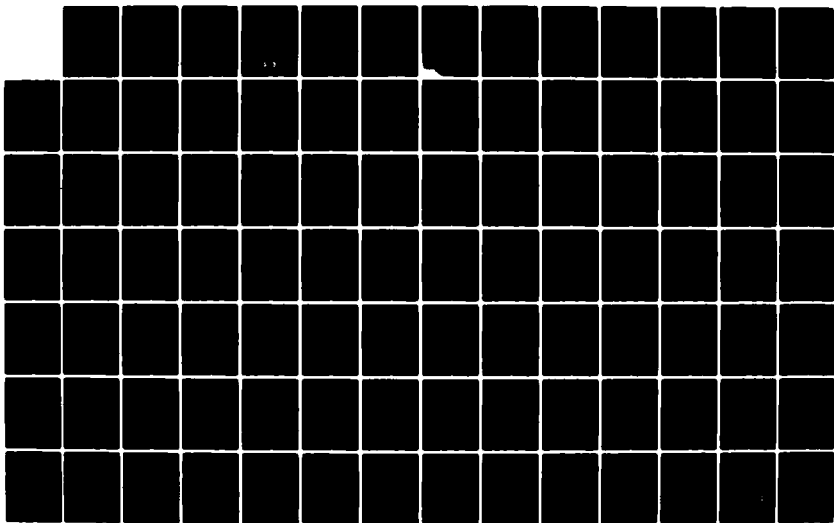
PROCEEDINGS OF THE WORKSHOP ON ION MIXING AND SURFACE
LAYER ALLOYING(U) SANDIA NATIONAL LABS ALBUQUERQUE NM
M NICOLET ET AL. 06 MAY 83 DE-AC04-76DP00789

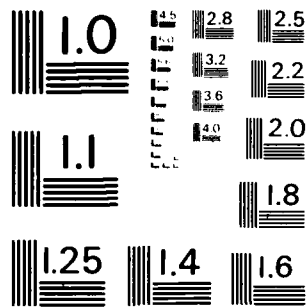
1/2

UNCLASSIFIED

F/G 20/8

NL





MICROCOPY RESOLUTION TEST CHART
NATIONAL BUREAU OF STANDARDS - 1963 - A

①

Proceedings of the Workshop on Ion Mixing and Surface Layer Alloying

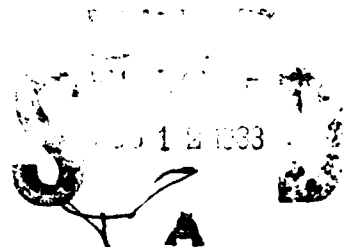
ADA131469

M-A. NICOLET, SAMUEL T. PICRAUX

Prepared by
Sandia National Laboratories
Albuquerque, New Mexico 87185 and Livermore, California 94550
for the United States Department of Energy
under Contract DE-AC04-76DP00789

DTIC FILE COPY

AD A 131 469



THIS DOCUMENT IS UNCLASSIFIED
DATE 11-19-83 BY 6032/UC/STP

Issued by Sandia National Laboratories, operated for the United States Department of Energy by Sandia Corporation.

NOTICE: This report was prepared as an account of work sponsored by an agency of the United States Government. Neither the United States Government nor any agency thereof, nor any of their employees, nor any of their contractors, subcontractors, or their employees, makes any warranty, express or implied, or assumes any legal liability or responsibility for the accuracy, completeness, or usefulness of any information, apparatus, product, or process disclosed, or represents that its use would not infringe privately owned rights. Reference herein to any specific commercial product, process, or service by trade name, trademark, manufacturer, or otherwise, does not necessarily constitute or imply its endorsement, recommendation, or favoring by the United States Government, any agency thereof or any of their contractors or subcontractors. The views and opinions expressed herein do not necessarily state or reflect those of the United States Government, any agency thereof or any of their contractors or subcontractors.

Printed in the United States of America
Available from
National Technical Information Service
U.S. Department of Commerce
5285 Port Royal Road
Springfield, VA 22161

NTIS price codes
Printed copy: A08
Microfiche copy: A01

COMPONENT PART NOTICE

THIS PAPER IS A COMPONENT PART OF THE FOLLOWING COMPILATION REPORT:

(TITLE): Proceedings of the Workshop on Ion Mixing and Surface Layer Alloying

held April 15 & 16 1983 at Pasadena, California.

(SOURCE): Sandia National Labs., Albuquerque, NM.

TO ORDER THE COMPLETE COMPILATION REPORT USE AD-A131 469.

THE COMPONENT PART IS PROVIDED HERE TO ALLOW USERS ACCESS TO INDIVIDUALLY AUTHORED SECTIONS OF PROCEEDINGS, ANNALS, SYMPOSIA, ETC. HOWEVER, THE COMPONENT SHOULD BE CONSIDERED WITHIN THE CONTEXT OF THE OVERALL COMPILATION REPORT AND NOT AS A STAND-ALONE TECHNICAL REPORT.

THE FOLLOWING COMPONENT PART NUMBERS COMPRISE THE COMPILATION REPORT:

AD#:	TITLE:
AD-P001 649	Effect of Temperature. Dose Rate and Projectile Mass on Ion Beam Mixing.
AD-P001 650	Models of Ion Mixing.
AD-P001 651	Spreads and Shifts of Markers in Ion Mixing.
AD-P001 652	Marker Experiments in Si and SiO ₂ .
AD-P001 653	Atomic Redistribution in Ion Mixing of Bilayer Thin Films.
AD-P001 654	Chemical Influence in Ion Irradiation-Induced Mixing.
AD-P001 655	Sputtering and Ion Mixing in CrSi ₂ : Temperature Effects.
AD-P001 656	Use of Free Energy Diagrams to Interpret Ion Beam Mixing Data.
AD-P001 657	Ion Mixing and Phase Diagrams.
AD-P001 658	Ion-Induced Reactions in Thin Film Structures of Al and Near-Noble Metals.
AD-P001 659	Ion-Beam Induced Changes in Alloy Composition.
AD-P001 660	High Energy Heavy Ion Induced Enhanced Adhesion.
AD-P001 661	Ion Mixing of Cr Layers on Steel: Effect of Impurities during Ion Mixing.
AD-P001 662	Mechanical Properties and Microstructure of Fe Alloys Implanted with Ti and C.
AD-P001 663	High Dose Ion Implantation and Corrosion behavior of Ferrous Metals.
AD-P001 664	Ion-Beam-Enhanced Deposition and Ionized Beam Deposition.
AD-P001 665	Ion Beam Mixing Research at Westinghouse.

This document has been approved for public release and sale; its distribution is unlimited.

DTIC
ELECTE
AUG 23 1983
A

Accession For	<input checked="" type="checkbox"/>	<input type="checkbox"/>	<input type="checkbox"/>
DTIC GRA&I			
DTIC TO			
Unannounced			
Justification			
By			
Distribution/			
Availability Codes			
Avail and/or			
Special			
DTIC			A

Proceedings of the
WORKSHOP ON ION MIXING AND SURFACE LAYER ALLOYING

April 15 & 16, 1983

California Institute of Technology
Pasadena, California 91125

sponsored by

Office of Naval Research (L. R. Cooper)

Co-Organizers:

M-A. Nicolet
California Institute of Technology
Steele Laboratory, 116-81
Pasadena, California 91125

S. T. Picraux
Sandia National Laboratories
Division 1111
Albuquerque, New Mexico 87185

This work relates to Department of Navy
Grant N00014-83-G-0057 issued by the Office
of Naval Research. The United States Govern-
ment has a royalty-free license throughout
the world in all copyrightable material
contained herein.

T A B L E O F C O N T E N T S

	<u>Page</u>
Address List of Participants	1
Workshop Summary	4
Processes and Nomenclature	8
PRESENTATIONS	
I. <u>Ion Mixing-Collisional Processes</u>	
1. R. S. Averback	10
2. S. Matteson	19
3. B. Paine	31
4. A. Barcz	41
5. H. Jorch	47
6. T. Banwell	59
II. <u>Ion Mixing-Material Processes</u>	
1. U. Shreter	68
2. W. L. Johnson	73
3. S. S. Lau	77
4. M. Nastasi	86
5. L. Rehn	96
6. M. Mendenhall	108
III. <u>Surface Modification-Ion Implantation and Mixing</u>	
1. K. Grabowski	117
2. D. M. Follstaedt	127
3. B. D. Sartwell	136

	<u>Page</u>
4. J. K. Hirvonen	150
5. R. Kossowsky	156
11. Report <u>Documentation Page</u>	170

ADDRESS LIST OF PARTICIPANTS

Dr. Robert S. Averback
Materials Science and
Technology Division
Argonne National Laboratory
Argonne, Illinois 60439
(312) 972-5141

Mr. Thomas Banwell
Electrical Engineering
Department, 116-81
California Institute of Technology
Pasadena, California 91125
(213) 356-4815

Dr. Adam Barcz
Electrical Engineering
Department, 116-81
California Institute of Technology
Pasadena, California 91125
(213) 356-4815

Dr. David M. Follstaedt
Sandia National Laboratories
Division 1112
Albuquerque, New Mexico 87185
(505) 844-2102

Dr. Kenneth S. Grabowski
Naval Research Laboratory
Washington, D. C. 20375
(202) 767-4800

Dr. James K. Hirvonen
Zymet, Inc.
Liberty Square
Danvers, Massachusetts 01923
(617) 777-5110

Professor William L. Johnson
Applied Physics Department, 138-78
California Institute of Technology
Pasadena, California 91125
(213) 356-4433

Dr. Harald Jorch
Chalk River Nuclear Laboratories
Chalk River, Ontario
Canada KOJ 1J0
(613) 584-3311

A



ADDRESS LIST (Continued)

Dr. Ram Kossowsky
Manager, Physical Metallurgy
Research and Development Center
Westinghouse
1310 Beulah Road
Pittsburgh, Pennsylvania 15235
(412) 256-3684

Professor S. S. Lau
Department of Electrical Engineering
and Computer Sciences
C-104
University of California, San Diego
La Jolla, California 92093
(619) 452-3097

Dr. Sam Matteson
Texas Instruments, Inc.
M.S. - 147
P.O. Box 225936
Dallas, Texas 75265
(214) 995-5113

Mr. Marcus Mendenhall
Physics Department, 301-38
California Institute of Technology
Pasadena, California 91125
(213) 356-4238

Mr. Mike Nastasi
Materials Science Department
Cornell University
Ithaca, New York 14853
(607) 256-5190

Professor Marc-A. Nicolet
Electrical Engineering
Department, 116-81
California Institute of Technology
Pasadena, California 91125
(213) 356-4803

Dr. Bruce M. Paine
Electrical Engineering
Department, 116-81
California Institute of Technology
Pasadena, California 91125
(213) 356-6555

ADDRESS LIST (Continued)

Dr. S. Thomas Picraux
Sandia National Laboratories
Division 1111
Albuquerque, New Mexico 87185
(505) 844-7681

Dr. Lynn E. Rehn
Materials Science and
Technology Division
Argonne National Laboratory
Argonne, Illinois 60439
(312) 972-5021

Dr. B. David Sartwell
Naval Research Laboratory
Washington, D. C. 20375
(202) 767-4800

Dr. Uri Shreter
Electrical Engineering
Department, 116-81
California Institute of Technology
Pasadena, California 91125
(213) 356-6555

WORKSHOP SUMMARY

The purpose of this workshop was to bring together in an informal setting individuals actively involved in ion mixing, and individuals working on high dose ion implantation and its application to the improvement of surface properties of solids. The objectives of the workshop included:

- 1) Outline present understanding of the basic physical processes underlying ion mixing.
- 2) Compare the approach of ion mixing to that of high dose ion implantation.
- 3) Assess the areas of greatest potential practical applications for ion mixing.
- 4) Identify critical areas on which future investigations should focus.

Summaries of the individual contributions presented at the workshop, along with the key illustrations, follow this workshop overview.

The workshop was primarily concerned with mixing phenomena observed for ion energies of about 50 to 500 keV. There is general agreement that the implantation of an ion into a solid initiates atomic redistribution by a number of processes as follows: Ballistic mixing occurs on a time scale $\approx 10^{-12}$ sec and contains those processes that can be explained on the basis of energetic displacements which result in atomic rearrangements in the solid.

These processes are athermal. In addition, other processes can contribute to the mixing in amounts which may depend on temperature. The present consensus is that the well-established processes described as radiation-enhanced diffusion are insufficient to explain the observations. Radiation-enhanced diffusion implies that a temperature dependence of mixing will correlate with a flux dependence and in the cases examined, flux dependences have not been observed. This suggests that processes within the immediate vicinity of a cascade may dominate.

The available experimental evidence is consistent with the existence of two temperature regimes. At low temperatures, the variation in mixing with temperature is weak. The amount of mixing observed there, however, varies noticeably between different systems. Attempts to identify this temperature-independent mixing with ballistic processes only are inadequate in two respects: i) small changes in masses between two systems are found to produce larger variations in mixing than can be explained by ballistic contributions; ii) theoretical calculations of the amount of mixing are numerically too uncertain to reliably identify ballistic mixing. At high temperatures, the mixing increases with temperature. However, the temperature ranges accessible so far have been too small to clearly establish the activated nature of that dependence.

There are indications that thermodynamic arguments may be able to explain and possibly predict the formation of metastable phases by ion mixing. Key factors are that the number of atoms involved in a cascade and the cooling time is long enough so that

thermodynamic states can be defined on a local scale. Free energy diagrams and characteristic times for nucleation then should predict which phases will form. For altering surface layer properties of solids (surface ennoblement), ion mixing has several advantages over ion implantation:

- 1) Much larger changes in concentration for the same irradiation dose.
- 2) Much reduced influence of sputtering.
- 3) Insensitive to ion species.
- 4) Facility in new phase formation (metastable, crystalline, amorphous).

Promising and critical areas for future studies should include:

- 1) Both experimental and theoretical studies of the functional dependences of mixing in the temperature-independent regime. There are probably several mechanisms contributing to the diffusion-like mixing that is observed in this regime, but none of them is yet well characterized.
- 2) Studies of molecular effects. These will help to identify non-linear cascade phenomena.
- 3) Development of models that explain mixing that varies with the temperature without varying with the flux of the irradiation.
- 4) Investigations of correlations between trends observed in ion mixing and those observed in

thermal processing (e.g., the dominant moving species in metal-silicide formation).

- 5) Studies at the microstructural level (e.g., in-situ TEM).
- 6) Investigation of differences between sequential and simultaneous deposition and bombardment. These processes, such as in cluster beam deposition and film deposition during irradiation, are of interest because of their possible economic benefits in applications. Combinations of ion mixing with simultaneous deposition may lead to rather simple implementations. Low ion energy, reduced beam selectivity, and limited vacuum are all compatible with the concept of ion mixing.

Fruitful applications appear to exist in wear, oxidation, and adhesion, particularly on critical surface regions of components.

Recent general references in the area of ion mixing include:

- Metastable Materials Formation by Ion Implantation, MRS Symposia Proceeding, Vol. 7, S. T. Pieraux and W. J. Choyke, Eds., (North-Holland, New York, 1982).
- "Ion Mixing", S. Matteson and M-A. Nicolet, Ann. Rev. Mat. Sci. 13, 339 (1983).
- Proceedings of the International Conference on Ion Beam Modification of Materials, Grenoble, France, (September 6-10, 1982); to be published in Nucl. Instr. & Meth.

PROCESSES AND NOMENCLATURE

(~ 100 keV)

Prompt Processes ($\lesssim 1$ ps).

Athermal; high energies.

Ballistic mixing.

- noninteracting collisions ("linear cascade")
- low order collisions ("recoil mixing")
- high order collisions (isotropic cascade mixing)
- interacting collisions (displacement spikes, energy spikes)

Cooling Down Period (~ 1 ps and ~ 100 ps).

Thermally assisted; intermediate energies; thermal spikes.

Delayed Processes (~ 1 ps and ~ 1 h).

Thermally activated; low energies.

Radiation-assisted Diffusion.

- transport by defect fluxes
- transport by enhanced diffusion

Persistent Effects (~ 1 h).

Thermally activated; energies $\sim kT$.

- modified physical and chemical properties
- applications

P R E S E N T A T I O N S

1. Ion Mixing-Collisional Processes

→ "Effect of Temperature, Dose Rate and Projectile Mass on Ion Beam Mixing**"

R. S. Averbach
Materials Science and Technology Division
Argonne National Laboratory
Argonne, Illinois 60439

The underlying diffusion mechanisms involved in ion beam mixing of layered materials are proving very elusive. It is known that mixing has both temperature dependent and independent components, but theoretical understanding of either component is lacking. We have initiated systematic studies of the temperature, dose-rate and projectile mass dependences of mixing to provide a basis for future theoretical considerations.

A. The Temperature Dependent Component-Radiation Enhanced Diffusion

From measurements of the mixing in Nb-Si⁽¹⁾ and Ni-Si⁽²⁾ as a function of temperature, values of 0.94 eV and 1.08 eV are deduced for the apparent activation enthalpies of diffusion respectively. These results might suggest that in the former case (Nb-Si) long-range vacancy migration controls the diffusion process and in the latter (Ni-Si) fast interstitial atoms are the dominant factor. Simple chemical rate theory shows that such an interpretation implies that the mixing should also depend on dose-rate. For both Ni-Si and Nb-Si, however, the measured thicknesses of the mixed layers were not affected by a change of

AD P 0 0 1 6 4 9

a factor of ten in the dose-rate, whereas the rate theory predicts that the thicknesses should have changed by a factor of ~ 1.8 . The null results suggest that the temperature dependent component of mixing is determined predominately by intra-cascade effects and not by long range migration of defects. These intra-cascade effects may be associated with the individual cascades themselves, or result from the superposition of cascades onto already highly ion-damaged material. An example of such a temperature dependent intra-cascade effect is the thermally stimulated collapse of point defects produced in the cascade, into dislocation loops.

B. Temperature Independent Component - Collisional Effects

Measurements of mixing at liquid helium temperature, where defect motion is suppressed, provide information about the athermal, or collisional aspects of mixing. It was observed that in Pt-Si bilayers, the mixing at 4.2 K was not solely a function of the deposited damage energy (i.e. collisional energy), but also a function of the energy density in the cascades. By irradiating with projectiles varying in mass from 4 amu to 84 amu the energy density in the cascades was systematically increased. It was observed that increasing the energy density in cascades enhanced the effectiveness of mixing. Each unit of damage energy deposited by 275-keV Kr ions was four times as effective as that for 300-keV He ions. This result and the fact that 300-keV He irradiation produces some cascades in addition to many low energy recoils (25% of the damage energy

for 300-keV He in Pt is deposited in primary recoils over ~ 7 keV), suggest that most of the mixing arises from cooperative phenomena within a cascade rather than to numerous, but individual, low-energy collisions. These results are consistent with a 'thermal spike' model of mixing. They could have important implications for materials modification considerations, since a thermal spike mechanism lends validity to the concept of a super-fast quench of microscopic volumes.

* Work supported by the U.S. Department of Energy

References

1. S. Matteson, J. Roth, and M-A. Nicolet, Radiation Effects, 42, 217 (1979).
2. R. S. Averback, L. J. Thompson, Jr., J. Moyle, and M. Schalit, J. Appl. Phys. 53, 1342 (1982).

Table 1. Effect of temperature and dose-rate on mixing in Ni-Si and Nb-Si. The table shows that there is a strong temperature dependence in ion-beam mixing, but no dose-rate dependence. The results suggest that mixing is predominantly an intra-cascade effect.

Target	Temp (k)	Dose-Rate* ($\mu\text{A}/\text{cm}^2$)	$\Delta x^2/\phi^{**}$ (arbitrary units)
Ni-Si	10	7.9	1.05
	373	7.9	2.47
	373	0.71	2.34
Nb-Si	293	7.0	2
	293	0.65	2
	600	7.9	41.0
	600	0.72	41.0

*300-keV Ar

**Nb-Si and Ni-Si are independently normalized.

Temp Dependence of Mixing

$$1) \Delta x^2 \propto Dt \quad t = \phi / \dot{\phi} \\ \propto D \phi$$

$$2) D = \sum_i D_i = D_{coll} + D_{th}$$

$$3) \Delta x^2 / \phi = D_{coll} + D_{th}$$

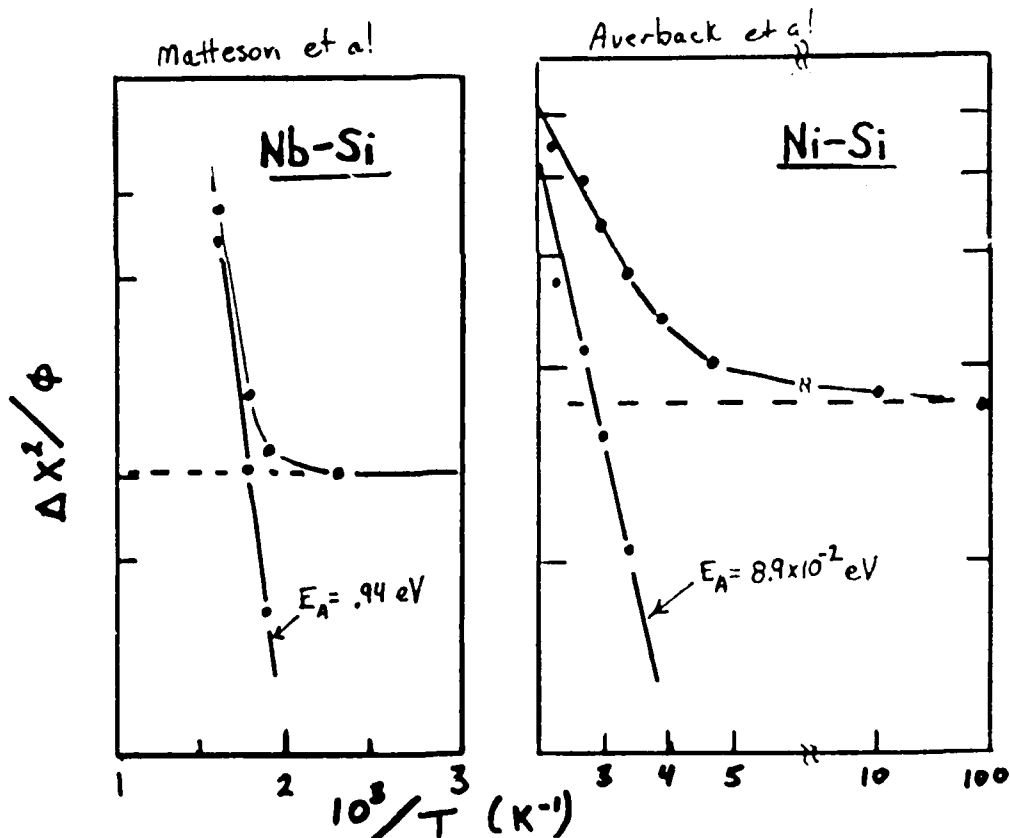


Fig. 1. Arrhenius plots of ion beam mixing in Nb-Si and Ni-Si. By assuming the diffusion coefficient is comprised of temperature dependent and independent components, the two components can be separated. This procedure yields apparent activation enthalpies of diffusion of .94 eV and .089 eV for Nb-Si and Ni-Si respectively.

300-keV Ar^+ irradiation of Ni-Si at 100°C
using different dose-rates.

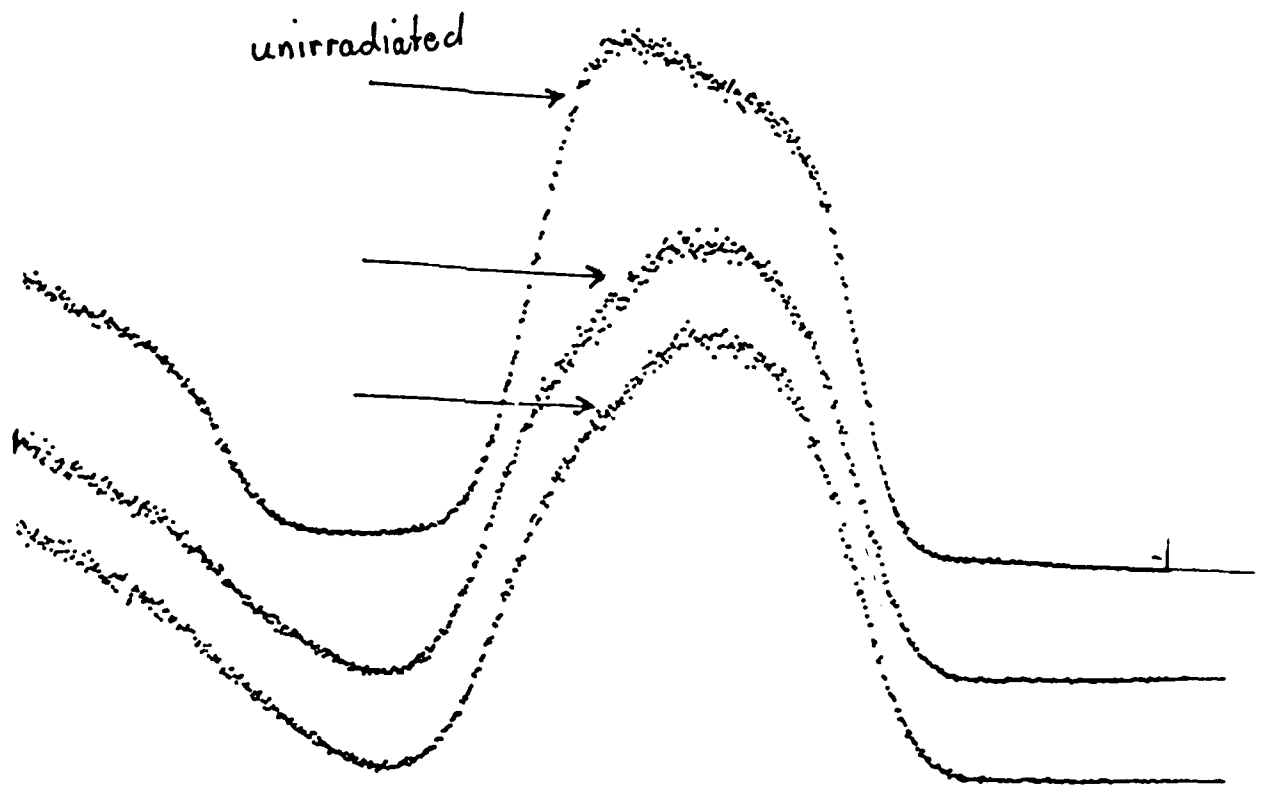


Fig. 2. RBS spectra of Ni-Si bilayers before and after irradiation at 373K with 300-keV Ar . The dose for each irradiation was $1.2 \times 10^{16}/\text{cm}^2$, but the dose-rates were $0.71\mu\text{A}/\text{cm}^2$ and $79\mu\text{A}/\text{cm}^2$. No effect of dose-rate is observed.

Damage Energy Profiles

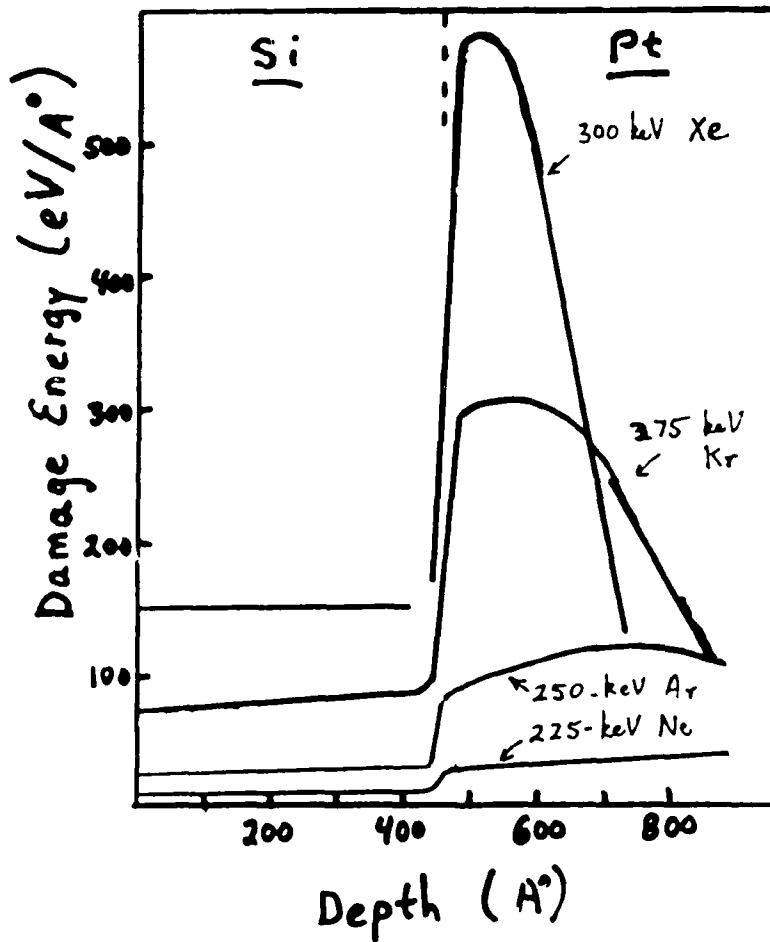


FIG. 3. Damage energy depth profiles for various ion irradiations of Pt-Si bilayers.

Recoil Spectra

$$W = \frac{L}{E_0} \int dE/s(E) \int dT \cdot \frac{dN(E,T)}{dT} \cdot E_D(T)$$

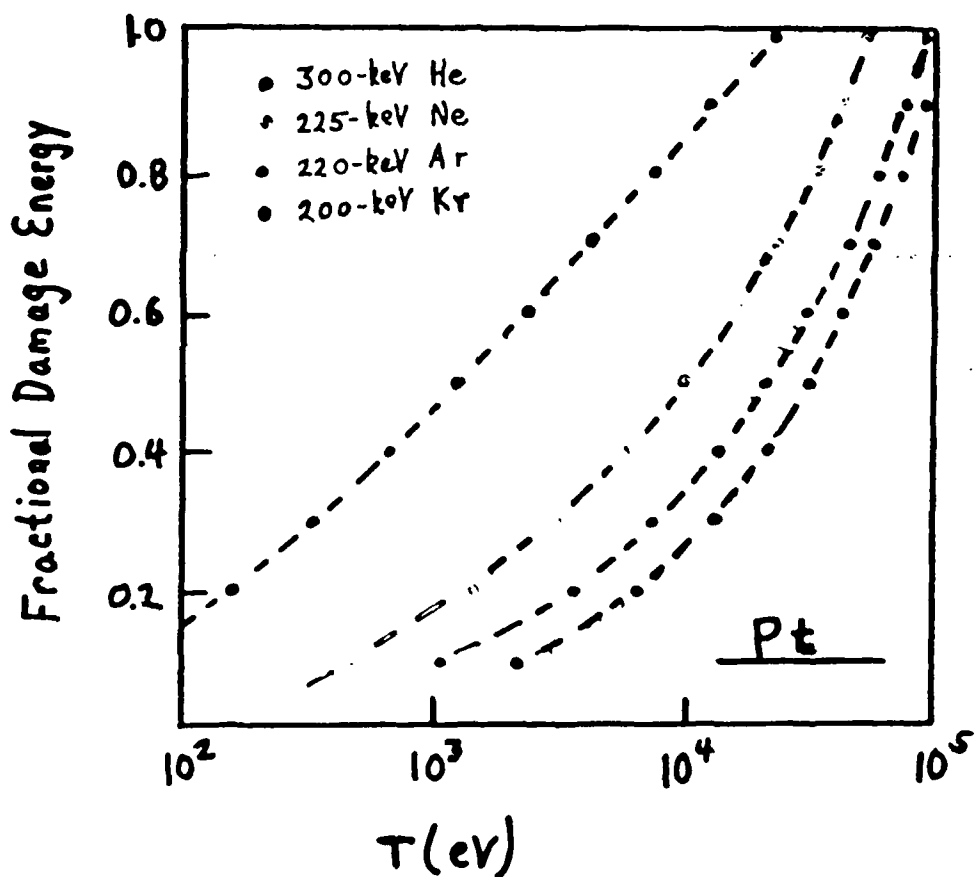


Fig. 4. Recoil energy distribution function. This plot shows the fraction of the total damage energy deposited in Pt resulting from primary recoils below energy T.

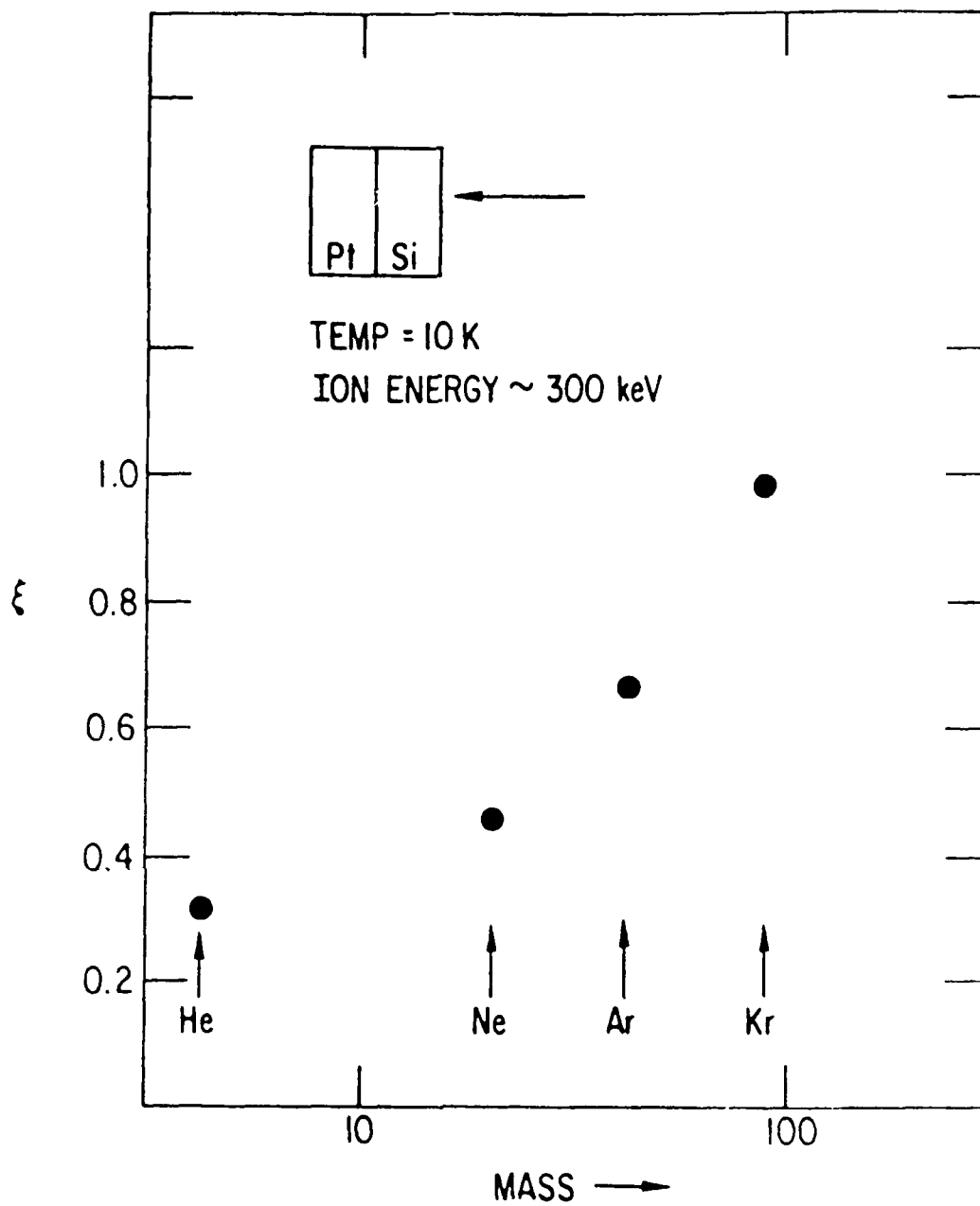


Fig. 5. Mixing efficiency as a function of ion mass in Pt-Si bilayers at 10 K. This plot shows that as the mass of the irradiation particle is increased and correspondingly the energy density in cascades is increased, the effectiveness of each unit of damage energy for inducing mixing is also increased. The efficiency for Kr irradiation was arbitrarily set equal to 1.0.

"Models of Ion Mixing"

S. Matteson
Texas Instruments Incorporated
Dallas, Texas 75265

The phenomenon of ion mixing has many facets which are not as yet well, fully, and accurately described in theory. Two general classes of models have been proposed:

- (1) Equilibrium models which describe transport resulting from thermal oscillation of the atoms in a high concentration of defects;
- (2) Ballistic models in which the transport is the product of the radiation damage itself.

Radiation enhanced diffusion (RED) is a description of the transport in terms of standard diffusion greatly enhanced by the increased concentration of defects (with respect to thermally generated defect concentrations) which are necessary for diffusion to occur. Radiation induced segregation is an extension of RED which emphasizes the gradient in the defect concentration and the particular boundary conditions that accompany ion irradiation. Both models predict a dependence on temperature in high damage rate regimes. The models are most important at high temperatures ($> 20^\circ$).

At low temperatures ballistic processes should dominate if they are of sufficient magnitude. Recoil mixing attempts to analyze the transport as resulting from the direct interaction of the ion with the atom; the model is characterized as

anisotropic, predicting drifts in the centroids of sharp impurity distributions. Collision cascade mixing treats the transport as a random walk-type problem in which the atom is displaced many times in small steps in successive collision cascades. Neither model has quantitatively described experimental observations to date with sufficient accuracy. However, a re-examination of the parameters entering the model may produce better agreement. For example, the range of recoil of very low energy atoms is not well known and is critical to the models.

While the detailed models are inadequate, it seems well justified by experimental evidence to use a diffusion-like treatment with appropriate drift terms. These ad hoc treatments have proven very powerful in describing observations. As an example, the drift of a thin Sn layer between intermixing Ge and Si layers is explained by the gradient in the "diffusion" coefficient as it increases on going from Si to Ge.

Careful measurement of the dependence on the various parameters is crucial to an accurate and quantitative understanding of ion mixing.

Figure Captions

- Figure 1 Temperature dependence of amount of intermixing of Nb and Si layers under Si irradiation. The high temperature portion of the curve is interpreted as a radiation enhanced diffusion. The low temperature part is approximately independent of temperature and has been interpreted as due to ballistic phenomena. (From Matteson et al., Rad. Effects, 42, 217 (1979)).
- Figure 2 Computer simulations illustrating ballistic processes: Collision cascade mixing (left) is a random walk problem which is a distribution in displacement lengths, is random in direction, and has a distribution in the number of displacements as well; recoil mixing is illustrated on the right in which each atom experiences only a few recoils, but often of large magnitude. Because of the much greater probability of lower energy transfers most of the recoils are oblique to the ion direction (from the left). Recoil mixing predicts a shift of the centroid of the peak with distributions which are more lorentzian than gaussian in shape.
- Figure 3 The theoretical behavior of thin Ge layers in a Si matrix under Xe irradiation as described by the collision cascade model. The qualitative description of nearly gaussian profiles with little shift in

Figure Captions (Continued)

the centroid as well as a depth dependence which is correlated with the deposited energy density compares well with experiment. Small shifts are predicted due to the gradient in the diffusion coefficient.

Figure 4 Schematic of potential of interstitial (left) and substitutional atom (right) in a Si crystal. The two atom potential is taken to be the Born-Mayer (exponential) potential for interstitials and the Lennard-Jones potential for the bound site of a substitutional atom. The energy required to displace an interstitial is significantly less than a substitutional atom. The substitutional atom must be displaced to the second nearest interstitial site (labeled by letter i). The small arrows indicate increasing potential. Previous calculations have considered only displacement of substitutional atoms. A significant increase in the prediction of the collision cascade model may result from the inclusion of such an effect, e.g., in the case of interstitial Pt in Si.

Figure 5 Calculations of the redistribution of Sb in SiO_2 during sputter depth profiling with oxygen. (The original material was Si with a thin evaporated layer of Sb.) The lower plot is the distribution

Figure Captions (Continued)

at various time intervals illustrating the effect of the surface erosion. No preferential sputtering is comprehended in the calculations.

Figure 6 Comparison of calculated surface concentrations of Sb and Sb secondary ion yields. The agreement is fairly good for the assumption of a SiO_2 matrix for the rise of the distribution. The fall of the distribution is slowed by the artifact of Sb ion pick up from the side walls of the sputter crater and preferential sputtering of Si. (Matteson, Appl. Surf. Sci. 9, 335 (1981)).

Figure 7 The redistribution of a 1 nm Sn layer "sandwiched" between a Ge and a Si layer under 360 keV As irradiation. The distribution is seen to shift into the Ge-rich layer. Other specimens confirm the shift into the Ge-rich layer. This can be understood by the collision cascade model in which the "diffusion" coefficient increases dramatically on passing from the Si to the Ge-rich layers.

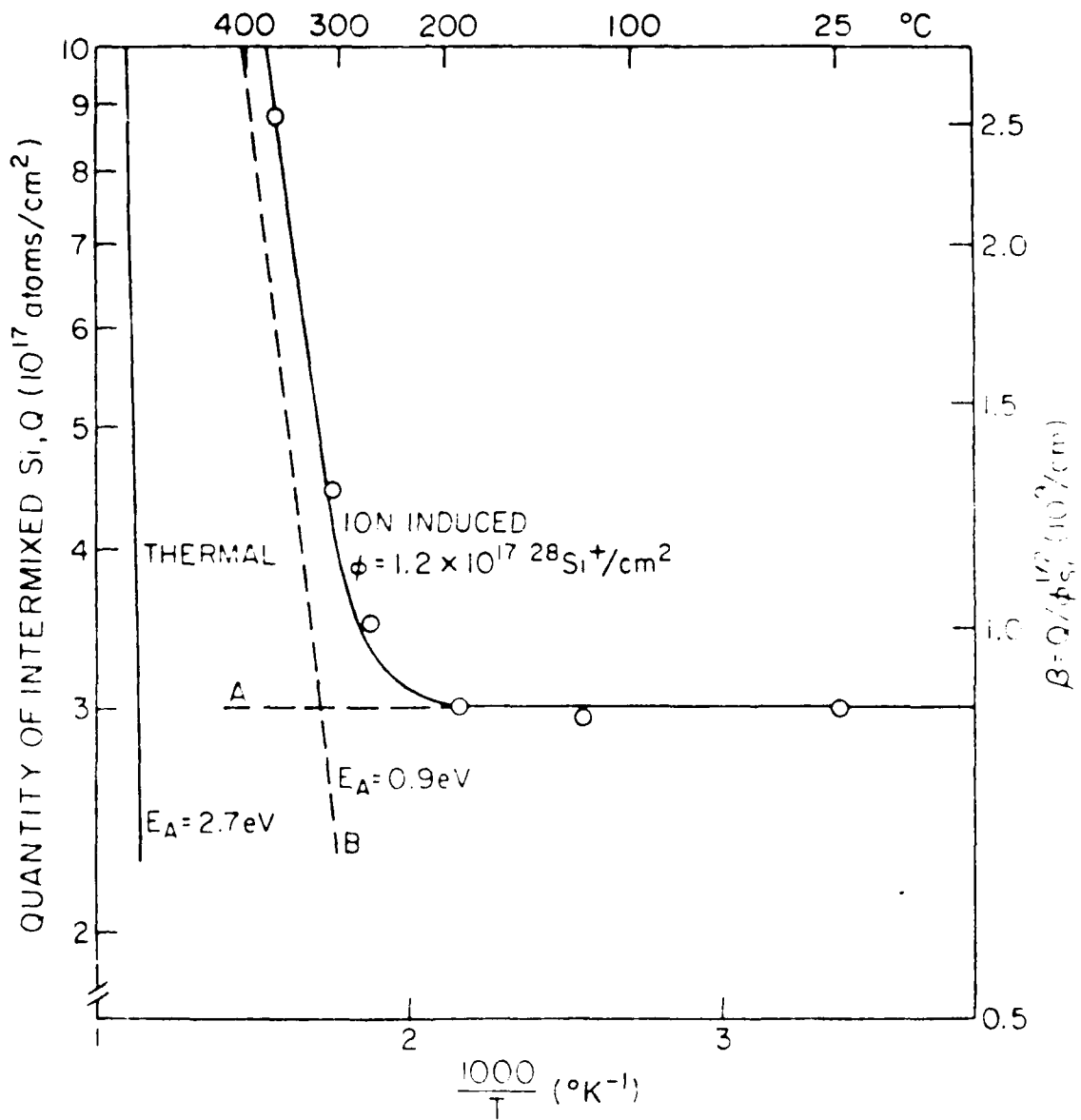


Figure 1

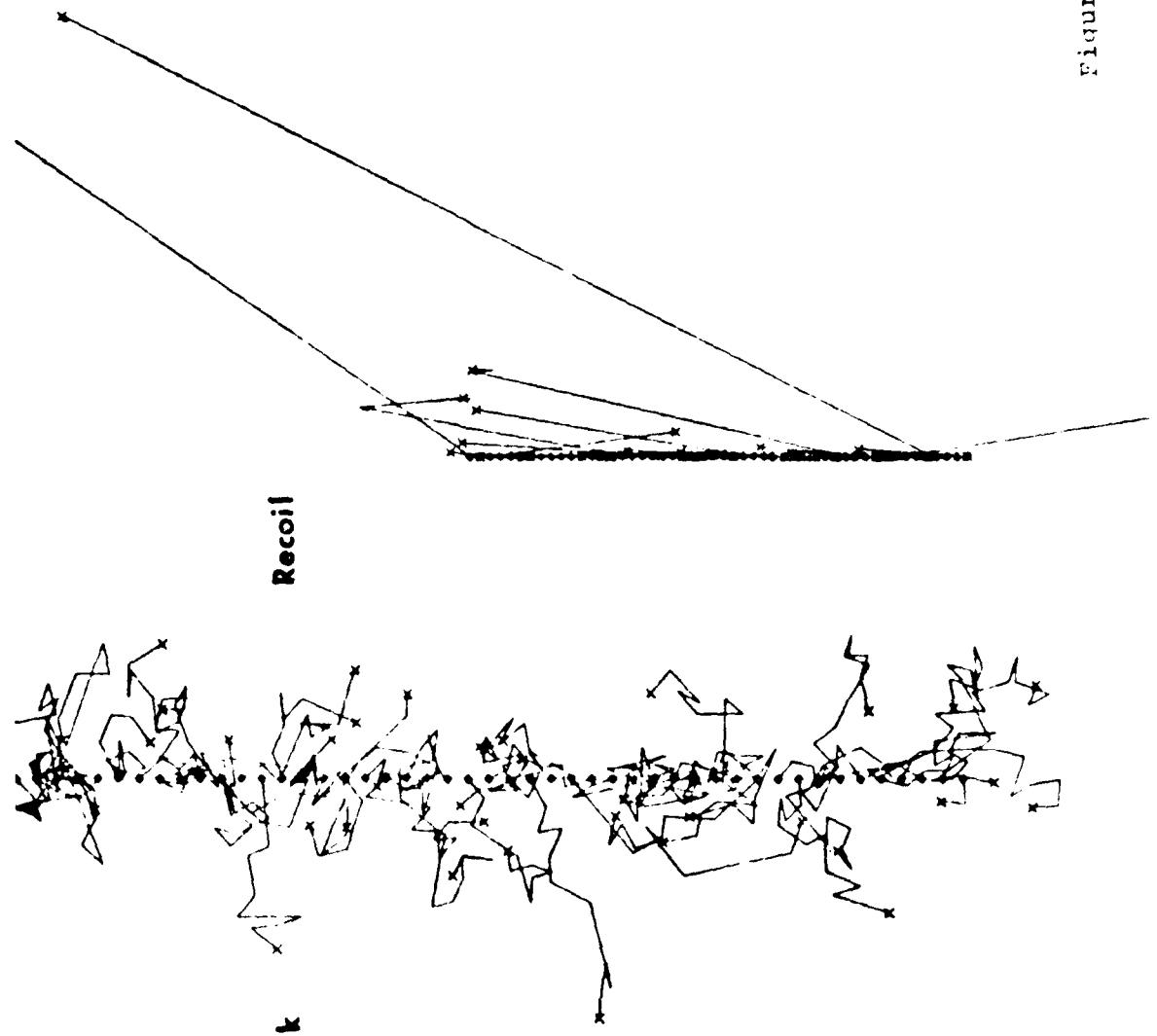


Figure 2

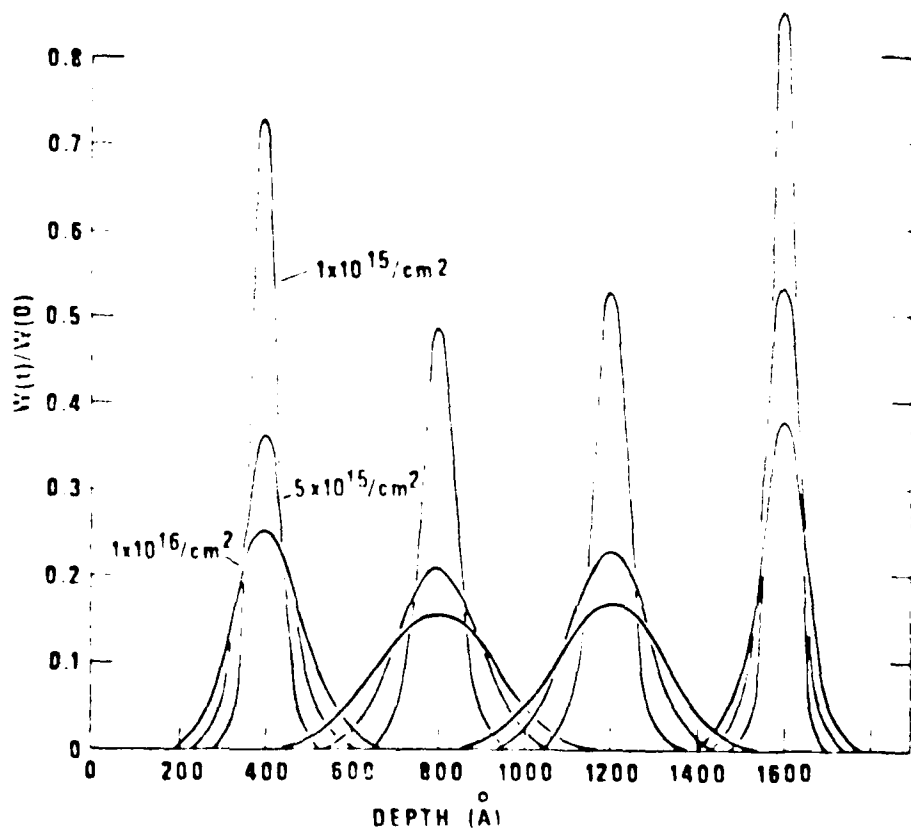
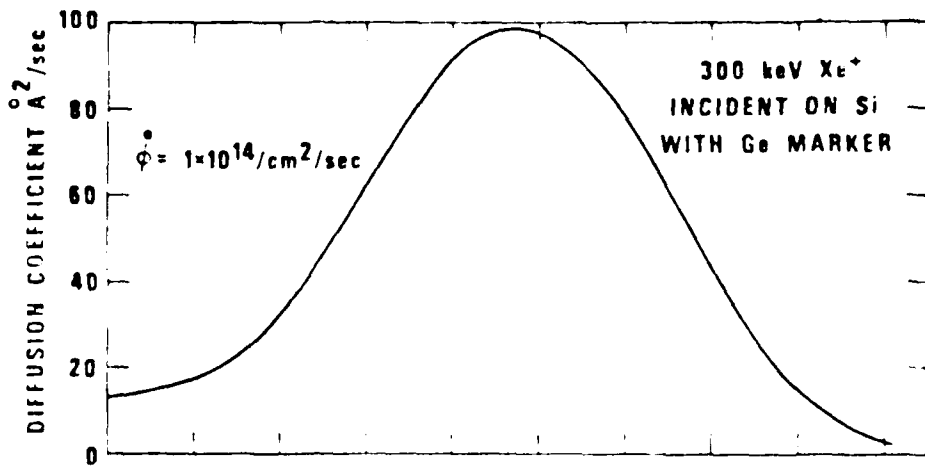


Figure 3

1λ \rightarrow

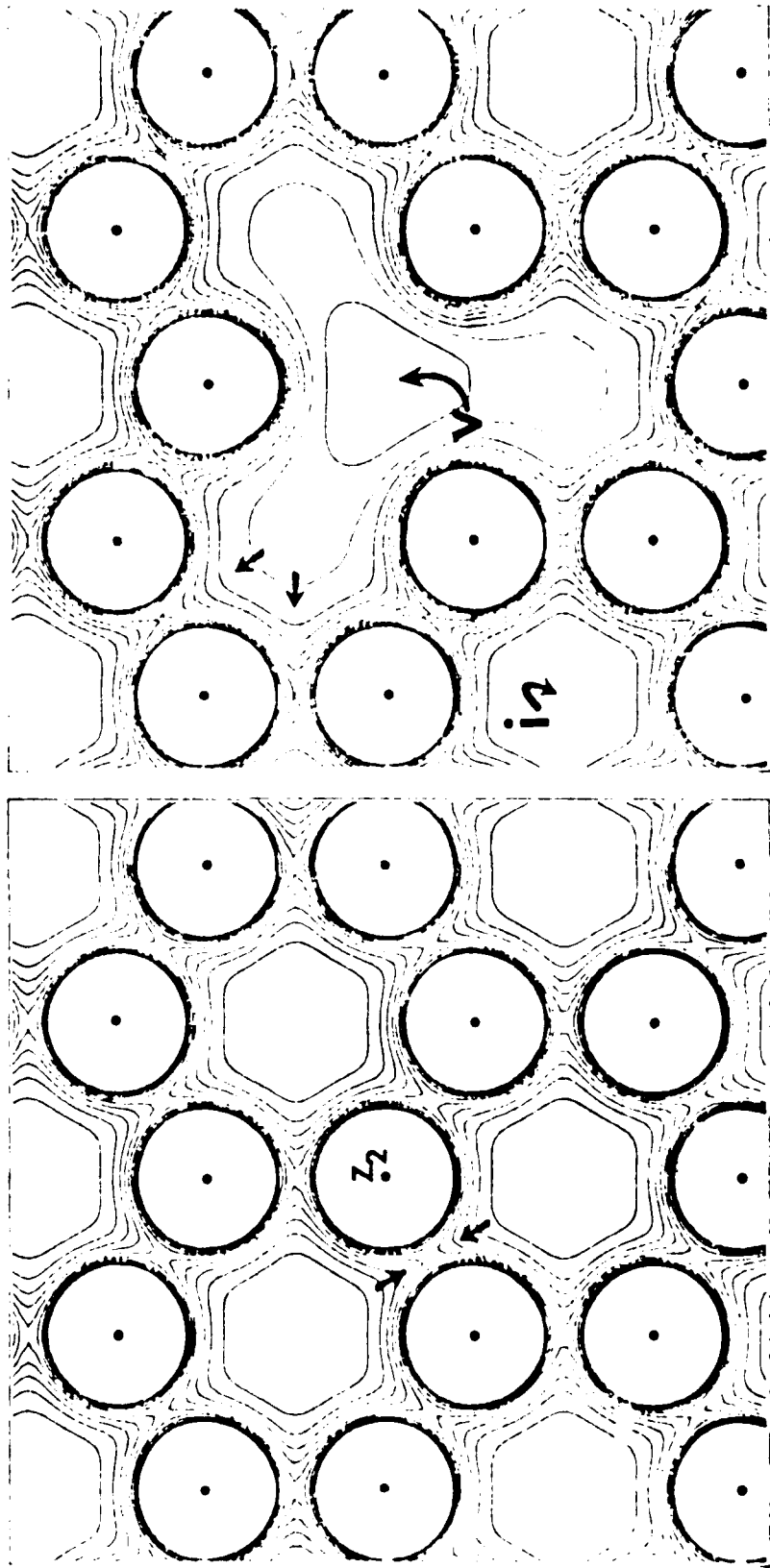


Figure 4

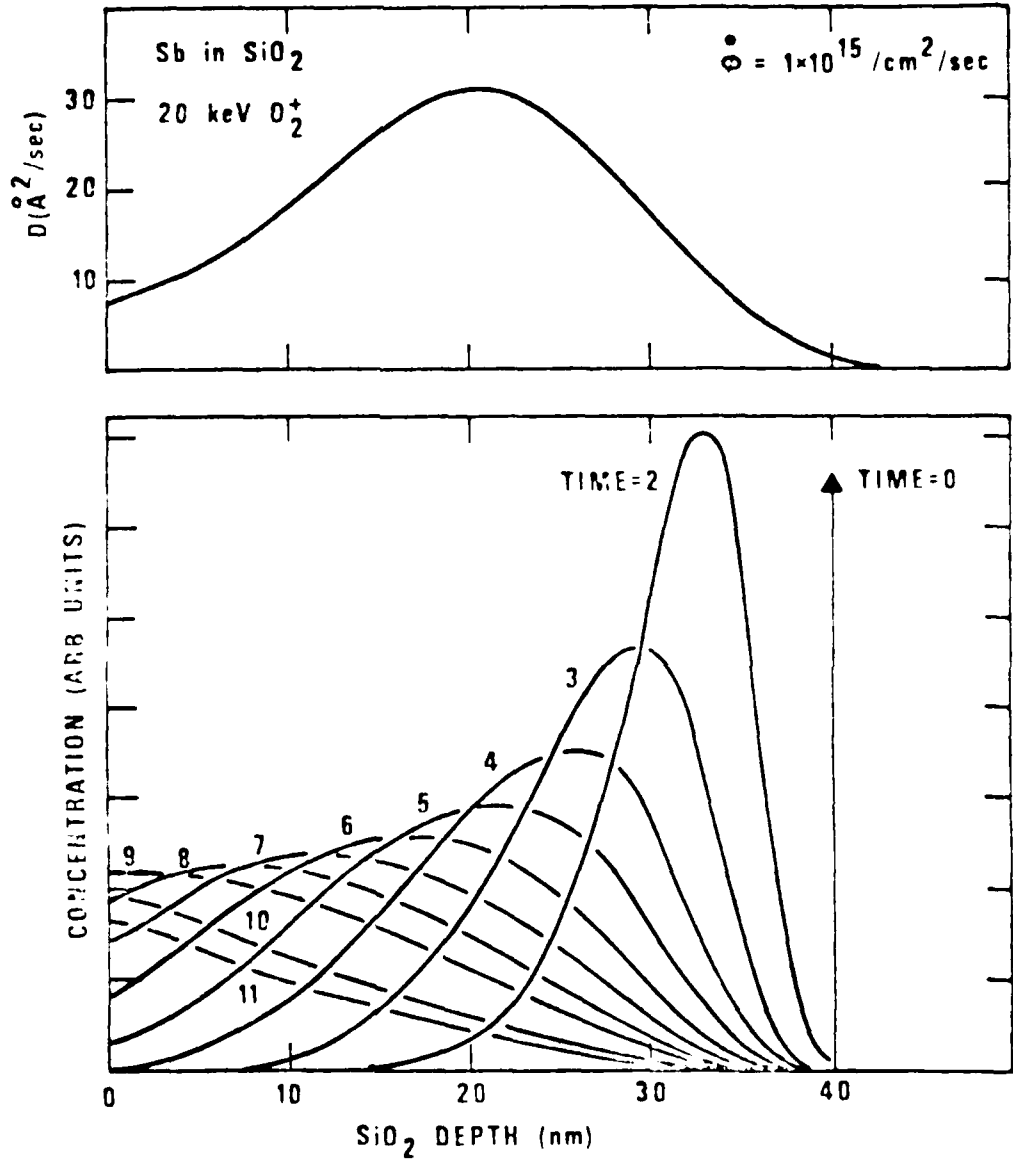
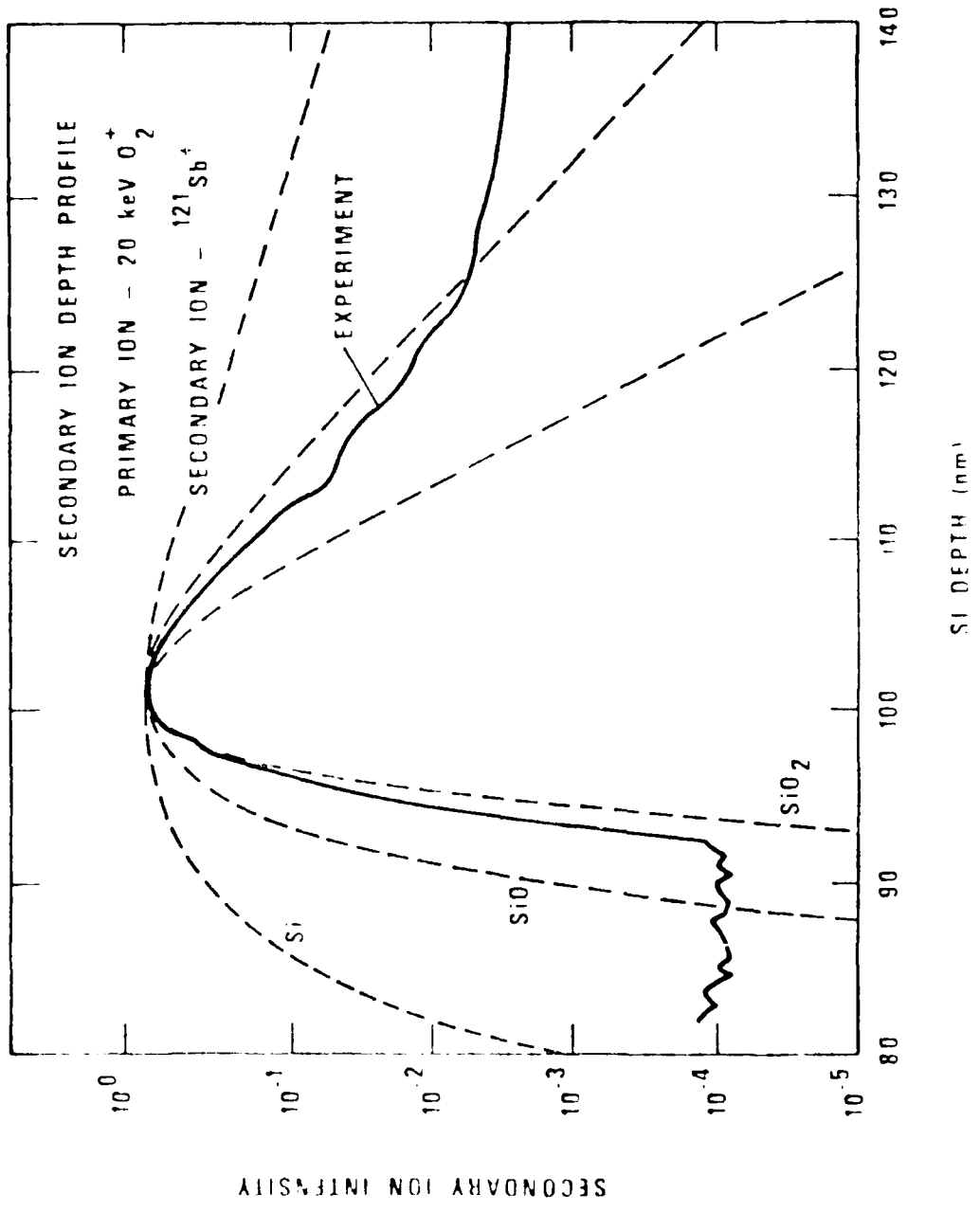
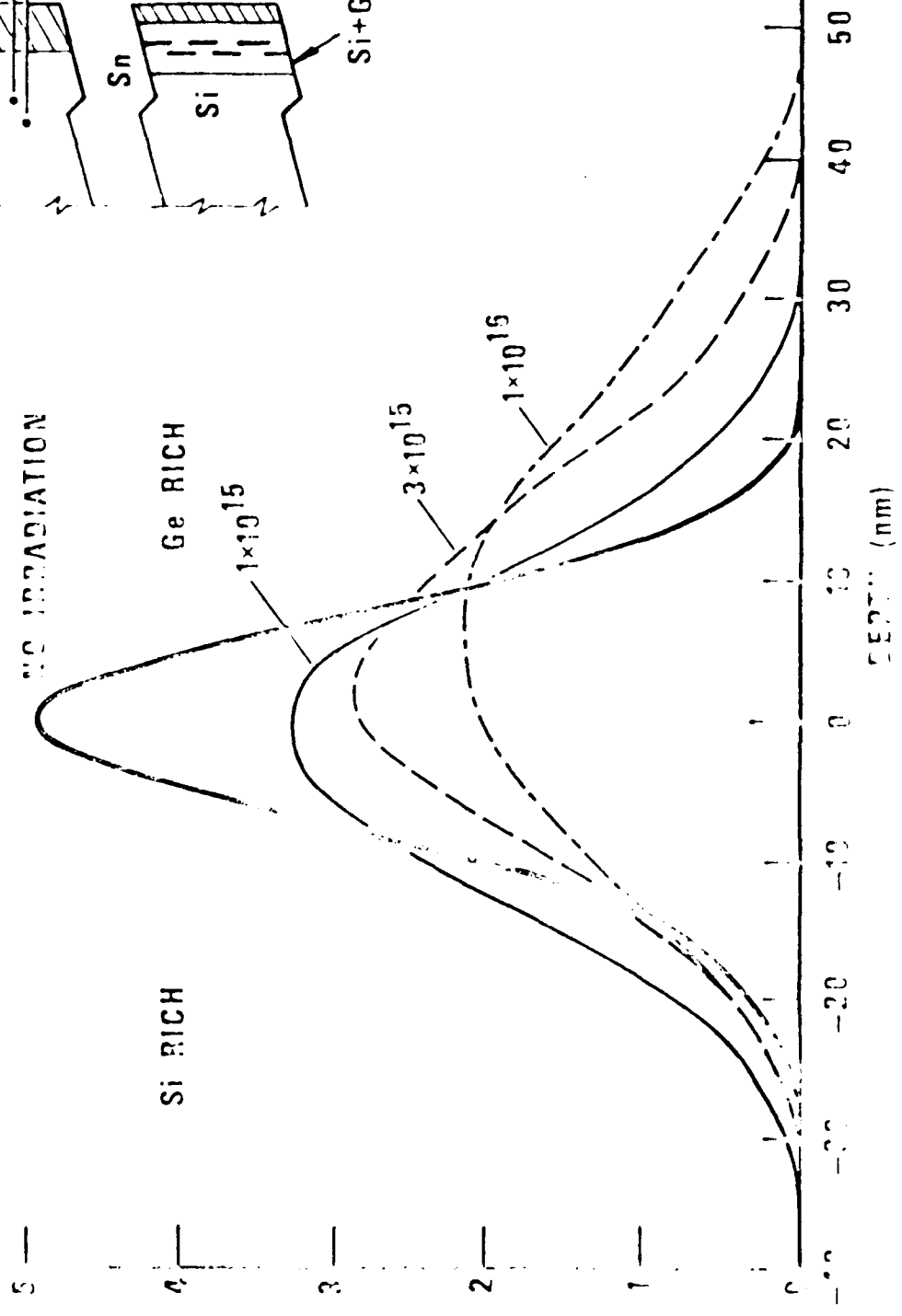


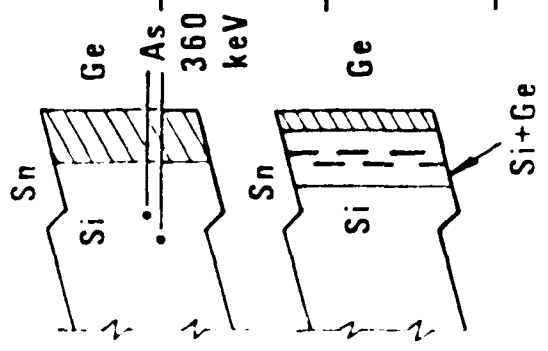
Figure 5



Ge CONCENTRATION (ARBITRARY UNITS)



⁶³Zn IRRADIATION



Si RICH

Ge RICH

DEPTH (nm)

AD P 001651

"Spreads and Shifts of Markers in Ion Mixing"

Bruce M. Paine
California Institute of Technology
Pasadena, California 91125

One of the simplest conceivable sample configurations for studying ion mixing in solids consists of a thin ($\sim 10^2 \text{ \AA}$) impurity layer (or "marker") buried several hundred \AA deep in an otherwise uniform medium. If the mass of the impurity is substantially greater than that of the medium, then the mixing of the marker can be monitored by backscattering spectrometry. Such experiments have been conducted for a variety of marker elements buried in Si plus markers buried in Al and SiO_2 . In these, the mixing is usually characterized by Dt , the product of the effective diffusion coefficient and time and Δx , the shift of the mean of the marker distribution. In this presentation, we outline the general results of these experiments to date, compare them with the predictions of published models, and finally comment briefly on present understanding of the mechanisms of the ion-induced mixing that is observed.

Below room temperature, the mixing profiles are approximately Gaussian for all marker elements M , in media A - denoted $A(M)$ - except Si(Pd). The mixing parameter varies linearly with fluence, and is essentially independent of temperature, except for Si(Pd). Also, Dt seems to scale with nuclear stopping power F_D for Si(Pd). These results are consistent with the qualitative Kinchin-Pease

model of collisional mixing. The quantitative pure-collisional models of Matteson, and Sigmund and Gras-Marti are in fair agreement with the data for Si(Pt). However, the mean shifts predicted by the latter authors to result from "matrix relocation" events are in the wrong direction. If "matrix relocation" events are taken to be suppressed somehow, then the mixing magnitudes predicted by Sigmund and Gras-Marti are 50 times too small. Monte Carlo calculations of shifts in this system by Roush et al. are in good agreement with experiment for both magnitude and direction.

Above room temperature, mixing profiles are frequently non-Gaussian, and depend strongly on temperature. No attempts at modeling these phenomena have been published.

It has been generally accepted that the mixing above room temperature is caused by thermally-assisted atomic migration. At lower temperatures, the mixing may be purely collisional or it may be collisional with some additional transport mechanisms. Evidence for such additional components in the low temperature regime is as follows:

- (a) One system - Si(Pd) - has been observed so far which does not have Gaussian mixing profiles and for which the mixing is not independent of temperature in this regime.
- (b) The magnitude of the mixing varies significantly, depending on which element is used as the marker.
- (c) Some of the T-dependent curves other than for Si(Pd)

that have been measured so far are not completely horizontal below room temperature: there is a small increase with increase in T.

References

Experiment: B. M. Paine, J. Appl. Phys. 53, 6828 (1982) and references contained therein.

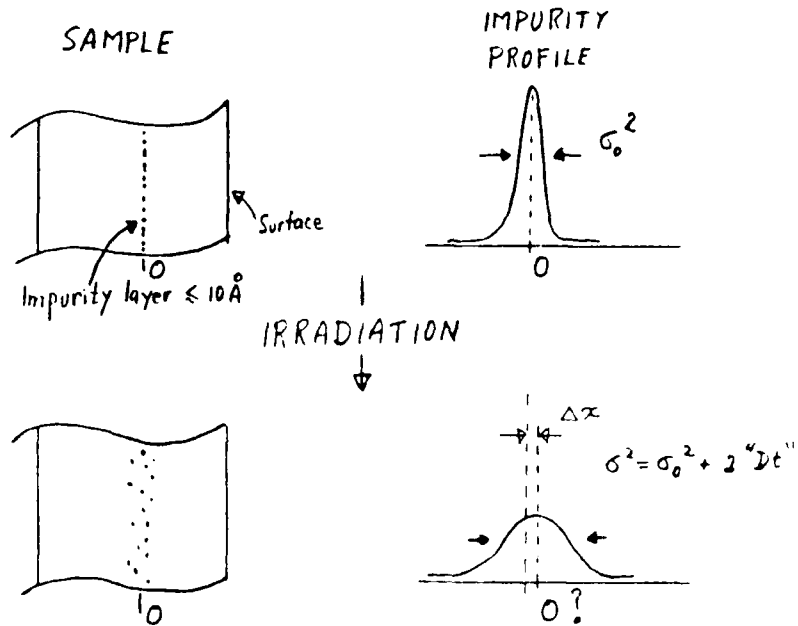
Models: H. H. Andersen, Appl. Phys. 18, 131 (1979).

S. Matteson, Appl. Phys. Lett. 39, 288 (1981).

P. Sigmund and A. Gras-Marti, Nucl. Instr. & Meth. 182/183, 25 (1981).

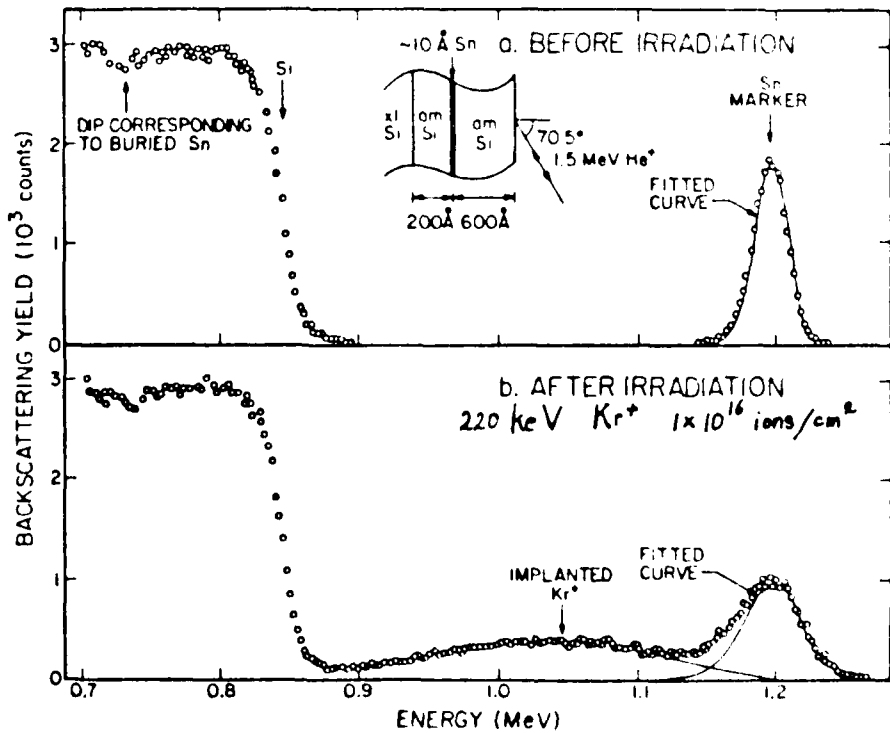
M. L. Roush, P. Davarya, G. P. Goktupo, Nucl. Instr. & Meth. (to be published).

GENERAL SCHEME



MARKER BROADENINGS

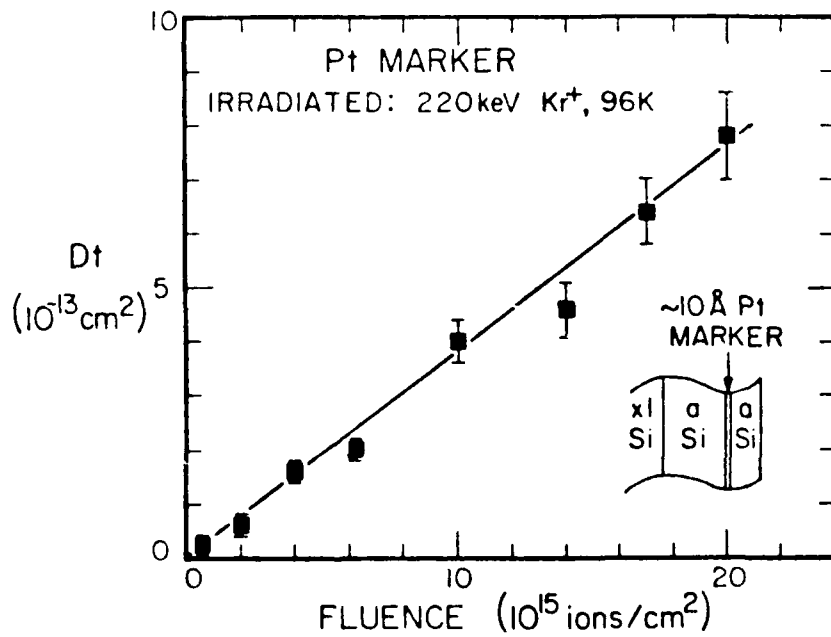
TYPICAL BACKSCATTERING SPECTRA



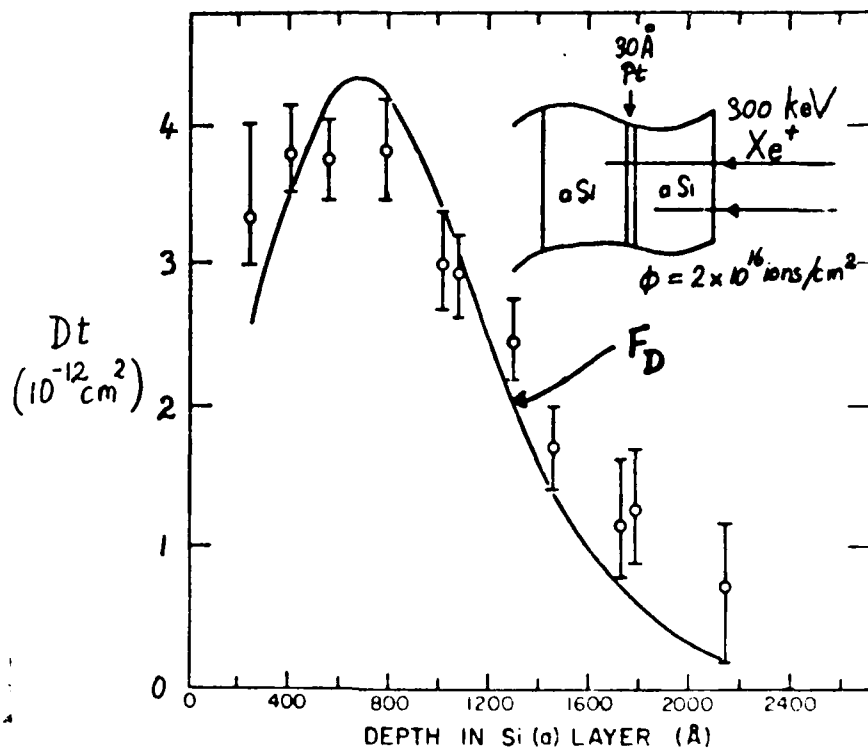
QUALITATIVE MODEL: KINCHIN-PEASE / ANDERSEN

EXPECT $Dt \propto \frac{F_D \phi \langle r^2 \rangle}{N_0 E_d^{eff}}$

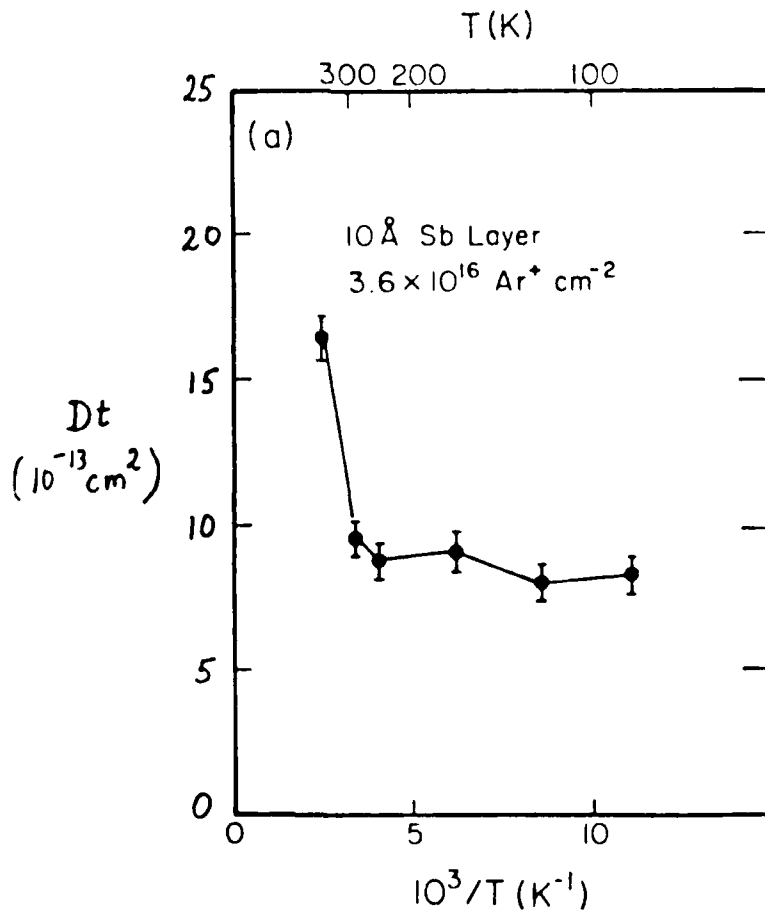
Φ -DEPENDENCE - EXAMPLE



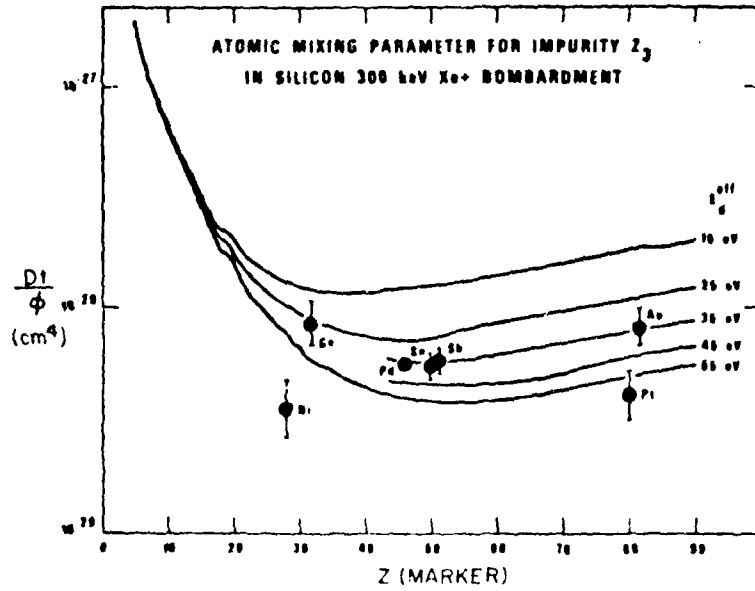
DEPTH DEPENDENCE



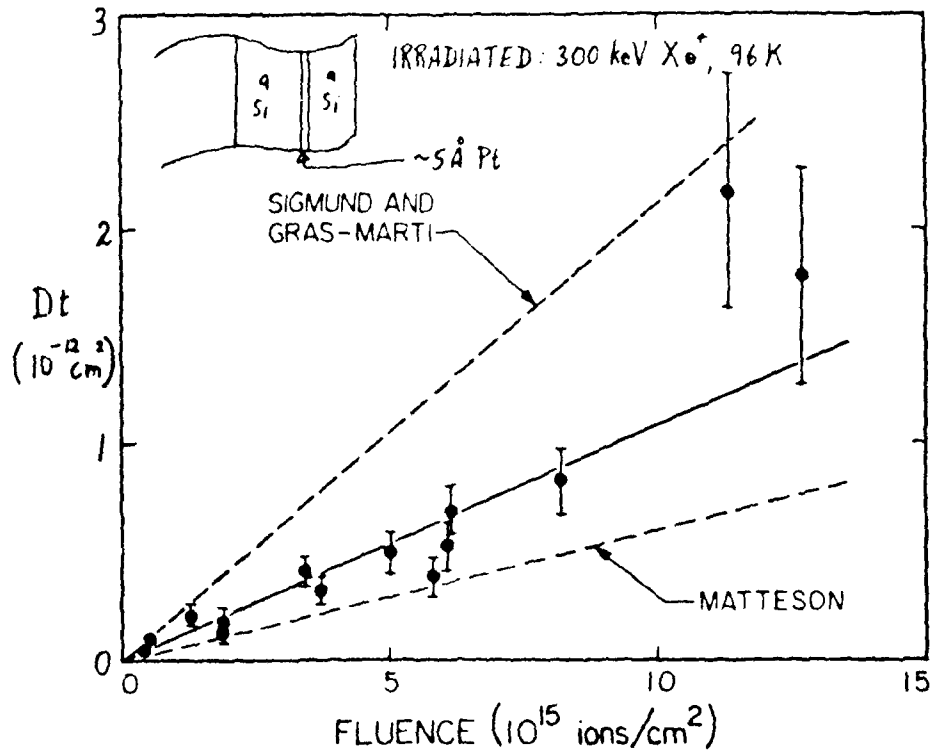
TYPICAL TEMPERATURE DEPENDENCE



QUANTITATIVE MODEL: MATTESON

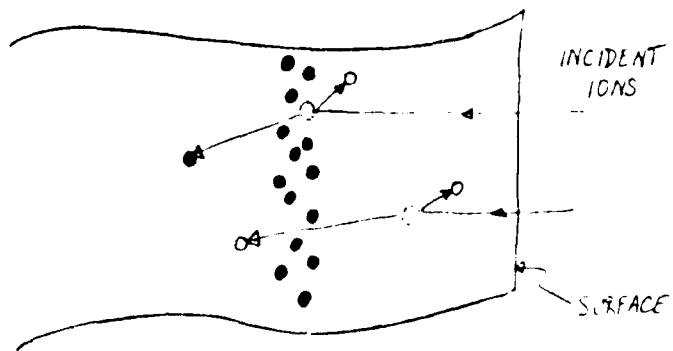


QUANTITATIVE MODEL: SIGMUND & GRAS-MARTI



MARKER SHIFTS

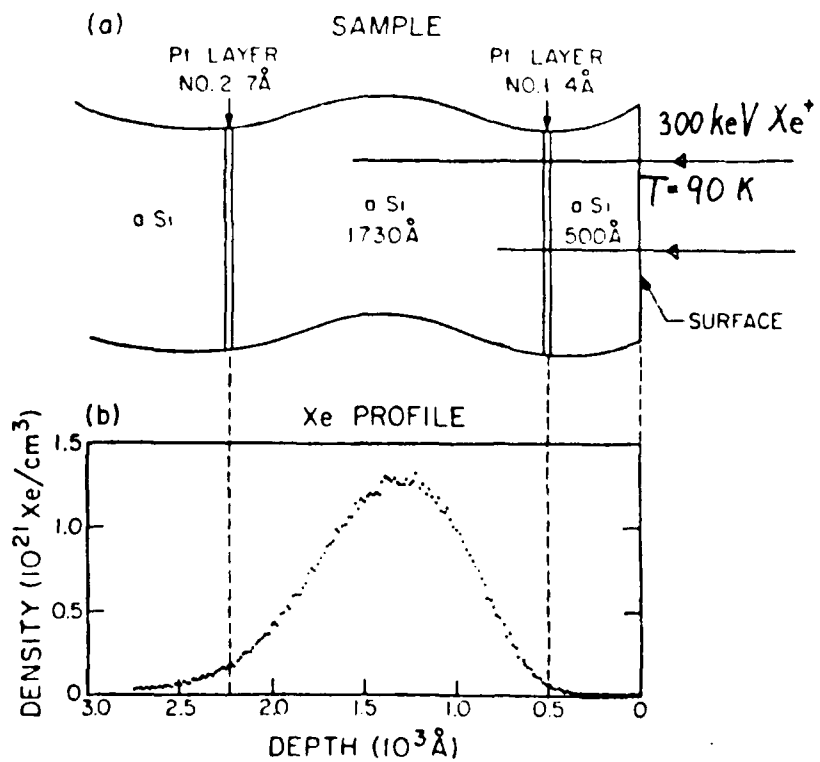
THEORY

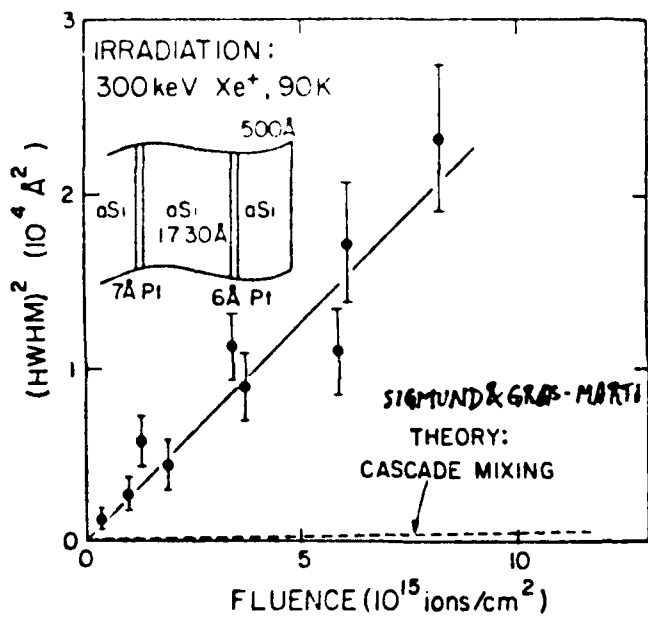
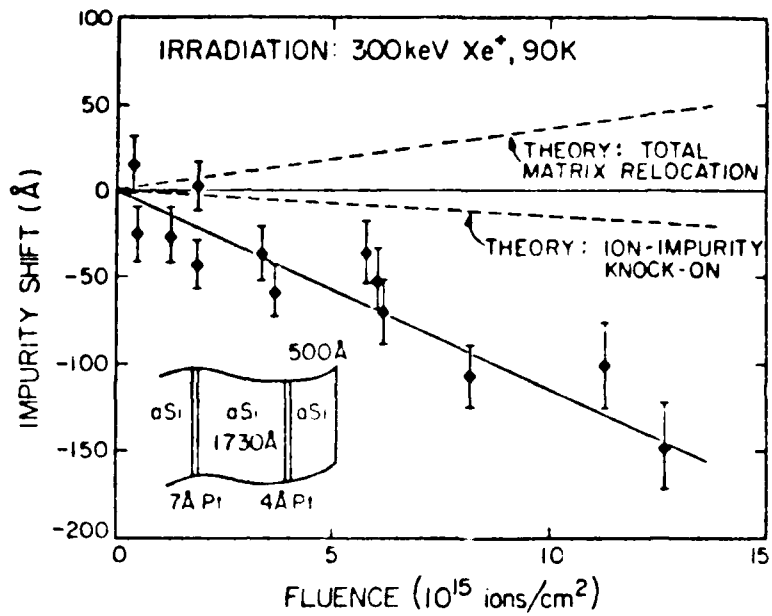


SIGMUND & GRAS-MARTI PREDICT:

FOR A HEAVY MARKER IN A LIGHT MATRIX:-
THE MARKER MOVES TOWARDS THE SURFACE

EXPERIMENT





SUMMARY

METHOD

OBSERVE SPREAD OF MIXING Dt AND SHIFT Δz FOR MARKER SPECIES M IN MATRIX A , DENOTED $A(M)$.

RESULTS

1. $T < T_c$

Expts.
 Mixing fn.
 ϕ -dep.
 F_D -dep.
 T -dep.

<u>Spreads</u>	<u>Shifts</u>
Gaussian except Si(Pd) ⁽²⁾	?
$\propto \phi^{1/2}$ ⁽³⁾	$\propto \phi$ ⁽¹⁾
? $\propto F_D$ ⁽¹⁾	-
$\neq f(T)$ except Si(Pd) ⁽²⁾	-

Models

Qualitative	Kinchin - Pense/Anderson	OK.	-
Quantitative	Matteson	OK.	-
	Sigmund and Gras-Marti Pouch	50x too small -	Trouble OK

2. $T > T_c$

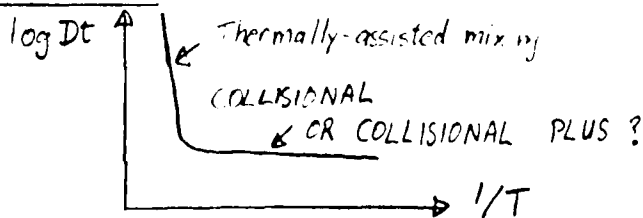
Expts
 Mixing fn
 T -dep.
 other deps.

often non-Gaussian	-
often strong	-
-	-

Models

Thermally-assisted mixing

STATE OF UNDERSTANDING



(1) for Si(Pt)

(2) for Si(Ni), Si(Ge), Si(Sn), Si(Sb), Si(W), Si(Pt), Si(Au), Al(Si), SiO₂(W), SiO₂(Pt)

(3) for Si(Ge), Si(Sb), Si(W), Si(Pt), Al(Sb), SiO₂(W), SiO₂(Pt)

"Marker Experiments in Si and SiO₂"

A. Barcz¹ and B. M. Paine
 California Institute of Technology
 Pasadena, California 91125

ONE SET

↓
 To investigate the role of the chemical nature of the medium and the impurity species in the ion mixing process, we have measured the apparent broadening of thin metal markers in SiO₂ and compared it with the broadening of markers in Si. Samples consisted of markers of thicknesses of the order of $\sim 10^2$ Å of W or Pt imbedded in Si, and of Pt, W, Hf, Co, Ni and Ti markers in SiO₂. The SiO₂ matrices were prepared by both chemical vapor deposition (CVD) and chemical oxidation of silicon in a steam atmosphere. The samples were irradiated with 300 keV Xe⁺ ions at 300 K and analyzed by 2 MeV RBS (Fig. 1). The efficiency of the mixing is expressed as σ_{mix}^2 - the variance of the redistribution of marker atoms due to the ion irradiation. The mixing is found to be independent of the method of preparation of the SiO₂. Furthermore, the values of σ_{mix}^2 for Pt and W markers in SiO₂ are equal to within experimental uncertainties while in silicon σ_{mix}^2 for Pt exceeds that for W by a factor of four. For all systems, the variance increases linearly with ion fluence (Fig. 2). The mixing parameter⁽¹⁾ in SiO₂ appears to increase monotonically with the atomic number of the marker species (Fig. 3).

In contrast, the amount of mixing reported previously in Si exhibits significant quantitative differences for elements of

similar mass. Our measurements for W and Pt markers in Si support this observation. Note that Dt/l of Fig. 3 is defined as $1/2 x_{mix}$. Also, note that the depth of our markers is 600 \AA compared to $\sim 200 \text{ \AA}$ for Ref. 1; this difference roughly accounts for the different values for the Pt marker data in Si.

Different efficiencies for the ion mixing process in Si and SiO_2 can also be observed directly from the asymmetric redistribution (preferentially toward silicon) of an initially thin Au marker located at a SiO_2 -Si interface and subjected to ion bombardment (Fig. 4). These results suggest that fast-diffusing atoms (e.g., Au or Pt in Si) can experience greater relocation under ion irradiation, than less mobile species (e.g., W). In SiO_2 , mixing is less dependent on the chemical nature of the marker because of much lower mobilities of impurities in general (e.g., for Au $D_{\text{Si}}/D_{\text{SiO}_2} \sim 10^8$) (2). A preliminary model is proposed according to which, in addition to prompt interactions in a cascade (two-particle collisions), delayed and extended perturbations (resulting for example from either excitations by very low energy recoils or relaxations of matrix atoms following a "prompt" displacement) may contribute significantly to the overall relocations of marker atoms. The magnitude of the latter mechanism should thus be related to the probability of thermally activated displacements (diffusion coefficient).

Permanent Address: Institute of Electrical Technology, Al.
Lotników 46, 02-668 Warsaw, Poland.

References

1. S. Matteson, B. M. Paine, M. G. Grimaldi, G. Mezey, and M-A. Nicolet, Nucl. Instr. & Meth. 182/183 (1981) 43.
2. H. F. Wolf, Semiconductors, (Wiley-Interscience, New York, 1971).

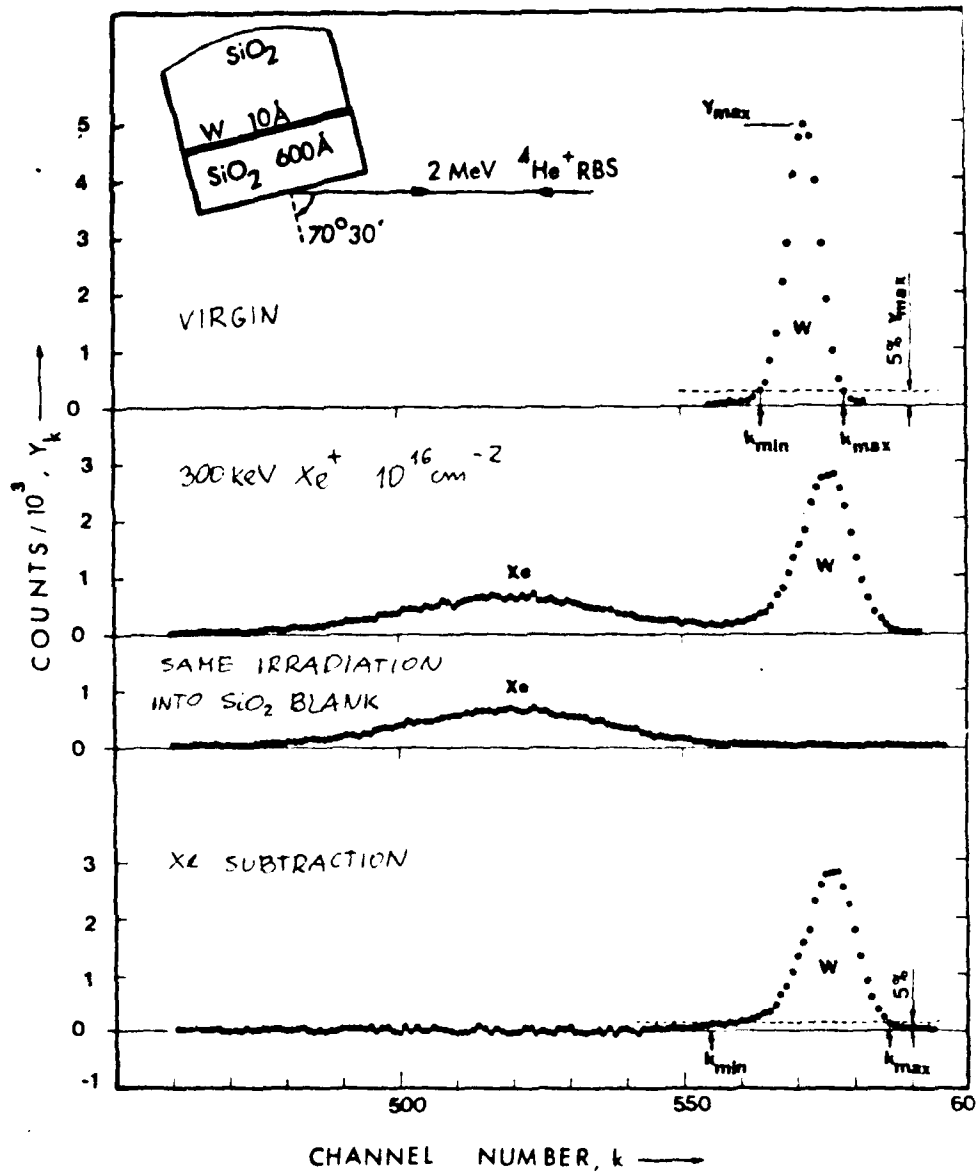


Fig. 1

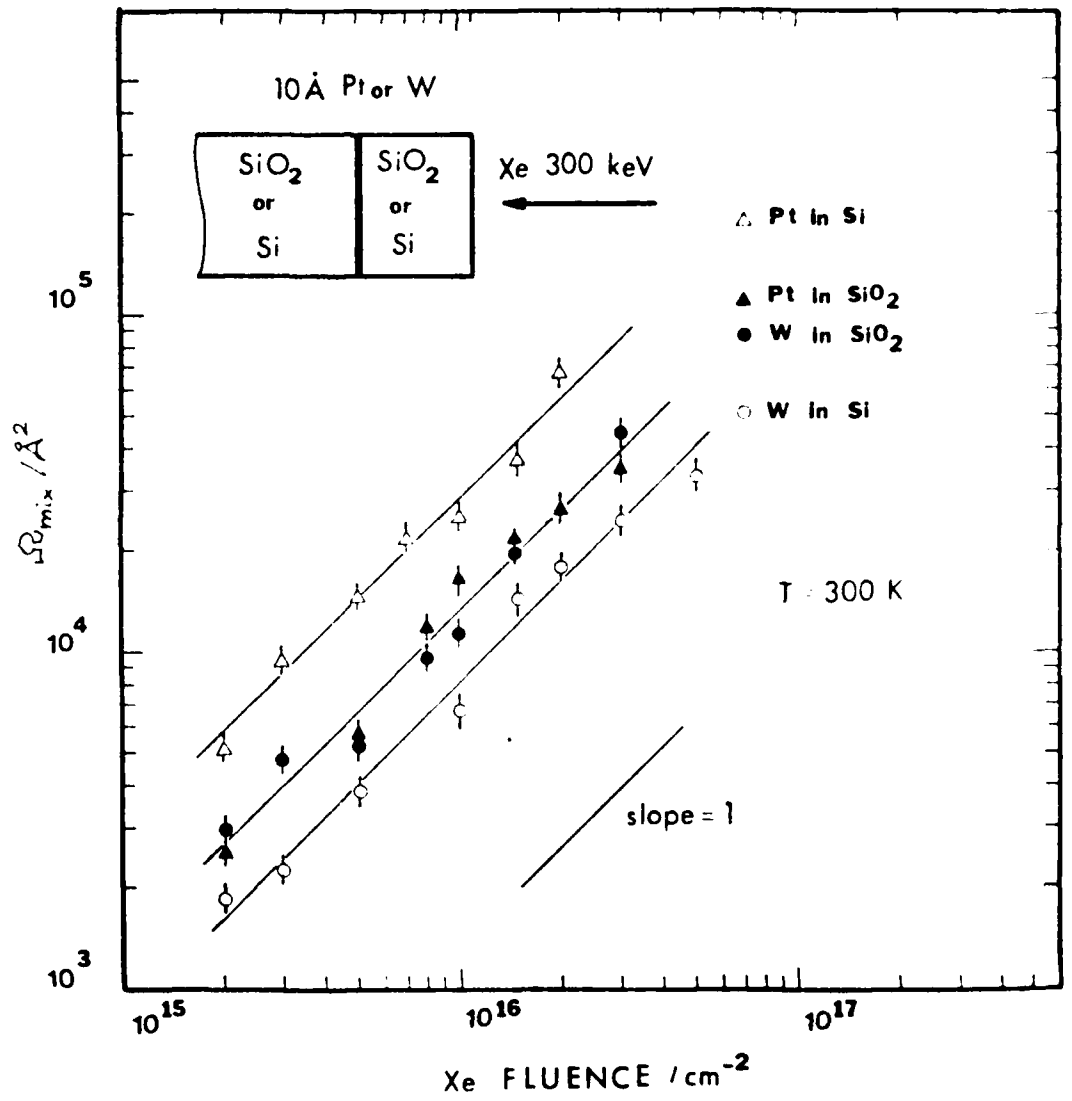


Fig. 2

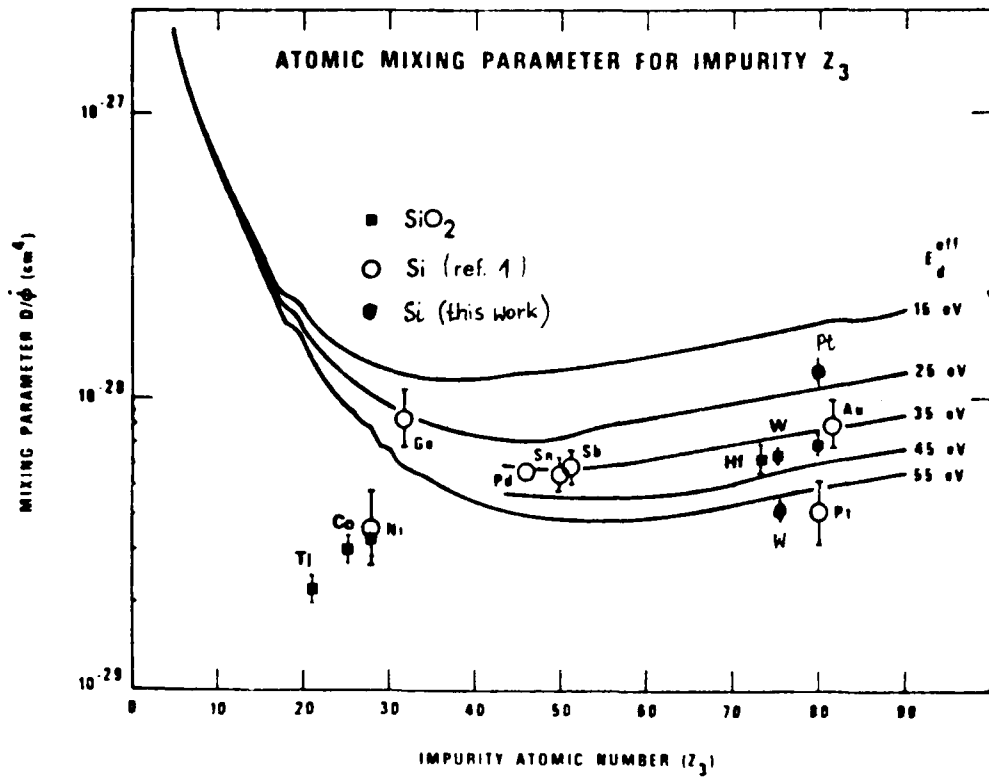


FIG. 3

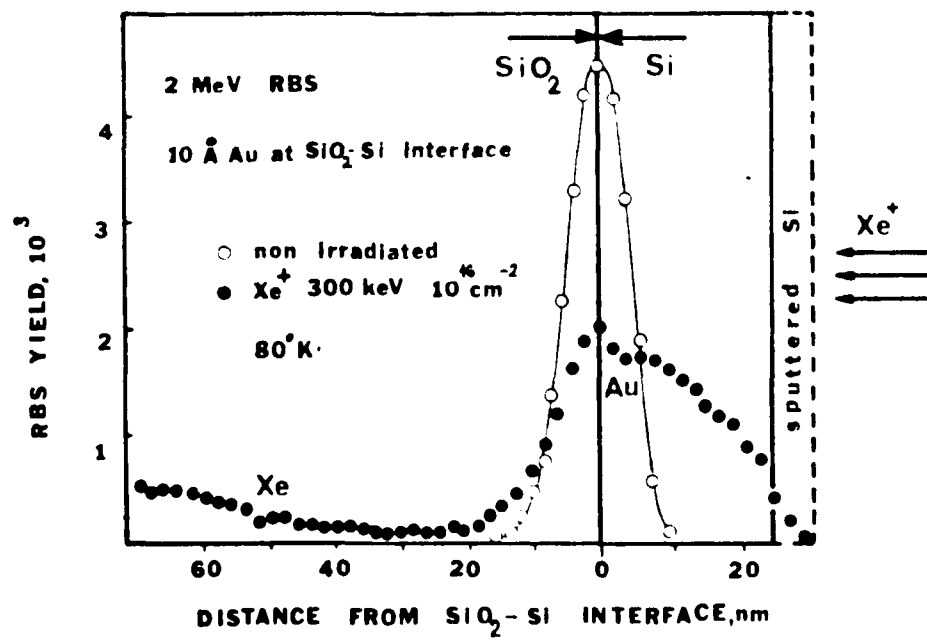


Fig. 4

AD P 001653

"Atomic Redistribution in Ion Mixing of Bilayer Thin Films"

H. H. Jorch and R. D. Werner
Chalk River Nuclear Laboratories
Atomic Energy of Canada Research Co. LTD.
Chalk River, Ontario, Canada (K0J-1J0)

An apparatus used for in-situ ion mixing and Rutherford Backscattering (RBS) analysis is described, and data are presented for thin film (i.e. "limited supply") structures of the Ag-Si and Au-Si simple eutectic systems. We find considerable preferred orientation in the Ag thin films which was not observed in the Au films although they were similarly prepared. This texturing is initially increased by Xe ion bombardment and then decreases (less preferred orientation), but even with 10^{17} Xe cm⁻² it is still far from random (Fig. 1). Caution is required in both RBS analysis and during the heavy ion bombardment to avoid misinterpretation due to this orientation problem.

Although there is no evidence for phase formation in the Ag-Si system (near room temperature), there are large differences in the degree of mixing of Si into Ag (Fig. 3) between 40 K and 280 K. This suggests thermodynamic forces play a role in hindering mixing at room temperature.

In the Au-Si system, no difference in the mixing behavior of Si into Au is observed from 55 K to 280 K (Fig. 5). At 300 K, however, a Au₅Si₂ metastable phase forms (Fig. 6) and after the entire Au layer has been converted, the mixing is inhibited.

Growth of this metastable phase proceeds linearly with Xe fluence (Fig. 7), suggesting supply-limited formation kinetics. The interplay of ballistic, cascade, and free energy (thermodynamic and chemical) effects severely complicate the evaluation of ion mixing mechanisms.

Figure Captions

- Figure 1 Preferred orientation effect in evaporated Ag thin film before irradiation (compare 20° higher "random" level in Fig. 2) is enhanced by 21% after 2.3×10^{15} Xe cm^{-2} ion fluence. Further irradiation doses start to decrease the degree of orientation (peak level rises closer to "random" height), but there is still a 27% difference at 10^{16} Xe cm^{-2} .
- Figure 2 With the same sample tilted to minimize the orientation problem, some effect remains ($\approx 2\%$), but the major features show interfacial mixing.
- Figure 3 Comparison of mixing at 40 K and near room temperature by measuring the mean atom fraction of Si in the Ag-Si mixed layer. Lines serve only to guide the eye. The ordinate value is determined from the average height of the Ag spectrum in the mixed layer (Ag peak).
- Figure 4 Low-temperature mixing of Au thin film on Si shows a widening concentration gradient at the interface along with a rapidly increasing Si content throughout the mixed Au layer.
- Figure 5 Mean atom fraction of Si in the Au-Si mixed film. At 300 K, a Au_5Si_2 metastable phase is formed and appears to retard the mixing after $\approx 5 \times 10^{15}$ Xe cm^{-2} .

Figure Captions (continued)

Figure 6 At 300 K, Si is seen to move from the substrate into the Au film and stepwise produce a Au_5Si_2 uniform phase across the film.

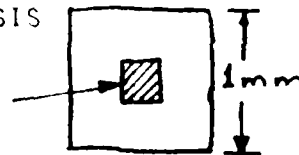
Figure 7 Growth of the Au_5Si_2 layer is shown. Faster growth at the high dose rate may be due to local heating of the sample.

CHALK RIVER HIGH VOLTAGE MASS SEPARATOR

FEATURES . . .

- HIGH ENERGIES (TO 2 MeV) WITH HEAVY IONS
 - : IMPLANT RANGE FAR BELOW FILM INTERFACE
 - : UNIFORM NUCLEAR STOPPING THROUGHOUT THIN FILM AND INTERFACE
- HIGH VACUUM
 - : 10^{-9} RANGE IN 30 K CRYOSHIELD
- TEMPERATURE RANGE
 - : SAMPLE TEMPERATURES 40 K TO 600 K
- RECTANGULAR PRECISION APERTURES
 - : X-Y TRANSLATIONAL REPRODUCIBILITY
 - : UP TO 100 INDEPENDENT RUNS ON EACH OF 5 SEPARATE TARGETS
 - : CENTRAL ANALYSIS

SPOT



MIXED
SPOT

- Y-AXIS ROTATION
 - : MONITOR PREFERRED ORIENTATION IN IMPLANTATION AND ANALYSIS

400 Å Ag on Si<111>
280 K
tilt = 0°
mixing : 1 MeV $^{132}\text{Xe}^+$

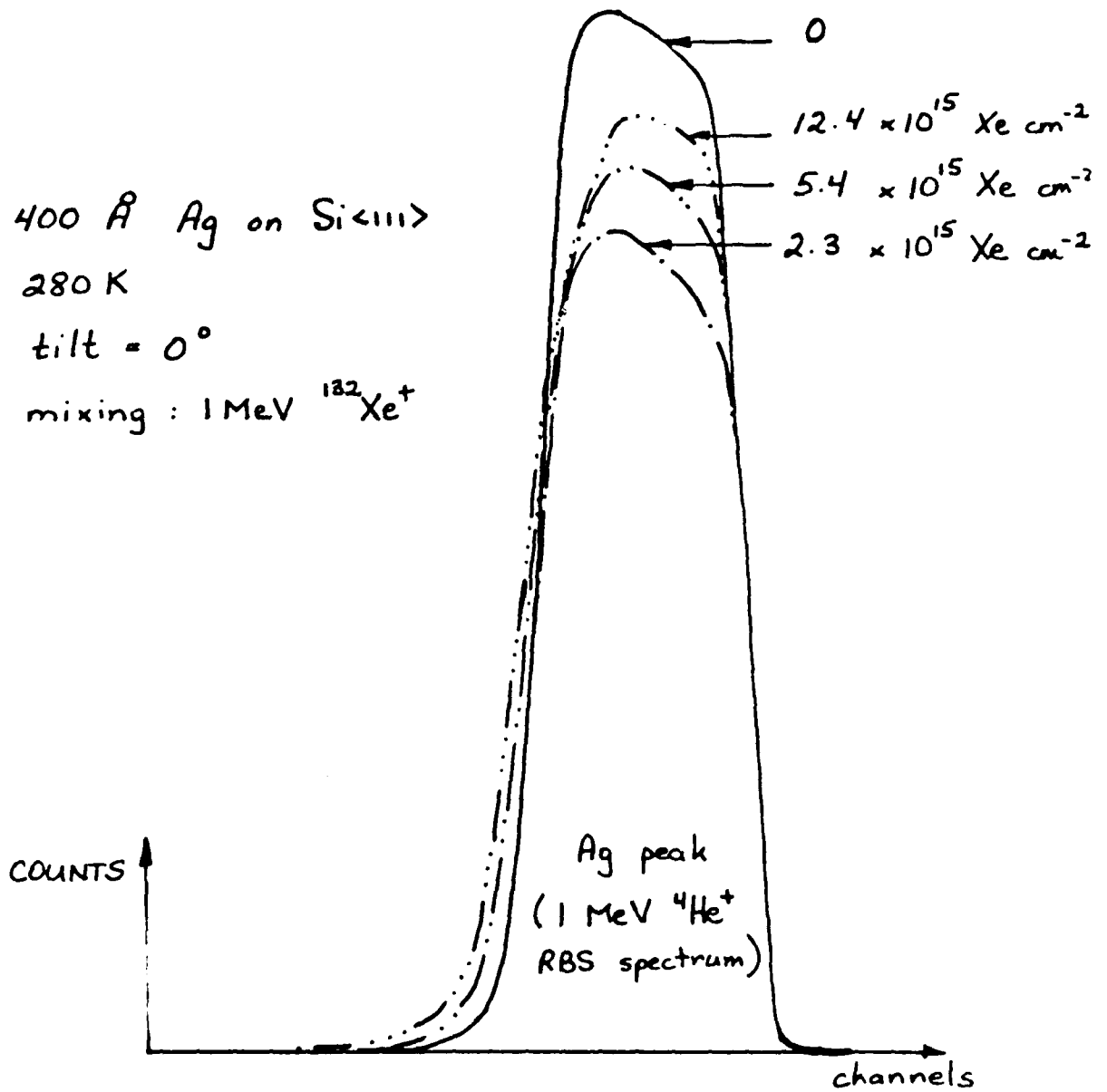


Fig.1

400 Å Ag on Si <111>
280 K
tilt = 8°
mixing : 1 MeV $^{132}\text{Xe}^+$

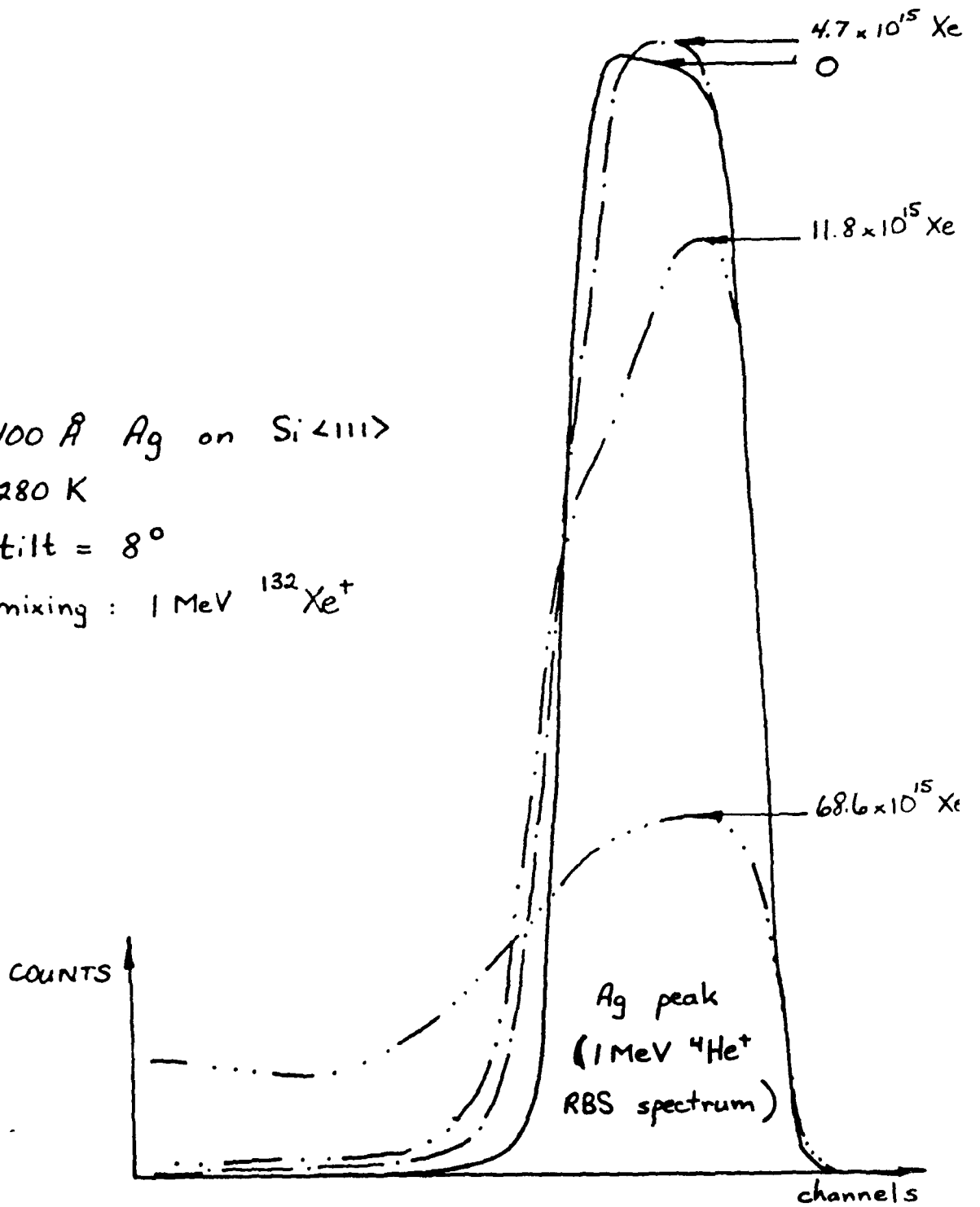
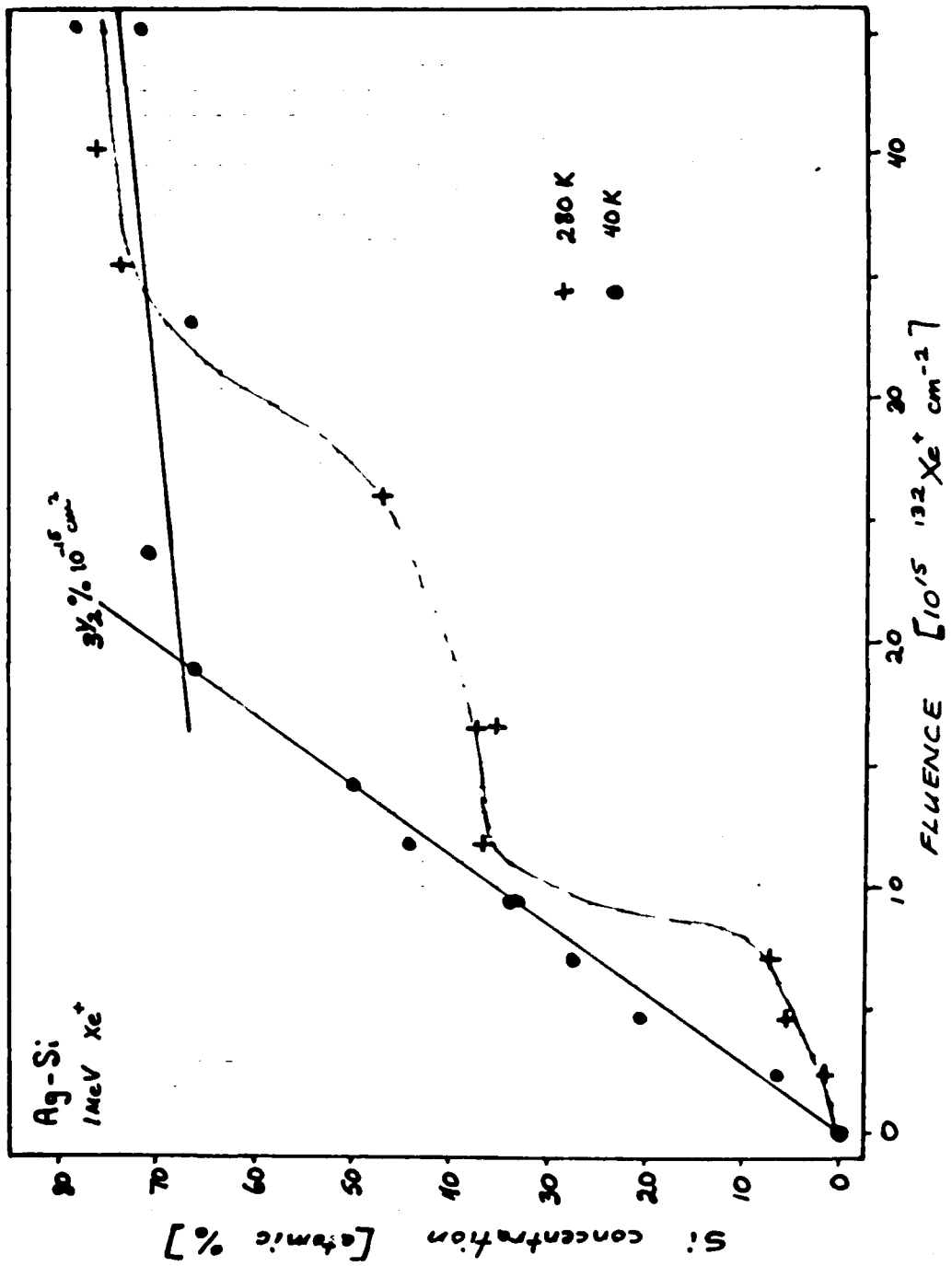
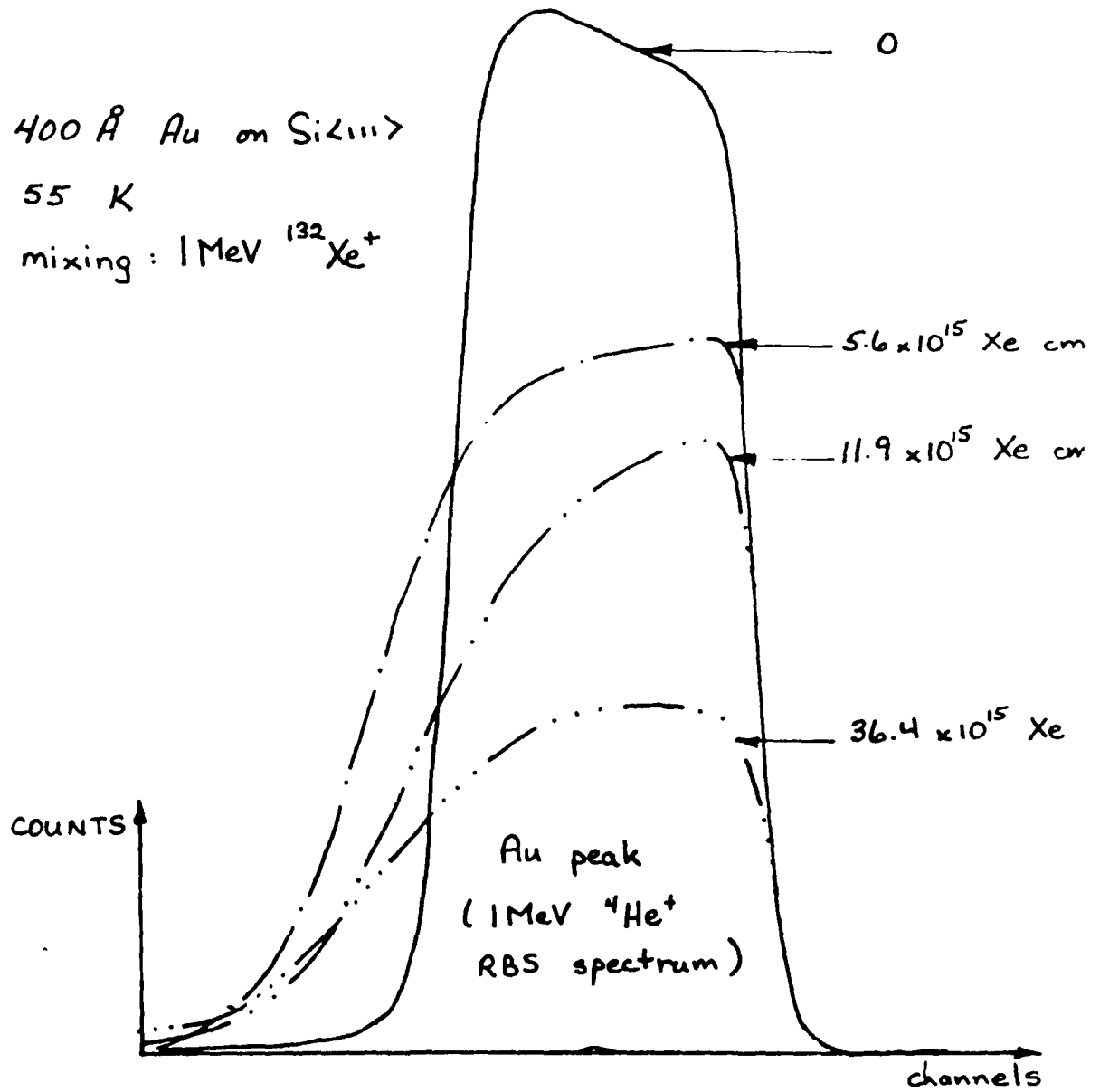
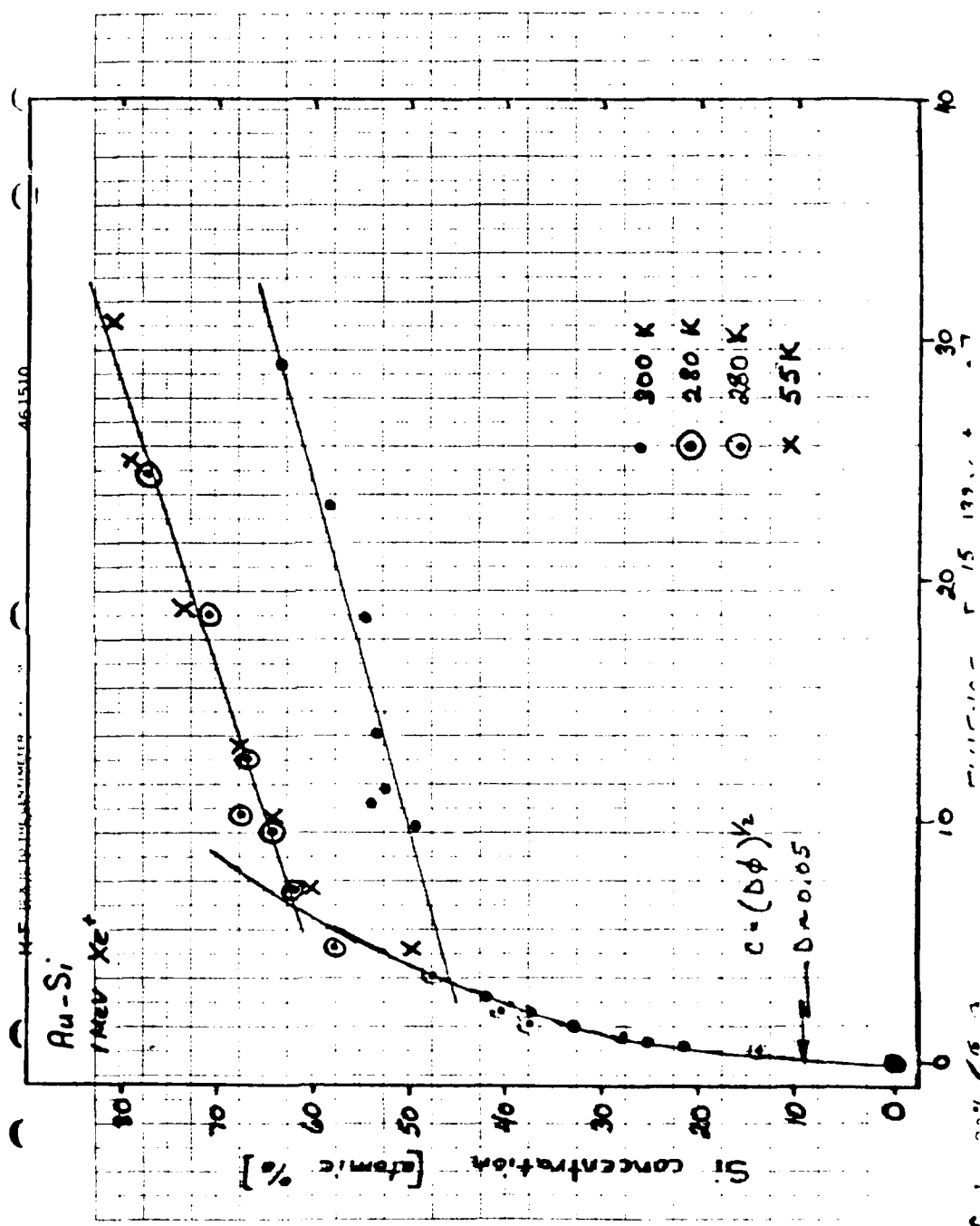


Fig. 2



400 Å Au on Si(111)
55 K
mixing: 1 MeV $^{132}\text{Xe}^+$

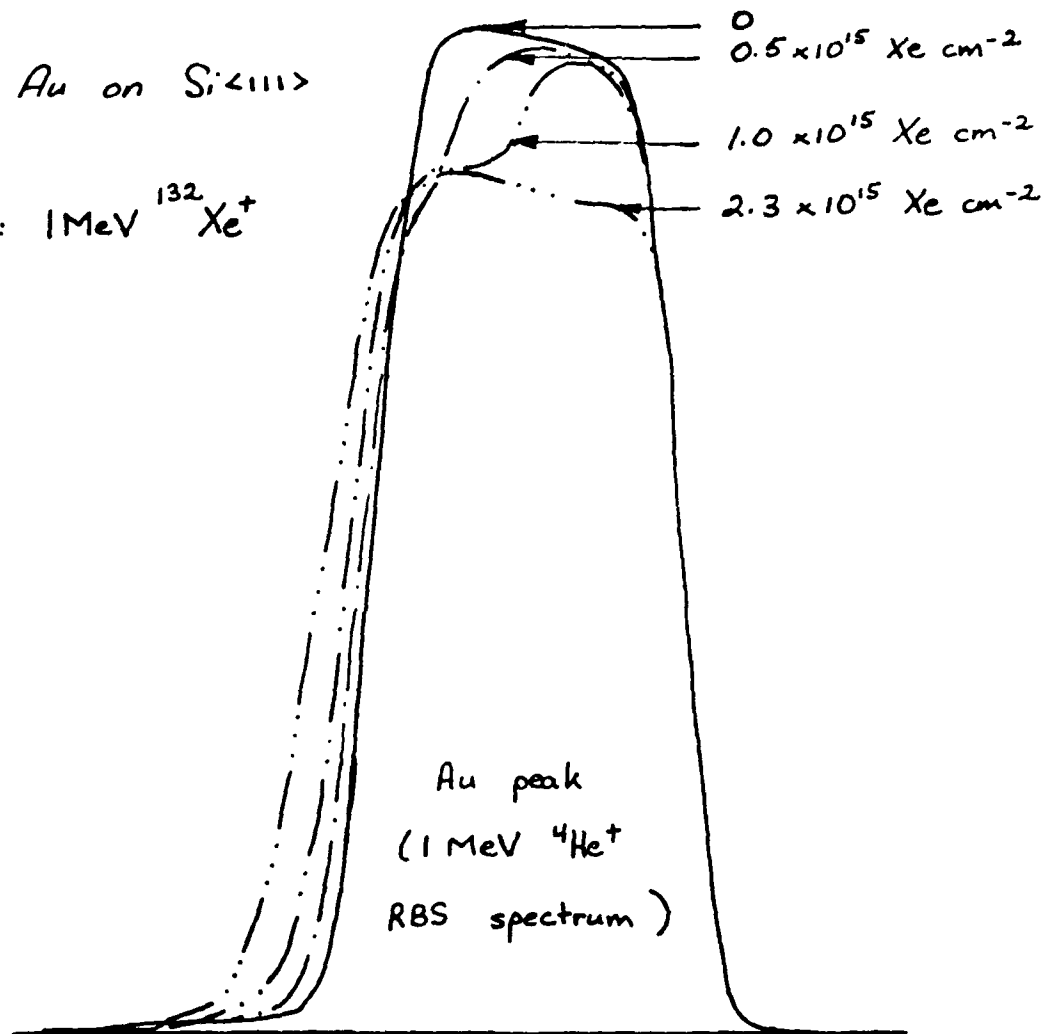




400 Å Au on Si<111>

300 K

mixing: 1 MeV $^{132}\text{Xe}^+$



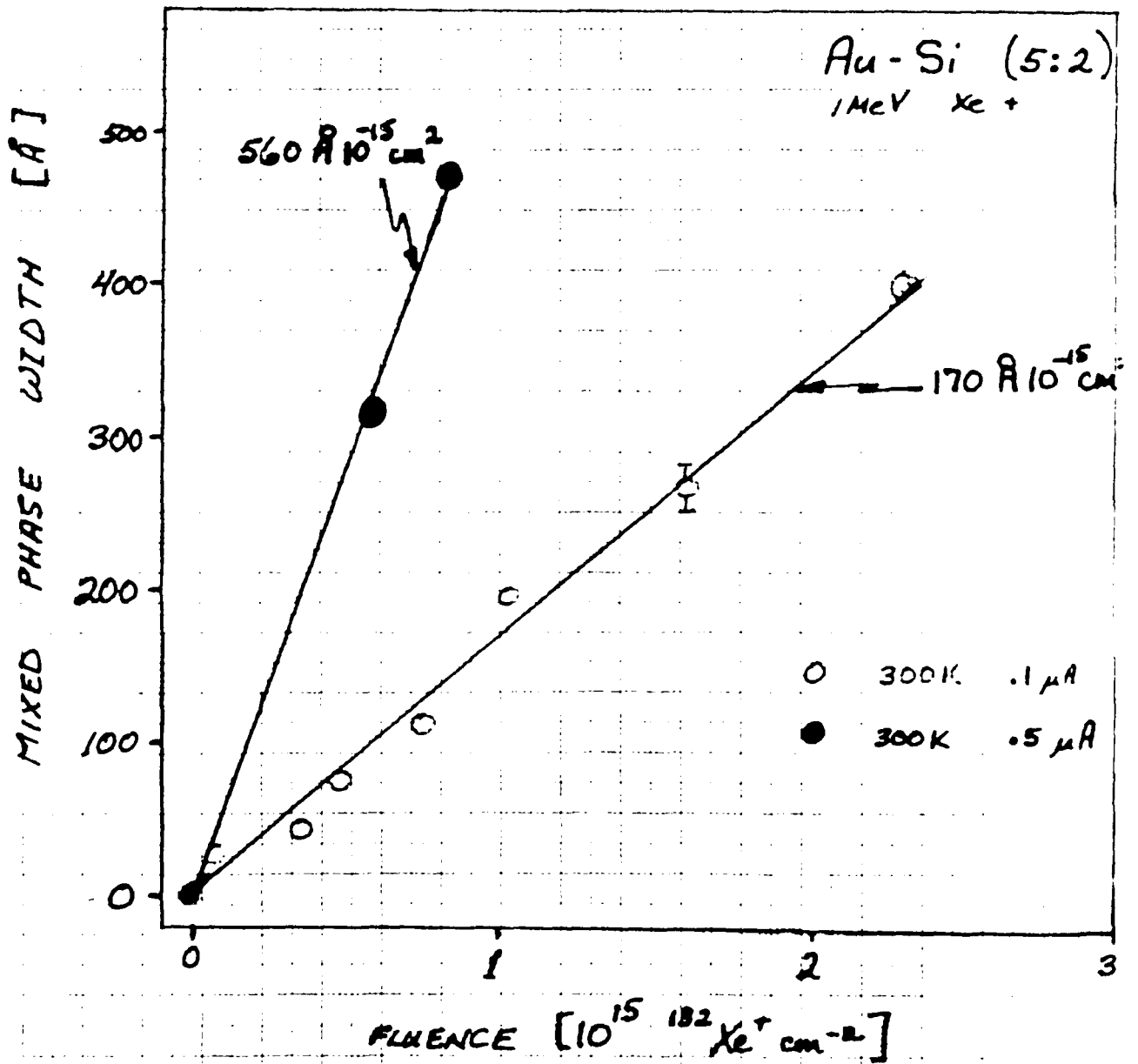


Fig. 7

AD P 001654

"Chemical Influences in Ion Irradiation-Induced Mixing"

T. Banwell and M-A. Nicolet
California Institute of Technology
Pasadena, California 91125

↓

Ion irradiation-induced mixing can be attributed to two principal types of processes; recoil implantation and "cascade" mixing, both of which may contribute significantly in bilayer mixing experiments. We have examined the influence of the chemical reactivity of the layers on these two mechanisms. For this study we chose the mixing of Ti/SiO₂, Cr/SiO₂ and Ni/SiO₂ bilayers induced by 290 keV Xe irradiation at irradiation temperatures of 77-750 K. The ballistic processes should be similar for all three systems since the metals have similar atomic masses; however, their chemical reactivities with SiO₂ are very different. Titanium readily reacts thermally with SiO₂ at temperatures above 900 K. Chromium reacts with SiO₂; however, the reaction is restricted by interfacial passivation. Nickel does not react with SiO₂; a Ni film on SiO₂ will coalesce into islands after only 1100 K annealing.

↖

The projected ranges and standard deviations for 290 keV Xe in these metals are 33±2 μg/cm² and 13±2 μg/cm², respectively. Metal films of 16, 24, and 34 μg/cm² were used. The unreacted metal was removed with hot HCl after the Xe irradiation. The metal and Xe remaining after etching were profiled by 2 MeV He backscattering spectrometry.

Figure 1 shows log-log plots of the areal density $[M]_s$ of the metal remaining after etching versus Xe fluence ϕ_{Xe} for R.T. irradiation. A predominately linear relationship is observed for the Xe fluence range considered, with $d \log[M]_s / d \log \phi_{Xe} = 0.57-0.73$. These results suggest that cascade mixing is the dominant process with a 10-20% contribution from recoil implantation at the lowest Xe fluence. Figure 2 shows the backscattering spectra for the $24 \mu\text{g}/\text{cm}^2$ Ni samples after R.T. Xe irradiation and etching. The inflections in the logarithmic plots of the Ni profiles around 1.4 MeV indicate that two processes contribute to Ni transport. Recoil implantation could produce the deep linear tail. Similar features are observed in the residual Ti profiles. Figure 3 shows that the integral of the Ni counts in the fixed portion of the Ni tail indicated is a linear function of Xe fluence ϕ_{Xe} for R.T. irradiation. A small dependence on Ni film thickness is noted. These results can also be attributed to recoil implantation. We conclude that the long range transport is predominately due to recoil implantation while cascade mixing dominates transport near the metal-SiO₂ interface.

Figure 4 shows the effect of temperature on the mixing process. Both Ti and Cr show enhanced mixing at 750 K while mixing is suppressed in Ni. There is strong correlation between these results and the chemistry associated with thermal annealing. Figure 5 shows the profiles for Ni and Ti with $10^{16} \text{Xe cm}^{-2}$ irradiation at R.T. and 750 K. The interfacial region is strongly affected by temperature whereas the deep tail is not.

Nickel irradiated at 750 K displays an exponential tail as in Fig. 2 with a linear $\ln \phi_{Xe}$ dependence as in Fig. 3, although the slope is $\sim 30\%$ less. The influence of chemistry is again seen in the results for mixing of Ti/SiO₂ induced by Xe irradiation at R.T. and 750 K, shown in Fig. 6. The enhanced mixing at 750 K is eliminated by incorporating 20-30 at. % O in the Ti layer prior to irradiation. The extra O may diminish the chemical driving force in the Ti-SiO₂ system.

From these results we conclude that chemistry has little direct effect on recoil implantation. "Cascade" mixing is strongly influenced by local chemical processes.

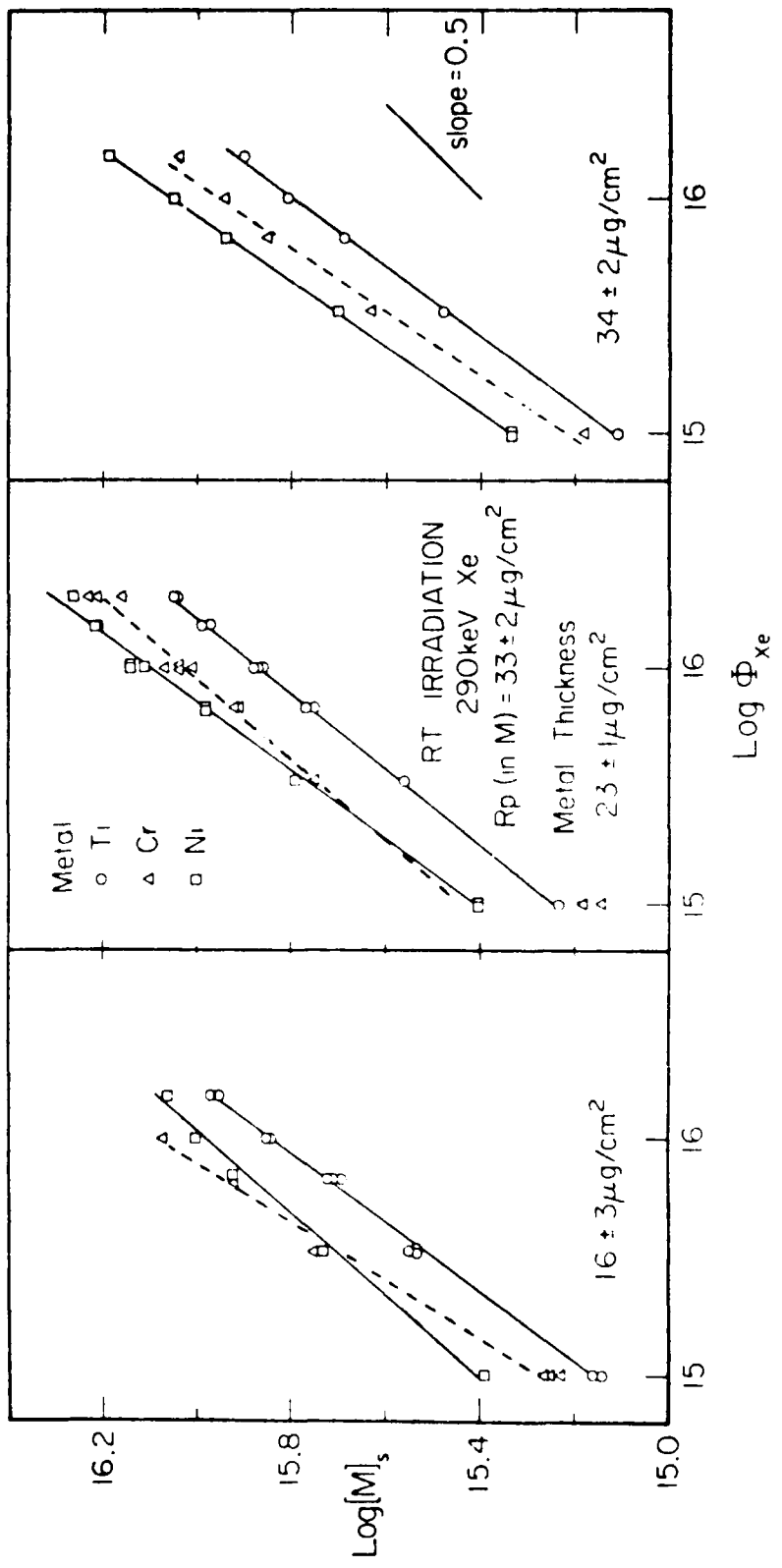
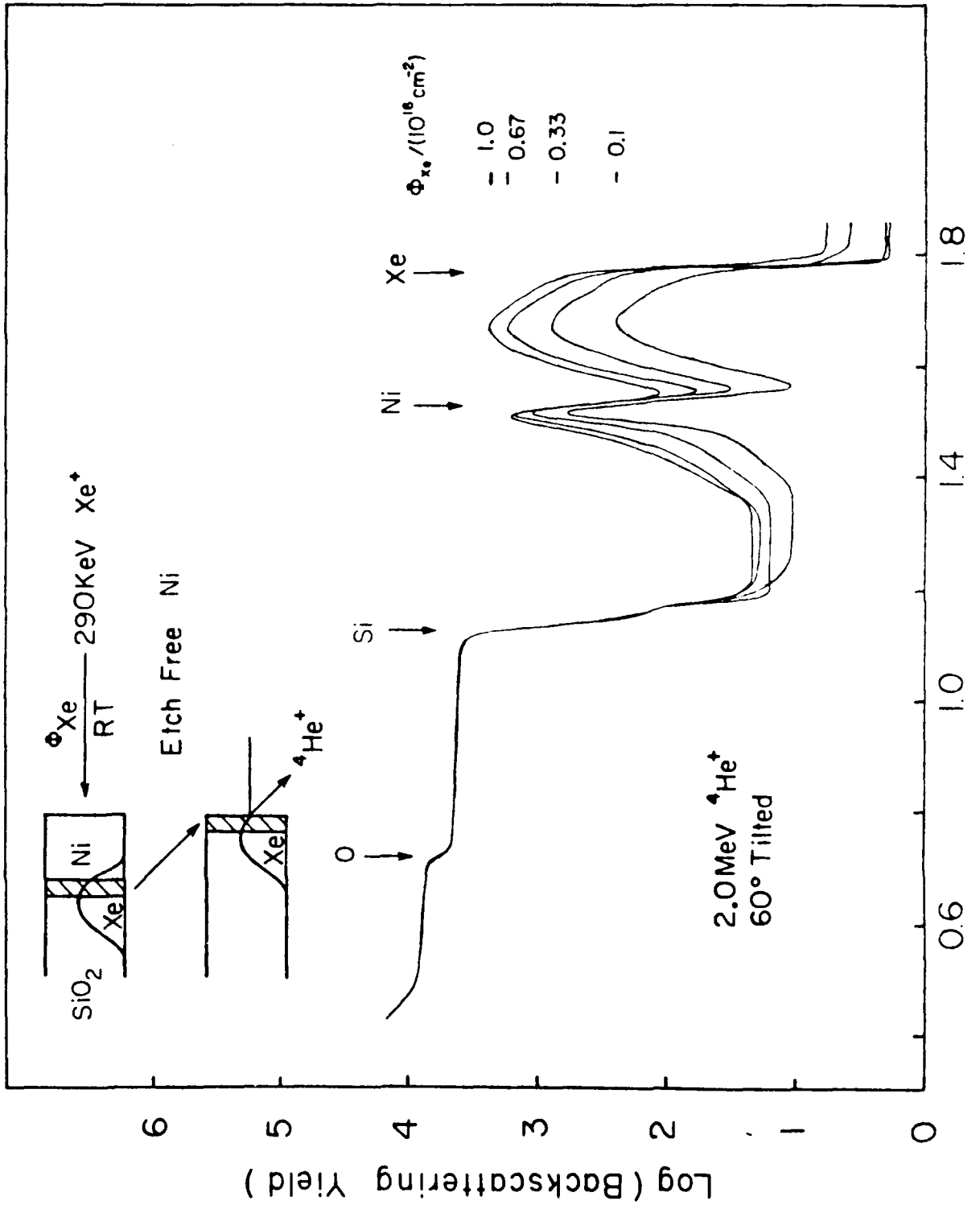


Fig. 1



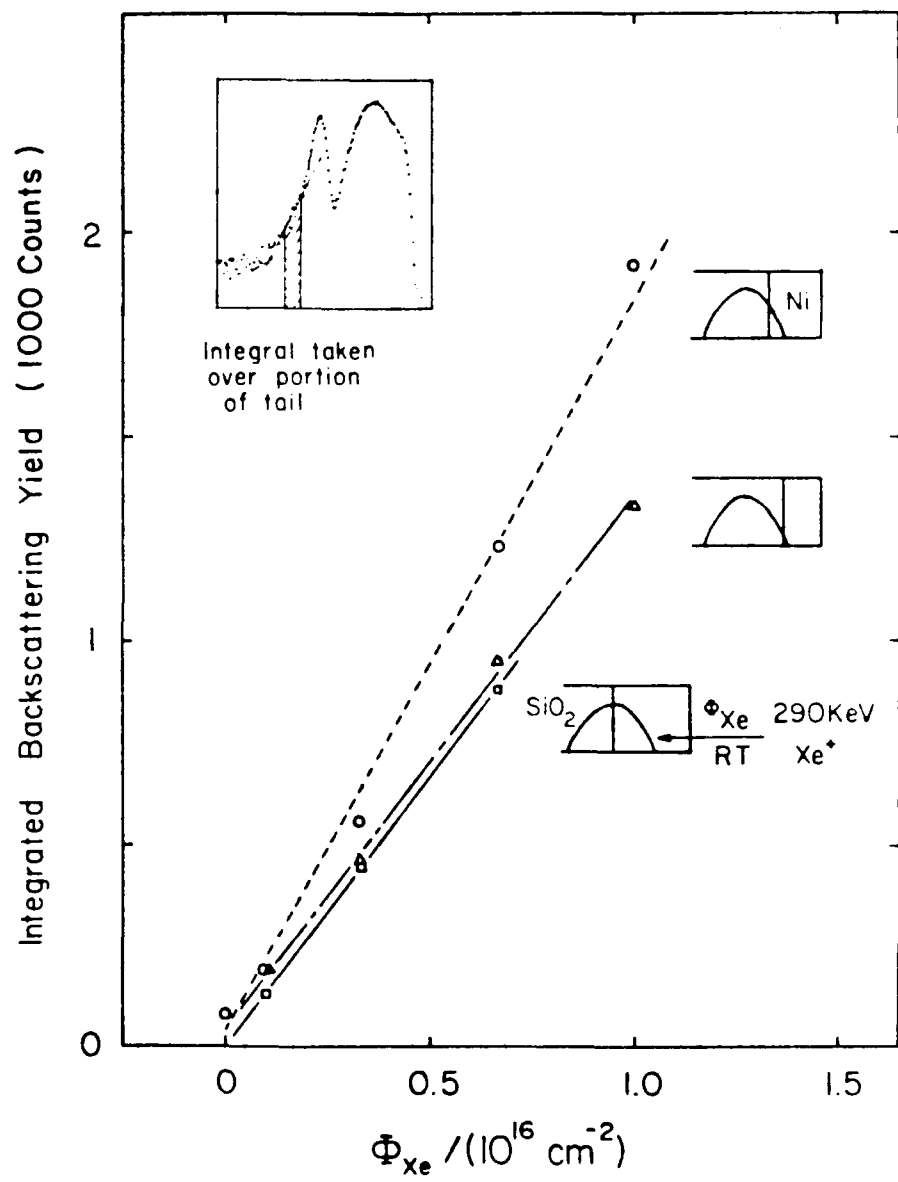
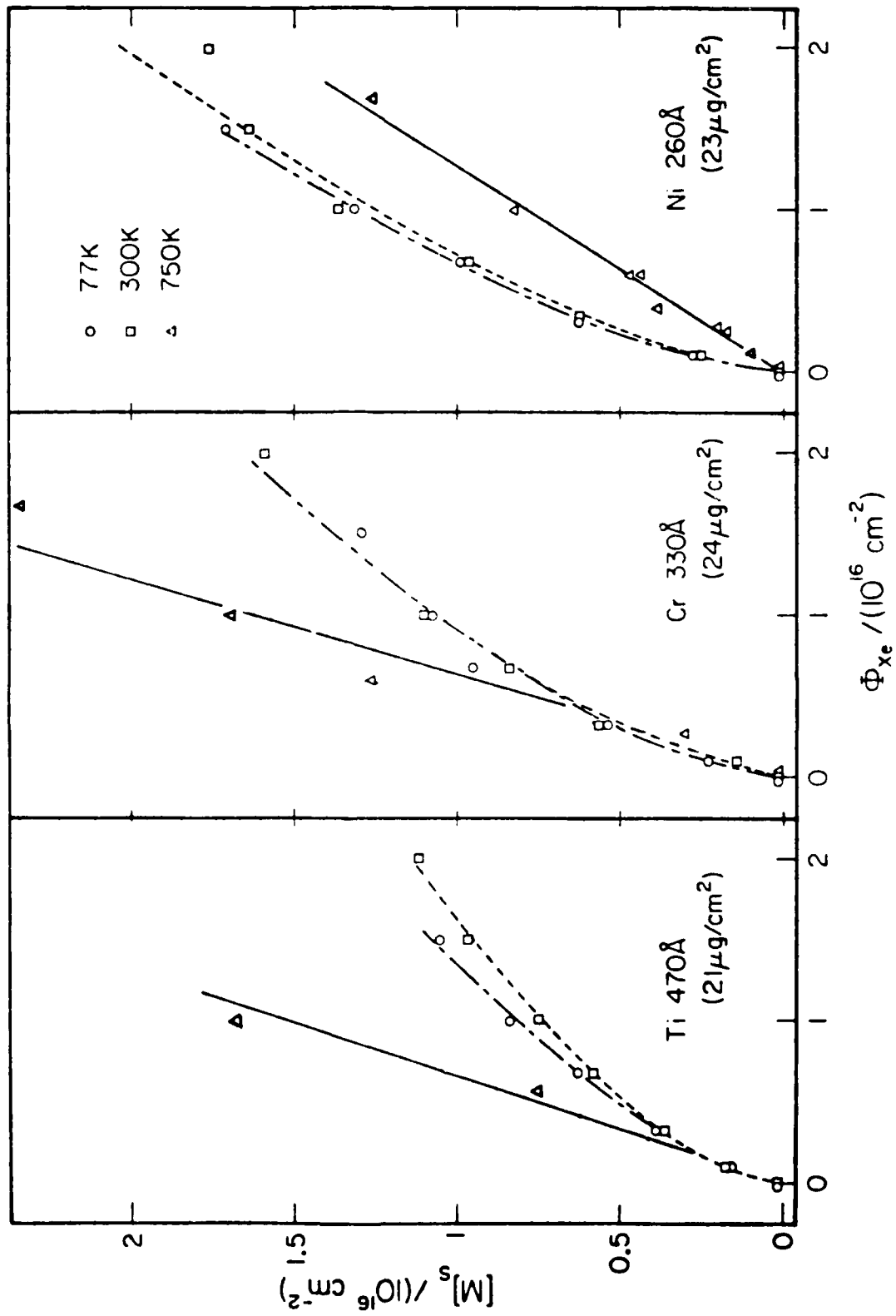
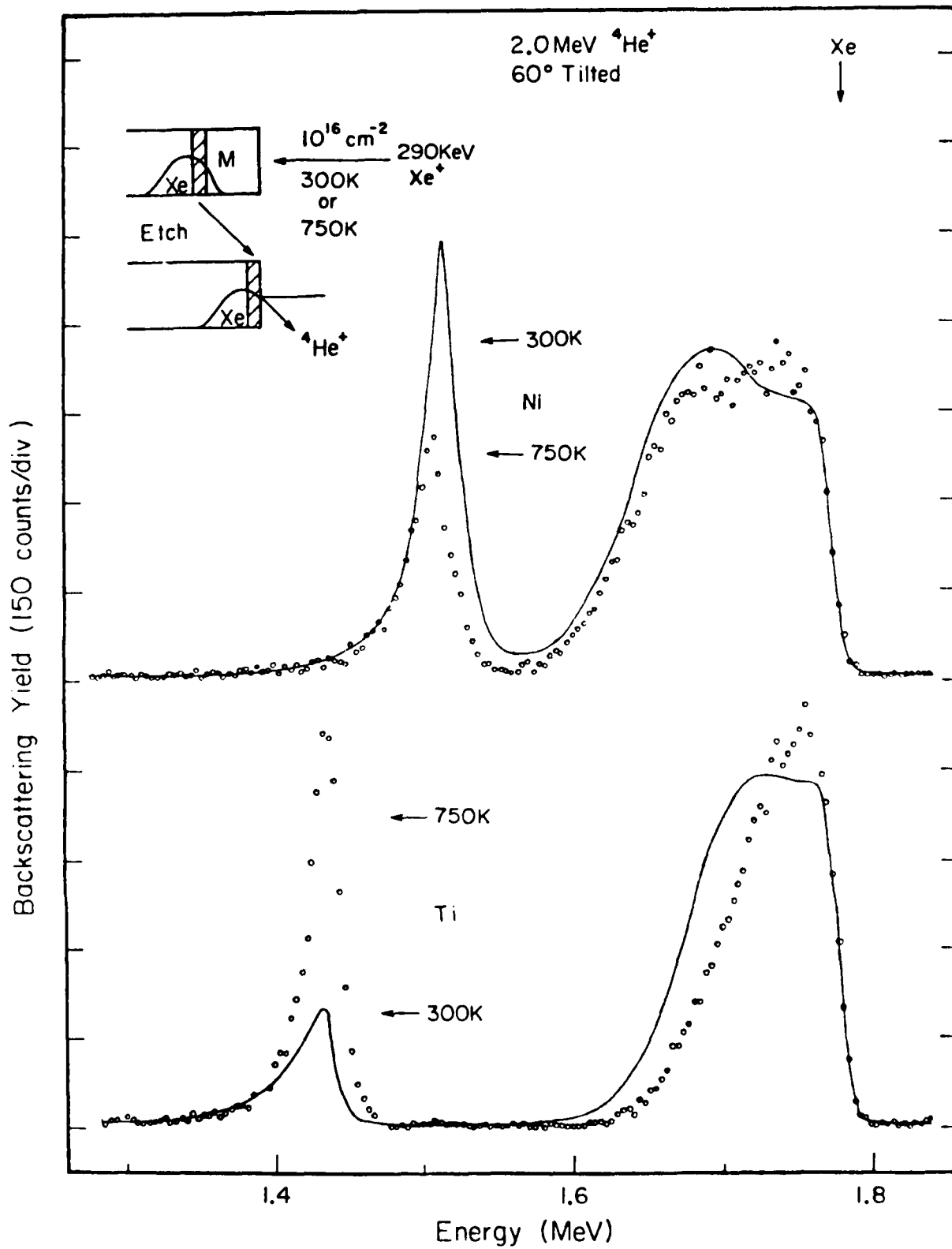


Fig. 3





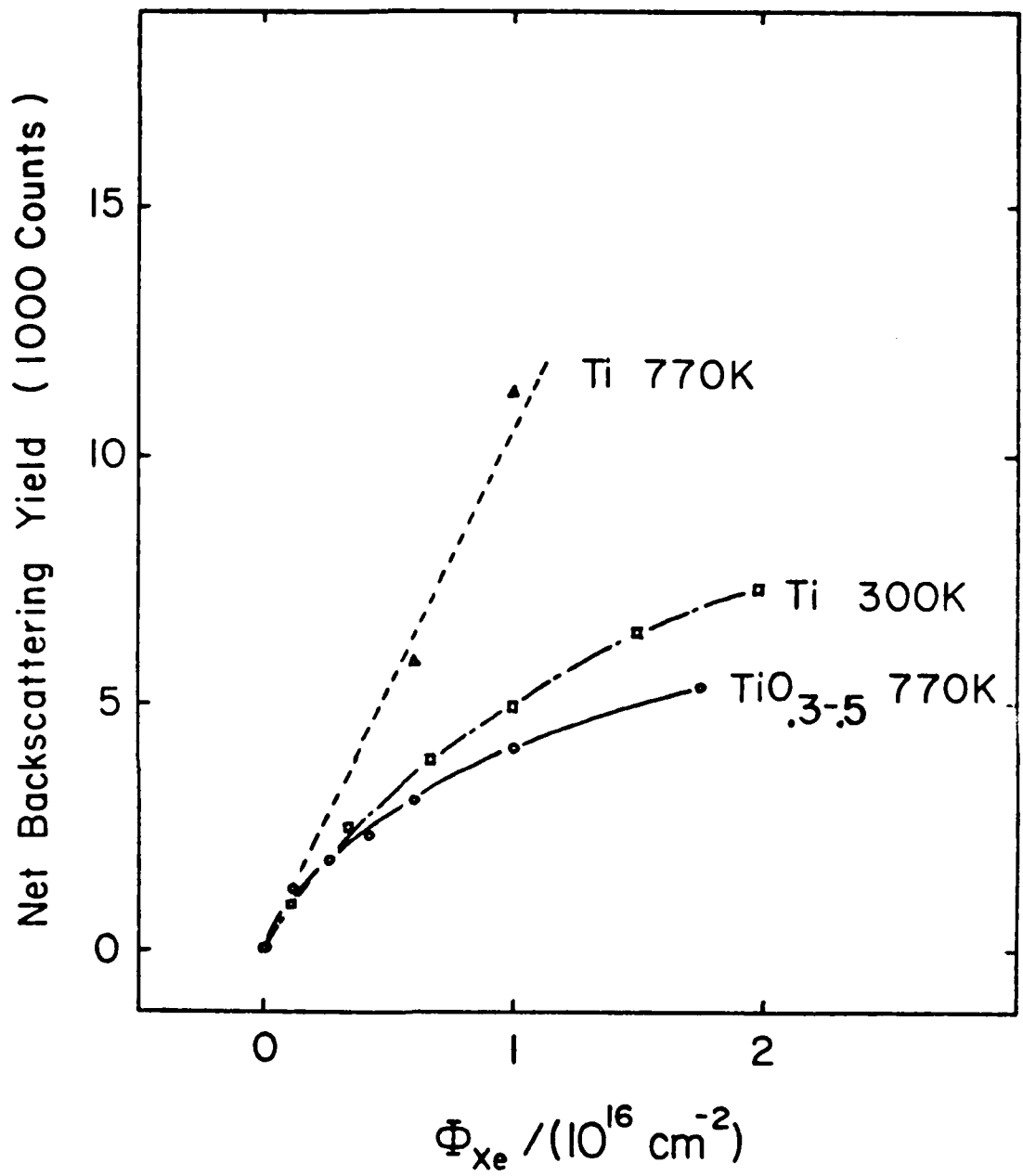


Fig.6

II. Ion Mixing-Material Processes

"Sputtering and Ion Mixing in CrSi_2 : Temperature Effects"

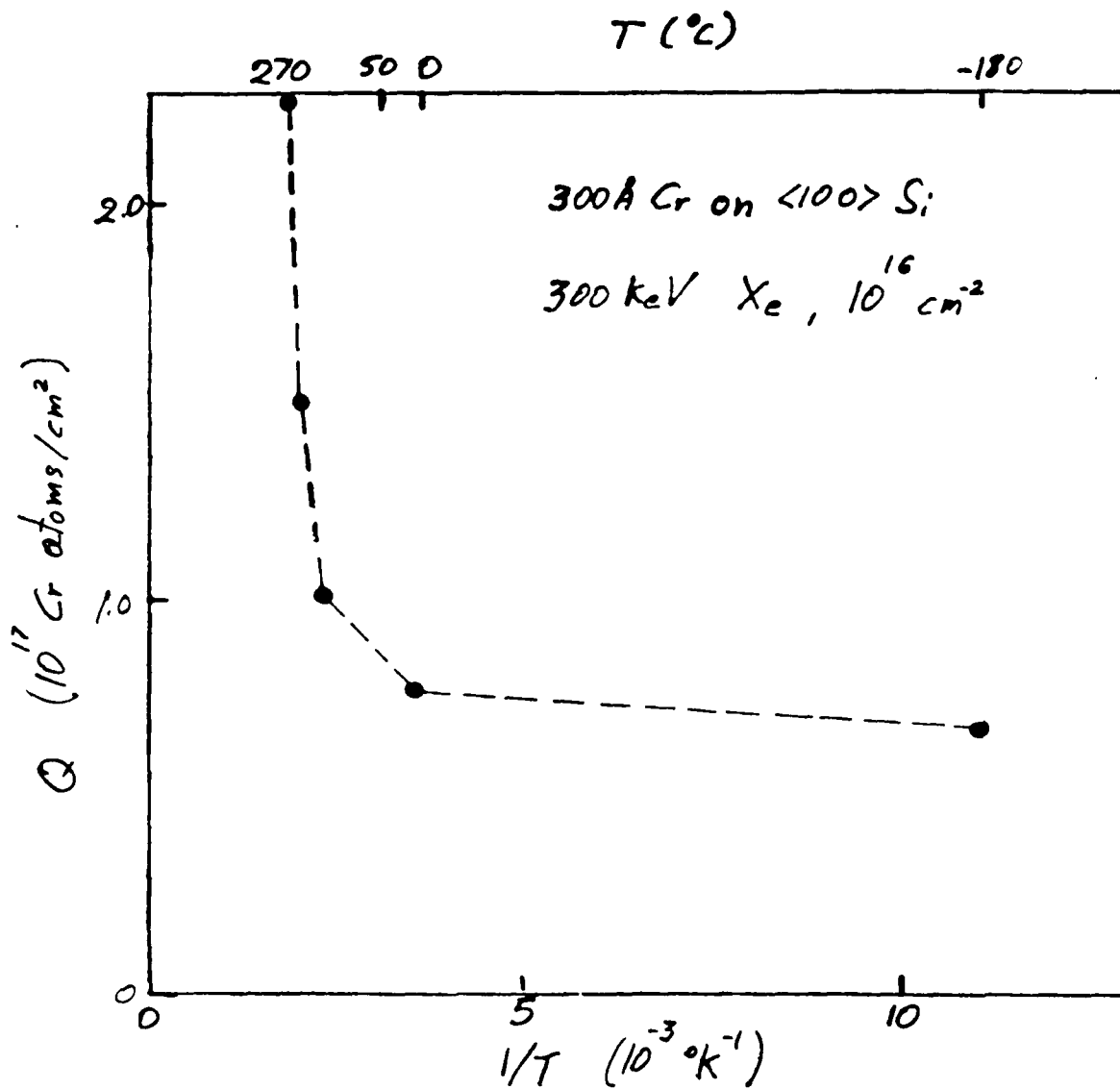
U. Shreter
California Institute of Technology
Pasadena, California 91125

Ion mixing and sputtering are influenced by the same transport mechanisms during irradiation. Both prompt and delayed processes are expected to affect mixing as well as sputtering.

It is known that mixing of a Cr layer on Si is strongly temperature-dependent above room temperature. CrSi_2^{-1} was chosen therefore for the investigation of temperature effects in sputtering.

Measurements of sputtering yields and composition profiles have been carried out using backscattering spectrometry for samples of CrSi_2^1 on Si irradiated with 200 keV Xe ions. When the CrSi_2^1 layer is thinner than the ion range, the sputtering yield ratio of Si to Cr increases from 3.5 for room temperature irradiation to 65 at 290°C. For a thick sample, the corresponding increase is from 2.4 to 4.0 only. These changes are explained in terms of a rise in the Si surface concentration at 290°C. The driving force for this process seems to be the establishment of stoichiometric CrSi_2 compound. Transport of Si to the surface is by ion mixing in the thin sample and thermal diffusion through the thick layer.

AD P 001655

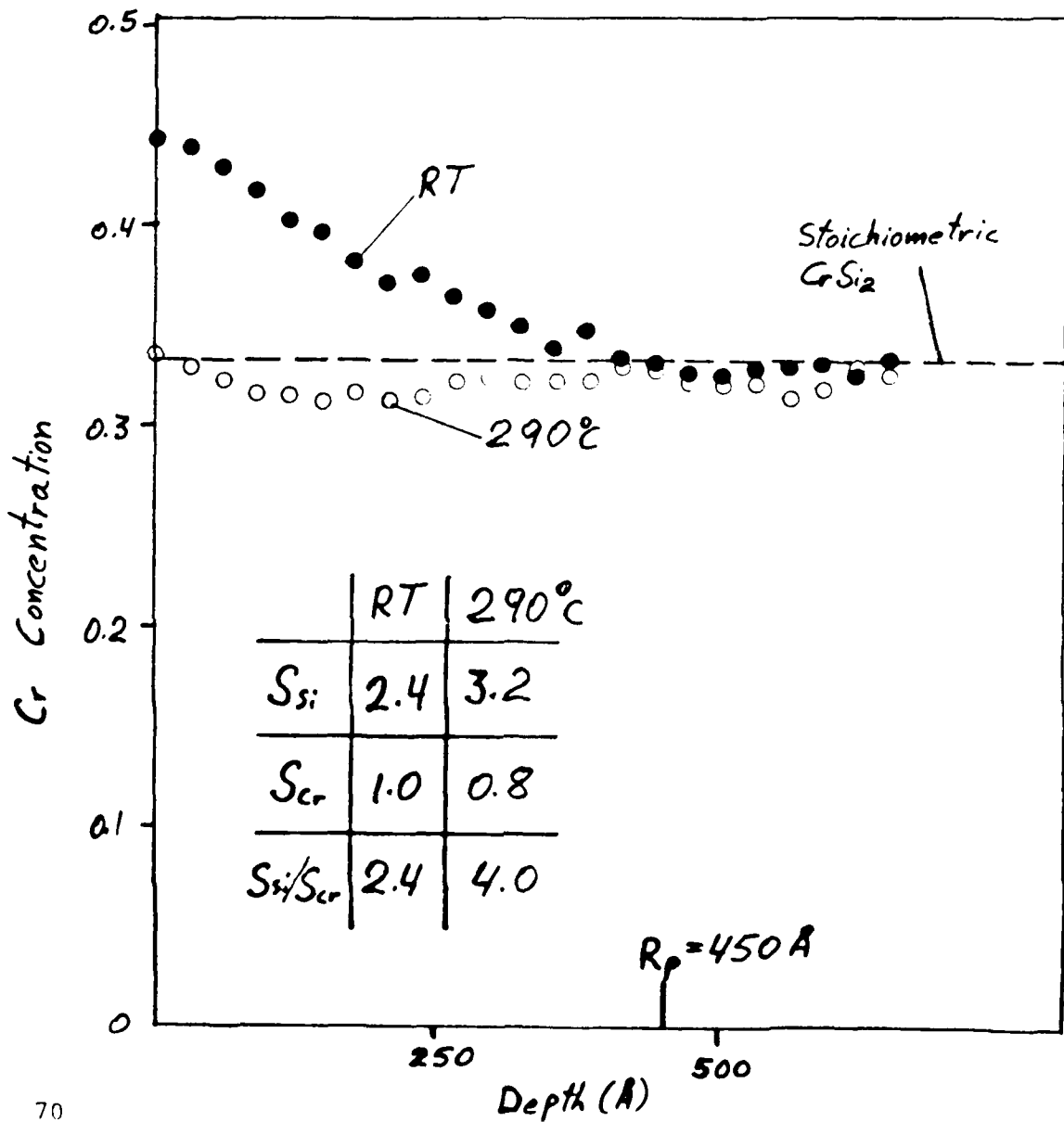


Mixing of a Cr layer on Si

Fig. 1

SiO ₂	Si	CrSi ₂
	580	1800 Å

← 200 keV Xe⁺
 ← 5 · 10¹⁶ ions/cm²



SiO ₂	Si	CrSi ₂
	1000 Å	370

← 200 keV Xe⁺
 ← 5 · 10¹⁶ ions/cm²

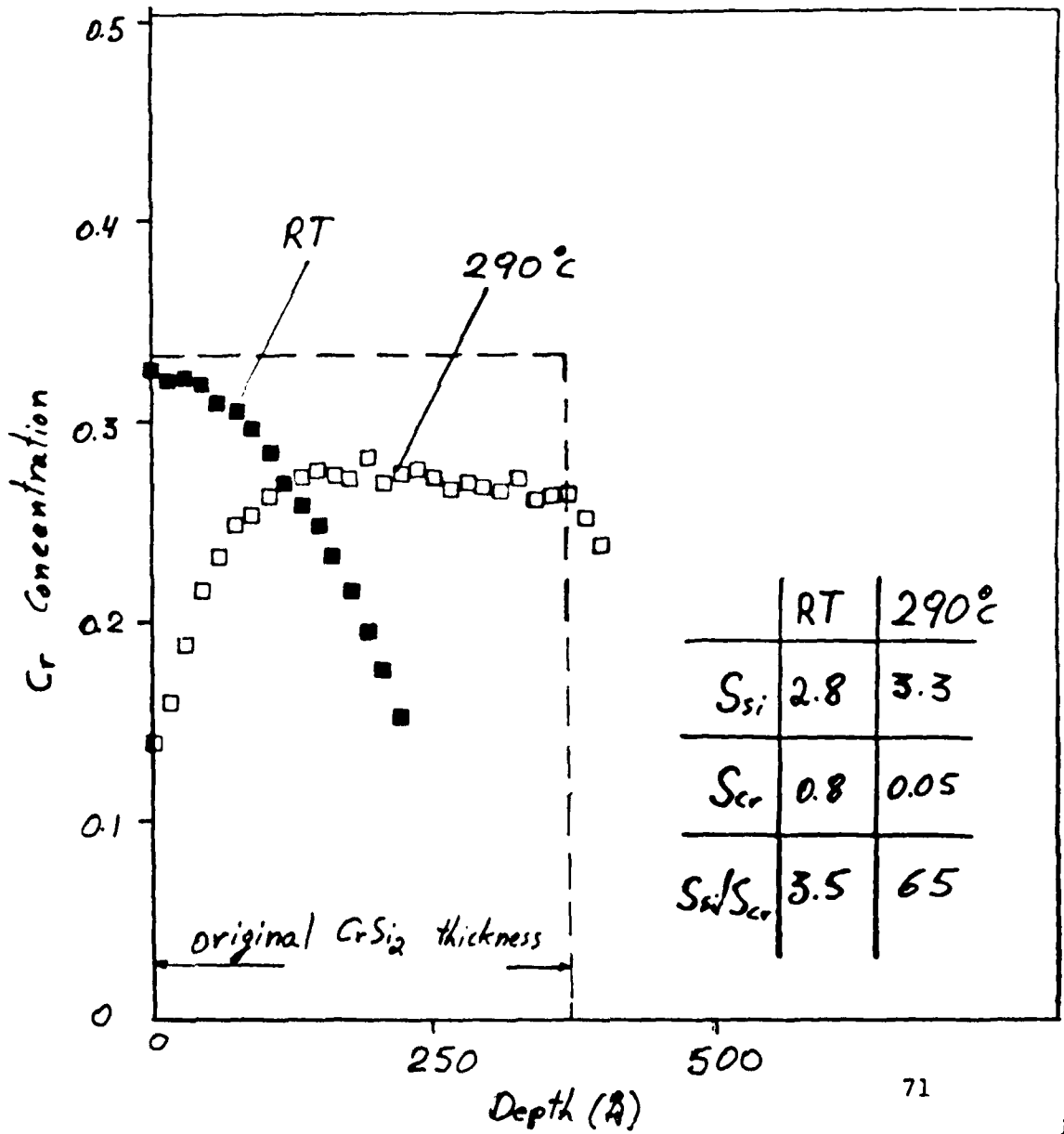
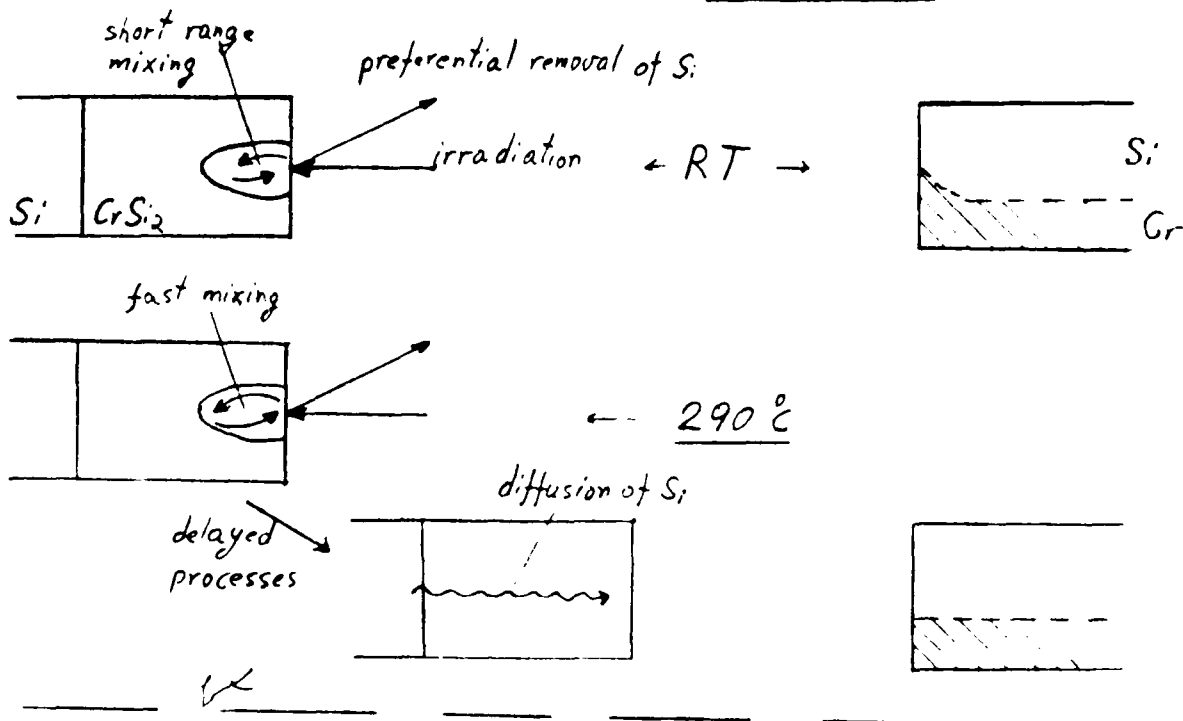


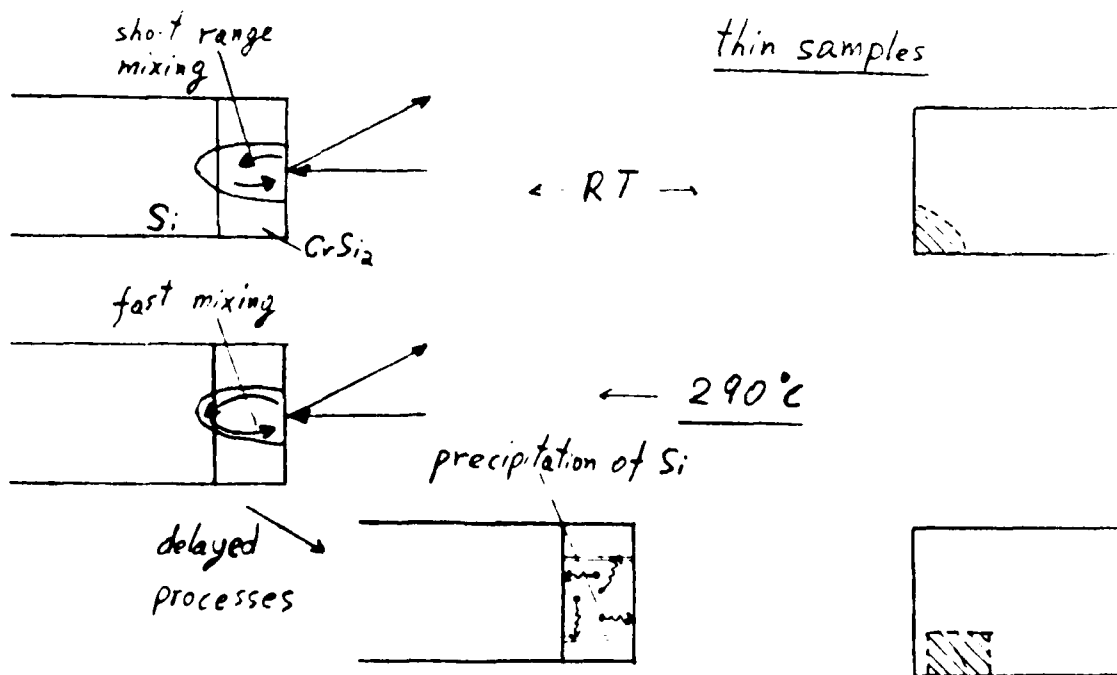
Fig.

Schematic description of processes and final compositions

thick samples



thin samples

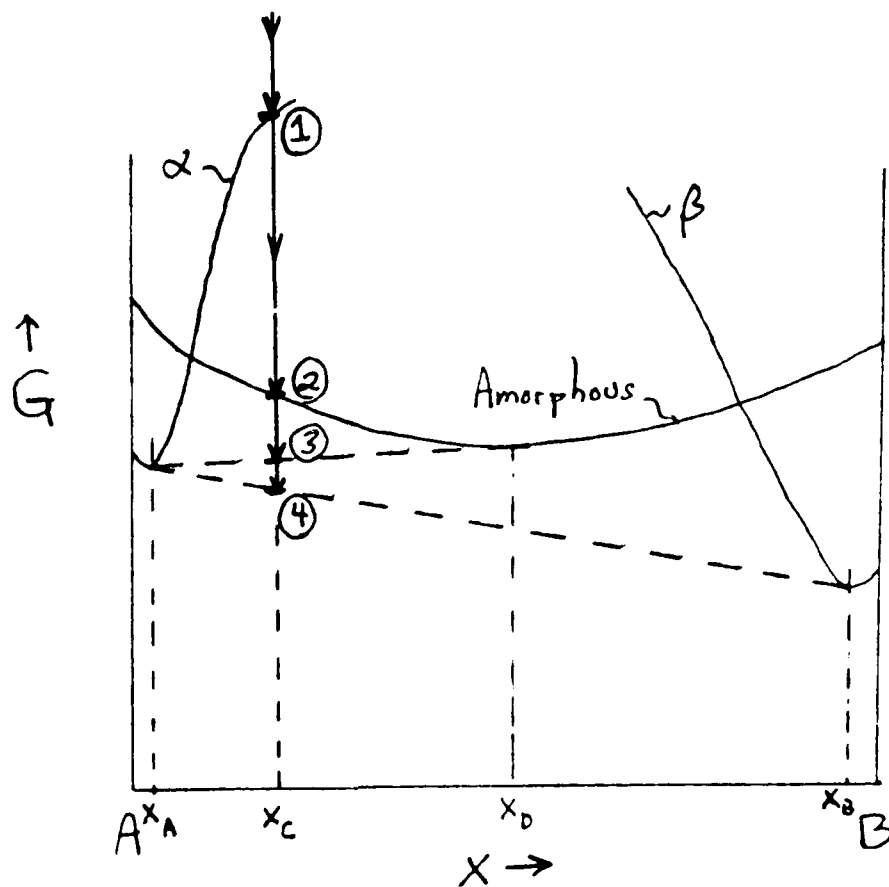


USE OF FREE ENERGY DIAGRAMS TO INTERPRET
ION BEAM MIXING DATA

W. L. Johnson

W. M. Keck Laboratory of Engineering Materials
California Institute of Technology

The interpretation of ion mixing results involves the combination of thermodynamic and kinetic concepts. The use of thermodynamic concepts implies that local regions in the vicinity of a cascade achieve some form of metastable equilibrium during the relaxation period following prompt cascade events. This implies that within these local regions, certain thermodynamic variables have well defined averages (e.g. temperature, composition, etc.) while other variables (e.g. long range order) are constrained to assume non-equilibrium values by the kinetic restrictions imposed during the relaxation process following the prompt cascade events. In order to describe the metastable thermodynamics, one can use free energy diagrams.¹⁻³ The diagrams describe both equilibrium and metastable equilibrium states. For example, the schematic figure following describes a simple binary eutectic alloy such as Au-Si at low temperatures. The curves α - and β - represent terminal solutions while the curve labeled Amorphous represents an under cooled liquid alloy. The lower horizontal dashed line is the common tangent of the α - and β - curves and represents the two-phase α - β equilibrium state between the terminal solubility limits X_A and X_B . The upper horizontal dashed line represents a two-phase metastable



equilibrium of α -solution and amorphous alloy. Curves α - and β - represent single phase metastable extended solutions between compositions X_A and X_B . The curve labeled amorphous represents another single phase metastable state. The diagram provides a direct measure of the free energy differences between the equilibrium and various metastable states. The downward vertical arrows represent various possible steps in the relaxation behavior of a locally excited region in the vicinity of a cascade. The local region of average composition X_C relaxes from a very high energy state downward into several possible final states. The possible final states are in order of decreasing free energy: 1) single phase α , 2) single phase amorphous, 3) two-phase α (composition $\sim X_A$) and amorphous (composition X_D), 4) two-phase α (composition X_A) and β (composition X_B). We notice that relaxation processes lead to final states of two types.

States (1) and (2) are compositionally homogeneous. We say that the reaction $1 \rightarrow 2$ is polymorphic (involving no composition changes). Reactions $2 \rightarrow 3$ and $3 \rightarrow 4$ involve compositional segregation. The time required for nucleation of polymorphic transformations should scale with the number of atoms in a critical nucleus of the new phase. For crystalline phases with large complex unit cells (e.g. σ -phase, μ -phase etc.) this time will tend to be longer than for simpler phases (e.g. Cs-Cl type) with small unit cells since critical nuclei sizes will tend to scale with unit cell sizes. The kinetic restrictions during relaxation following cascade events should thus favor polymorphic reactions into simple byproduct phases. Compositionally segregated final states (3 and 4 above) require longer nucleation and growth times than polymorphic final states since atoms in the nuclei must not only order but differentiate compositionally within the nucleus of each new phase. Such processes require times which scale roughly with the square of the number atoms in a critical nucleus of the new phase. The time scales for nucleation of a segregated state will thus tend to be far larger than those for polymorphic reactions. We can summarize by saying that ion mixing should most readily produce polymorphic final states of simple crystal structure (or no crystal structure, i.e. amorphous). Formation of complex crystalline final states with large unit cells or compositionally segregated final states should be suppressed during relaxation following prompt events in cascades. Together with free energy diagrams, these "rules" should allow one to predict the preferred final states arising following ion mixing of binary layers or irradiation of binary alloys. The above summary is brief, a more detailed discussion will be published shortly.

References on free energy diagram

1. R. A. Swalin, Thermodynamics of Solids, (John Wiley & Sons, New York, 1962) see especially Chapters 9, 10, 11.
2. A. R. Miedema, "The Heats of Formation of Alloys", Phillips Tech. Rev., 36, 217 (1976).
3. L. Kaufman and H. Bernstein, Computer Calculations of Phase Diagrams, (Academic Press, New York, 1970) Chapters 3 and 4.

AD P 00 1657

"Ion Mixing and Phase Diagrams"

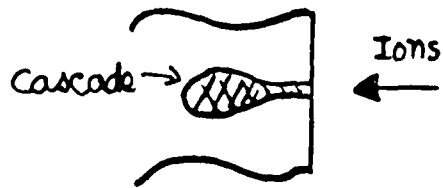
S. S. Lau
University of California, San Diego
La Jolla, California 92093

B. X. Liu, M-A. Nicolet and W. I. Johnson
California Institute of Technology
Pasadena, California 91125

Interactions induced by ion irradiation are generally considered to be non-equilibrium processes, whereas phase diagrams are determined by phase equilibria. These two entities are seemingly unrelated. However, if one assumes that quasi-equilibrium conditions prevail after the prompt events, subsequent reactions are driven toward equilibrium by thermodynamical forces. Under this assumption, ion-induced reactions are related to equilibrium and therefore to phase diagrams. This relationship can be seen in the similarity that exists in thin films between reactions induced by ion irradiation and reactions induced by thermal annealing. In the latter case, phase diagrams have been used to predict the phase sequence of stable compound formation, notably so in cases of silicide formation.

Ion-induced mixing not only can lead to stable compound formation, but also to metastable alloy formation. In some metal-metal systems, terminal solubilities can be greatly extended by ion mixing. In other cases, where the two constituents of the system have different crystal structures,

extension of terminal solubility from both sides of the phase-diagram eventually becomes structurally incompatible and a glassy (amorphous) mixture can form. The composition range where this bifurcation is likely to occur is in the two-phase regions of the phase diagram. These concepts are potentially useful guides in selecting metal pairs that form metallic glasses by ion mixing. In this report, phenomenological correlation between stable (and metastable) phase formation and phase diagram is discussed in terms of recent experimental data.



Prompt events

Displacement of atoms \approx Random
 No correlation with phase diagrams is expected

Relaxation



Delay Effects

High Temp. & Pressure in local region
 If phase diagrams are pertinent \Rightarrow High pressure phase diagrams.

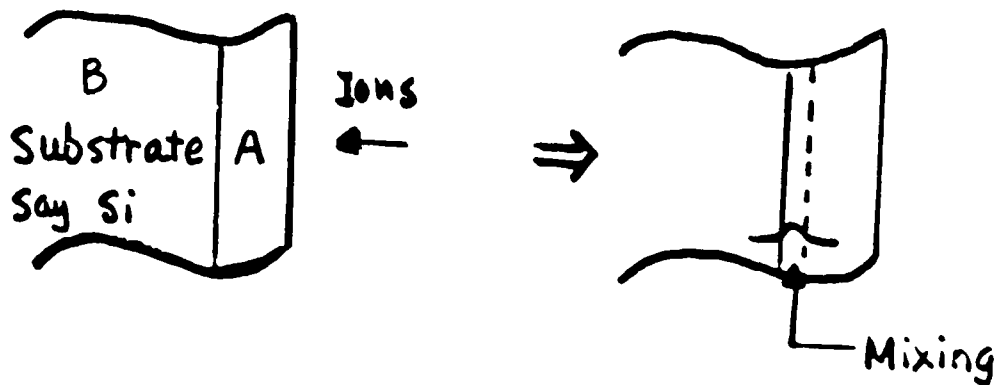
Further relaxation



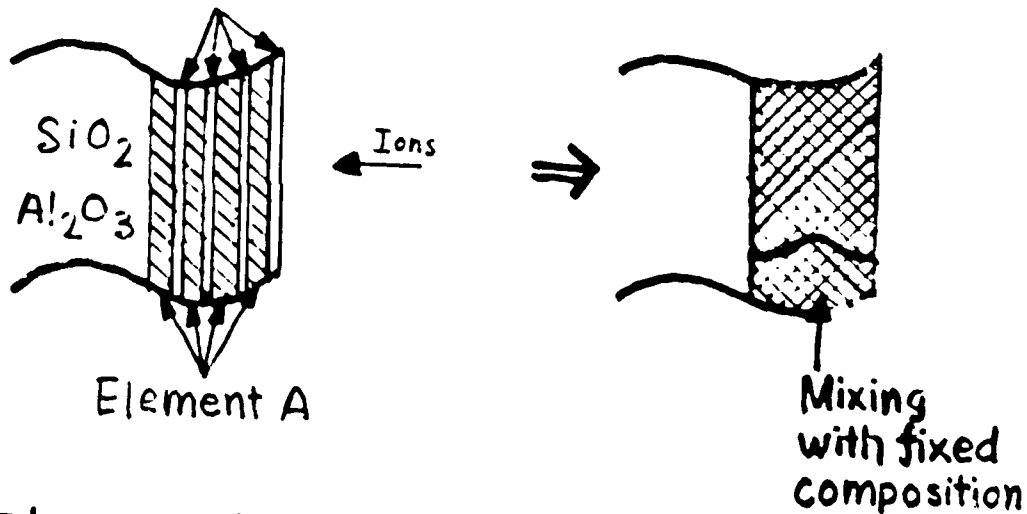
Further relaxation to normal temp. and pres. toward equilibrium.

\Rightarrow Any correlation with commonly available phase diagrams ?

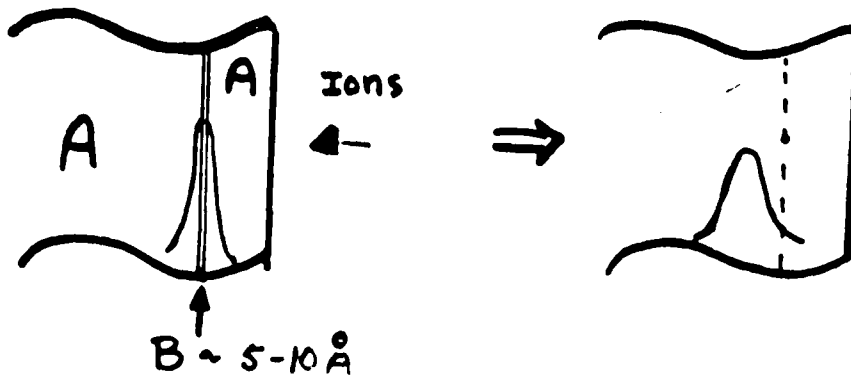
Bilayer - Unlimited supply



Multi-Layer - Limited supply



Thin Markers



BILAYER CASE

Laser Case, Very Different

TABLE I. Ion-Induced Interactions in Transition Metal/Si Systems (adopted from Ref.: B.Y.Tsaur, in Proceedings of the Symposium on Thin Film Interfaces and Interactions, J. E. E. Badlin and J. M. Pate, Eds., (The Electrochemical Society, Princeton, 1983), Vol. 2, p. 205).

Metal/Si	Ions	Compounds Observed		Phase Formed by Thermal Annealing
		Composition	Phase	
Ti/Si	N ⁺ , B ⁺	Ti ₅ Si ₃	-	TiSi ₂
Ti/Si	Ar ⁺ , Kr ⁺ , Xe ⁺	TiSi ₂	-	TiSi ₂
V/Si	Ar ⁺ , Kr ⁺ , Xe ⁺	VSi ₂	-	VSi ₂
Cr/Si	Ar ⁺ , Kr ⁺ , Xe ⁺	CrSi ₂	-	CrSi ₂
Fe/Si	Ar ⁺ , Kr ⁺ , Xe ⁺	FeSi	-	FeSi
Co/Si	Ar ⁺ , Kr ⁺ , Xe ⁺	Co ₂ Si	Co ₂ Si*	Co ₂ Si
Ni/Si	Ar ⁺ , Kr ⁺ , Xe ⁺	Ni ₂ Si	Ni ₂ Si*	Ni ₂ Si
Nb/Si	Ar ⁺	NbSi ₂	NbSi ₂ **	NbSi ₂
Nb/Si	Si ⁺	NbSi ₂	NbSi ₂ †	NbSi ₂
		Nb ₅ Si ₃	Nb ₅ Si ₃ ††	NbSi ₂
Pd/Si	Ar ⁺ , Kr ⁺ , Xe ⁺	Pd ₂ Si	Pd ₂ Si	Pd ₂ Si
Hf/Si	Ar ⁺ , Kr ⁺ , Xe ⁺	HfSi	-	HfSi
Pt/Si	Ar ⁺ , Kr ⁺ , Xe ⁺	Pt ₂ Si	Pt ₂ Si	Pt ₂ Si
W/Mo/Si	As ⁺	WSi ₂ /MoSi ₂		WSi ₂ /MoSi ₂
Mo/Si	As ⁺ , Ge ⁺	MoSi ₂		MoSi ₂
Nb/Si	As ⁺ , Ge ⁺	NbSi ₂		NbSi ₂

FOR TRANSITION METAL-SI SYSTEMS, THE FIRST PHASE FORMED IS THE SAME FOR ION MIXING AND THERMAL ANNEALING.

∴ IM ↔ THERMAL ANNEALING

NOW, IS THERE A CORRELATION BETWEEN THERMALLY INDUCED PHASE AND PHASE DIAGRAMS?

YES. VIA THE WALSER AND BENÉ RULE.

THE WALSER AND BENÉ RULE STATES:

"THE FIRST PHASE FORMED IS THE HIGHEST CONGRUENTLY MELTING COMPOUND NEAR THE LOWEST EUTECTIC COMPOSITION."

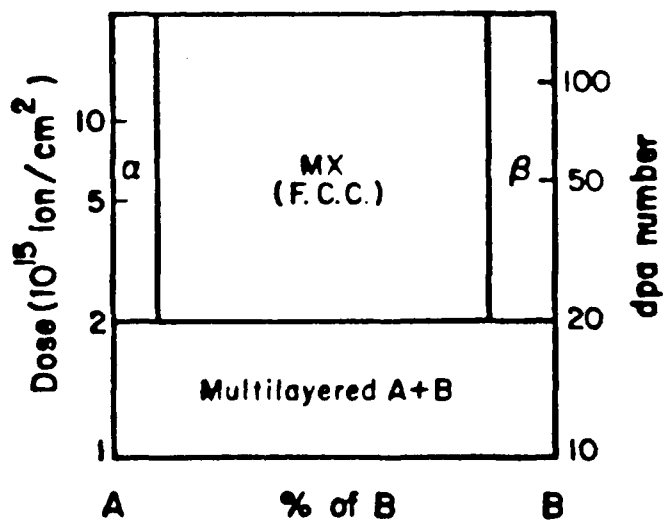
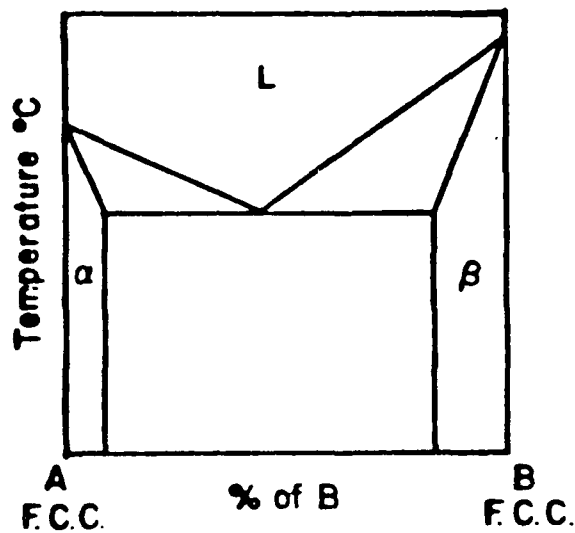
EXAMPLE: PT_2SI IS THE FIRST PHASE FORMED IN PT-SI SYSTEM.

NI_2SI IS THE FIRST PHASE FORMED IN NI-SI SYSTEM.

∴ FOR COMPOUND FORMING TRANSITION METAL-SI SYSTEMS (BILAYER - UNLIMITED SUPPLY)

IM ↔ THERMAL ANNEALING ↔ PHASE DIAGRAM
↑ CORRELATES ↑

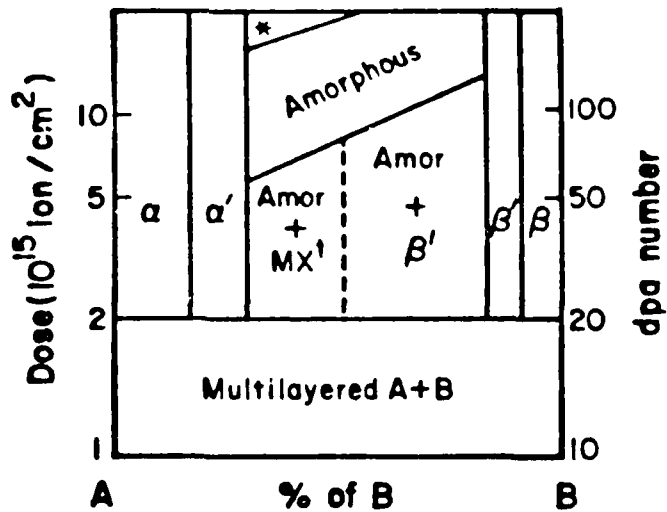
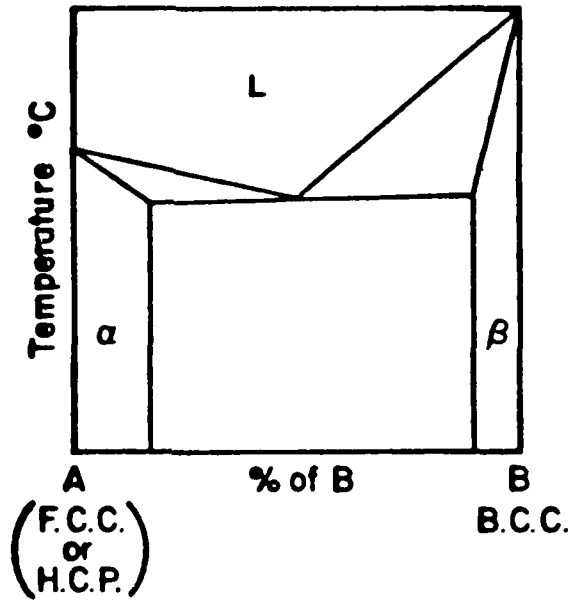
NEED METAL-METAL EXPERIMENTAL RESULTS TO CONFIRM THIS CORRELATION!



CU-AG
 ~ AU-NI

STRUCTURAL DIFFERENCE RULE: TO MAKE METALLIC GLASS
IN BINARY SYSTEM

- (I) DEPENDS ONLY ON CRYSTAL STRUCTURES OF A & B
- (II) NOT ON ELECTRONEGATIVITY
- (III) NOT ON ATOMIC SIZE



* sometime amorphous phase dissociates upon relatively high dose irradiation.

† MX is of h.c.p. structure but is different from the H.C.P metal A in size.

SUMMARY

- 1) GENERALLY SPEAKING, IF PHASE DIAGRAMS SHOW IMMISCIBILITY
→ DIFFICULT TO MIX BY IONS (I.E. CU-W)

- 2) BILAYER - UNLIMITED SUPPLY
FOR METAL-SI SYSTEMS, IM ↔ PHASE DIAGRAM
VIA
WALSER AND BENÉ RULE
NEED METAL-METAL DATA

- 3) MULTILAYERS - LIMITED SUPPLY
METALLIC GLASS → CHOSE BINARY SYSTEMS WITH
DIFFERENT CRYSTAL STRUCTURES.
GENERALLY SPEAKING - PREFER TWO PHASE REGIONS.

- 4) THIN MARKERS - BALLISTIC EFFECT EXPERIMENTS
COMPOUND FORMATION, THEREFORE PHASE DIAGRAM,
PLAYS A ROLE IN THE SPREAD OF THE MARKERS.



AD P 001658



"Ion-Induced Reactions in Thin Film Structures of
Al and Near-Noble Metals"

M. Nastasi, L. S. Hung and J. W. Mayer
Department of Materials Science and Engineering
Cornell University
Ithaca, New York 14853

Thin film Pd/Al, Ni/Al and Pt/Al interdigitated samples, either thermally reacted to form intermetallic compounds (Fig. 1) or left in their unreacted state, were irradiated with Xe ions to doses of 2×10^{14} to 2×10^{15} Xe ions/cm². Only crystalline compounds of the simplest structure, eP_2 could be identified by electron diffraction (Fig. 2). Compounds of a more complex structure than eP_2 decompose upon irradiation into an amorphous mixture and elemental constituents. Table 1 presents a summary of the results found in all three metal/Al systems (1).

When Pd/Al, Ni/Al and Pt/Al bilayers are ion reacted, RBS studies show the evolution of steps in the backscattered signals (Fig. 3). Electron diffraction studies of the mixed samples do not confirm the presence of the compound suggested by RBS. Instead it is found that the only crystalline phases formed by ion reaction are of the eP_2 structure type (Fig. 4). In the Pd/Al system, the broadening of Pd diffraction lines (Fig. 5), as a result of mixing, indicates an enhancement of the Al solubility above that found thermally. In situ TEM thermal

studies were carried out to determine the first crystal phase formed through thermal reactions (Fig. 6). Table 2, below, lists the results of this work. The fact that fair agreement exists between the first ion induced composition, determined by RBS, and the first thermally formed compound, suggests that chemical driving forces are in operation during the mixing process. But, the observation that the ion induced compositions do not correspond to crystalline phases identified by diffraction indicates that the high quench rate, non-equilibrium character of the cascade presents limitations on what phases are kinetically possible from a nucleation point of view. Figure 7 presents the equilibrium phase diagrams for the metal/Al systems studied and indicates the reactions observed in the bilayered structures.

TABLE 2
BILAYER THERMAL & ION BEAM REACTIONS

SYSTEM	FIRST THERMAL PHASE (TEM)	FIRST ION MIXED COMPOSITION (RBS)	FIRST ION MIXED CRYSTALLINE PHASE (TEM)
Pt/Al	Pt ₂ Al ₃	Pt ₄₀ Al ₆₀	α
Ni/Al	NiAl ₃	Ni ₂₅ Al ₇₅	NiAl
Pd/Al	PdAl ₄	Pd ₆₇ Al ₃₃	PdAl

Reference

- i. L. S. Hung, M. Nastasi, J. Gyulai, and J. W. Mayer, Appl. Phys. Lett. 42 (April, 1983).

Interdigitated Samples, Thermal and Ion Reactions

System	Thermal Reactions		Ion Beam Reactions 500 KeV Xe, $2 \times 10^{15} / \text{cm}^2$
	Compounds	Structure	
Pd/Al	PdAl ₃		$\alpha + \text{Al}$
	Pd ₂ Al ₃	hP ₅	PdAl(H) + α
	PdAl(H)	cP ₂	PdAl(H)
	Pd ₂ Al	oP ₁₂	$\alpha + \text{Pd}$
Ni/Al	NiAl ₃	oP ₁₆	$\alpha + \text{Al}$
	Ni ₂ Al ₃	hP ₅	NiAl + α
	NiAl	cP ₂	NiAl
Pt/Al	PtAl ₂	cF ₁₂	} α
	Pt ₂ Al ₃	hP ₅	
	Pt ₂ Al		
	Pt ₃ Al	tP ₄	

Remarks: c, h, o and t refer to cubic, hexagonal, orthorhombic and tetragonal. F and P refer to all face-centered and primitive. Numbers refer to the number of atoms in the unit cell.

Table 1. Interdigitated sample results for the Pd/Al, Ni/Al and Pt/Al systems. These results indicate that only the compounds, PdAl and NiAl, with the simplest structure, cP₂ (i.e. cesium chloride), survive Xe irradiation while compounds with a more complex structure decay into amorphous and elemental material.

ANNEAL 350°C, 1 hour

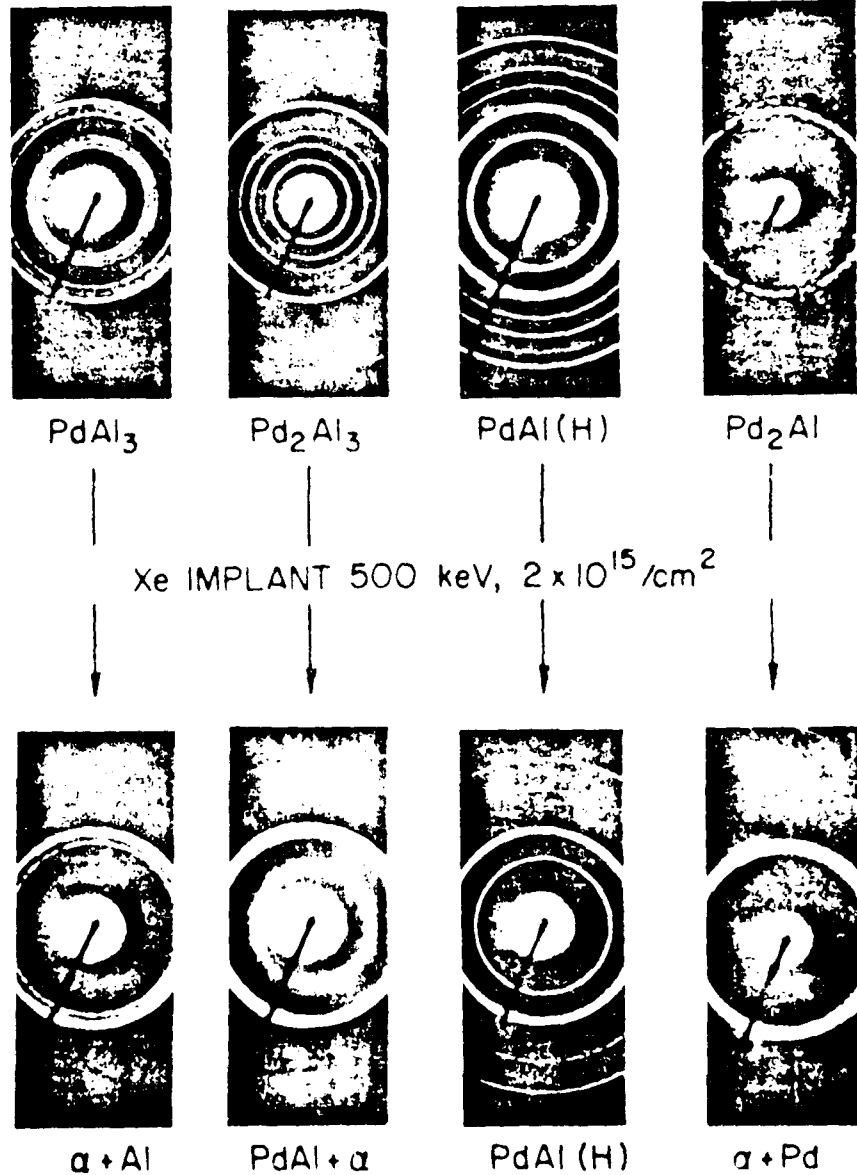
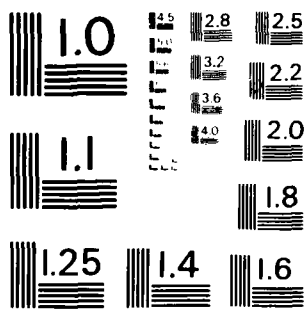


Fig. 5. Electron diffraction patterns of preannealed Pd-Al complex followed by patterns from samples implanted with 2×10^{15} Xe ions/cm² at 500 keV. Note that phases PdAl_3 and Pd_2Al become amorphous while Pd_2Al_3 decomposes into PdAl(H) plus an amorphous phase. PdAl(H) remains crystalline after implantation.



MICROCOPY RESOLUTION TEST CHART
NATIONAL BUREAU OF STANDARDS-1963-A

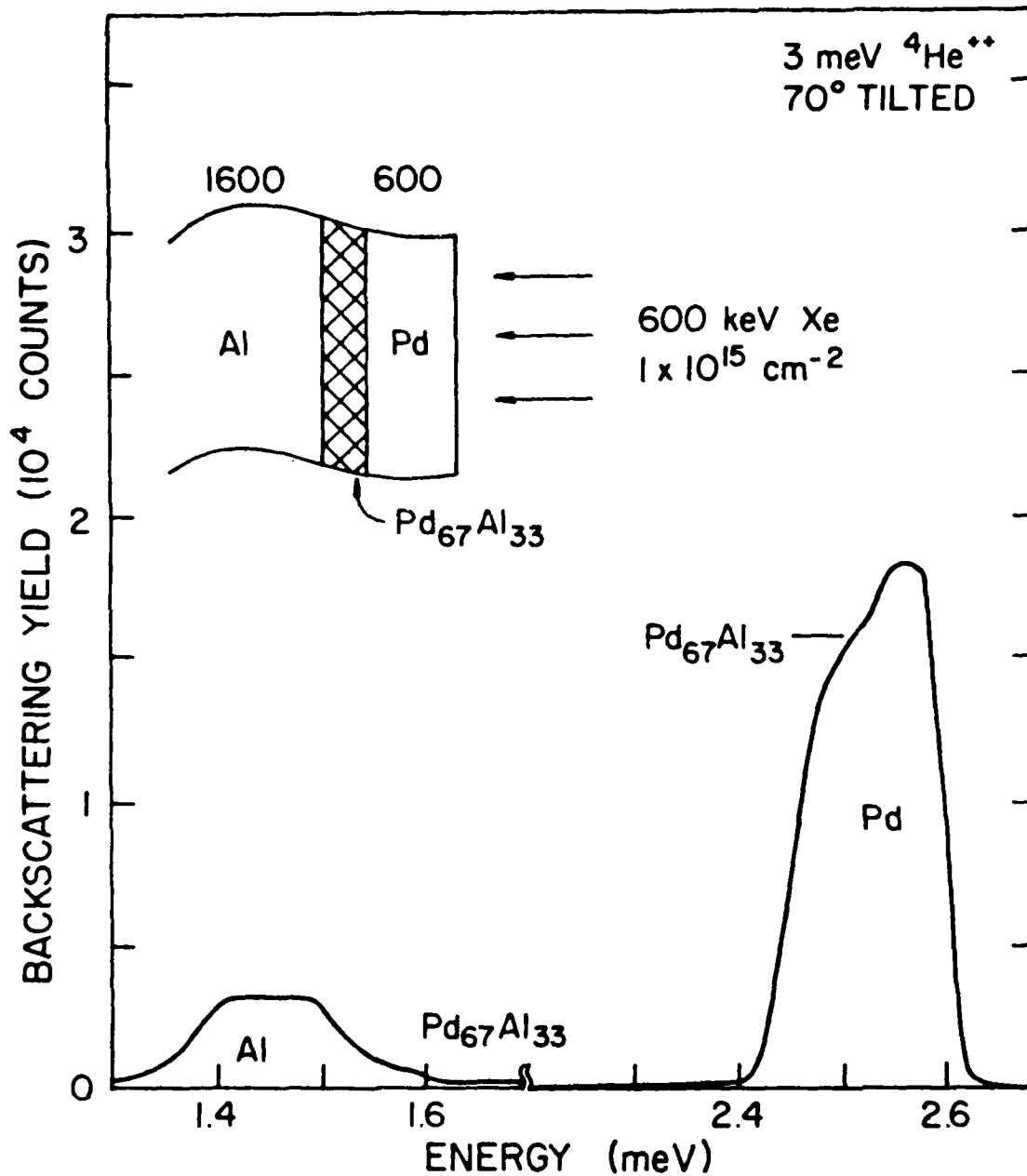


Fig. 3. RBS spectra from an ion reacted Pd/Al bilayer. Step evolution in the spectra resulted from mixing by 1×10^{15} Xe ions/cm² at 600 KeV. Step highs indicate the formation of a mixed layer with an approximate composition of $\text{Pd}_{67}\text{Al}_{33}$.

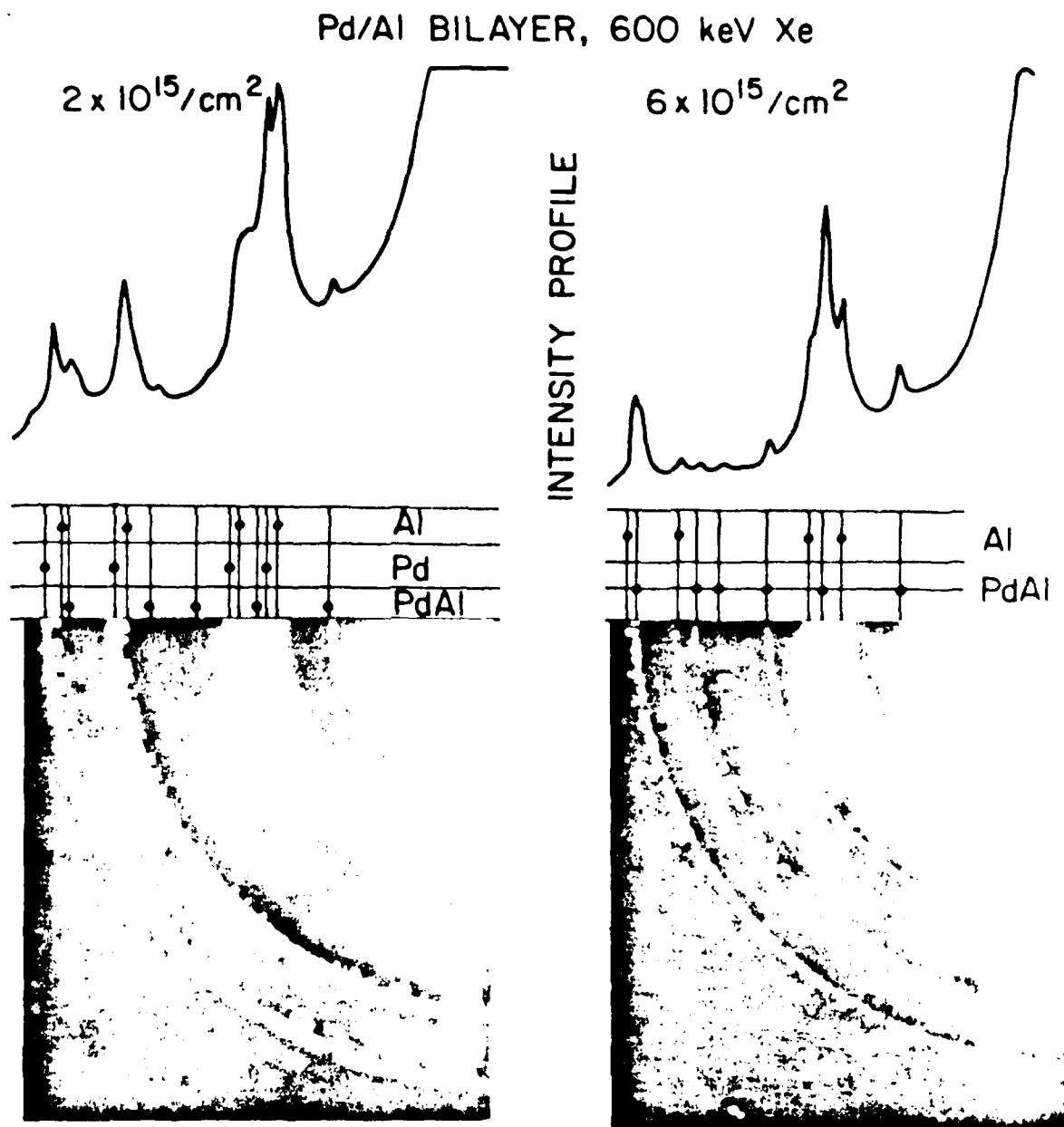
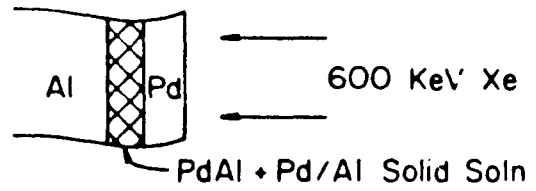


Fig. 4. Electron diffraction patterns of 600 KeV Xe reacted bilayers. Diffraction rings from samples implanted with 2×10^{15} Xe ions/cm² indicate the presence of Pd, Al and the compound PdAl. At a higher dose, 6×10^{15} /cm², complete attenuation of the elemental Pd signal is observed along with an enhancement in the PdAl signal.



	a_0 , Lattice Parameter (\AA)
Al	4.049
Pd	3.890
PdAl	3.049
Pd/Al Solid Soln	3.89-3.98

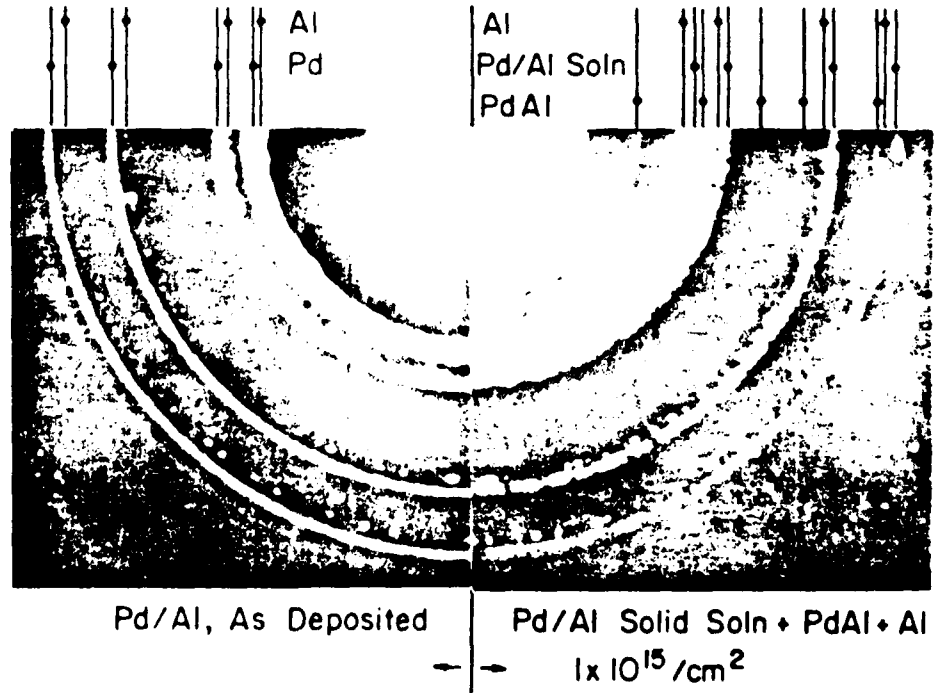


Fig. 5. Diffraction patterns from both as deposited and ion mixed Pd/Al bilayers. After mixing the diffraction lines become broader indicating the incorporation Al into the Pd lattice beyond the equilibrium solid solubility.

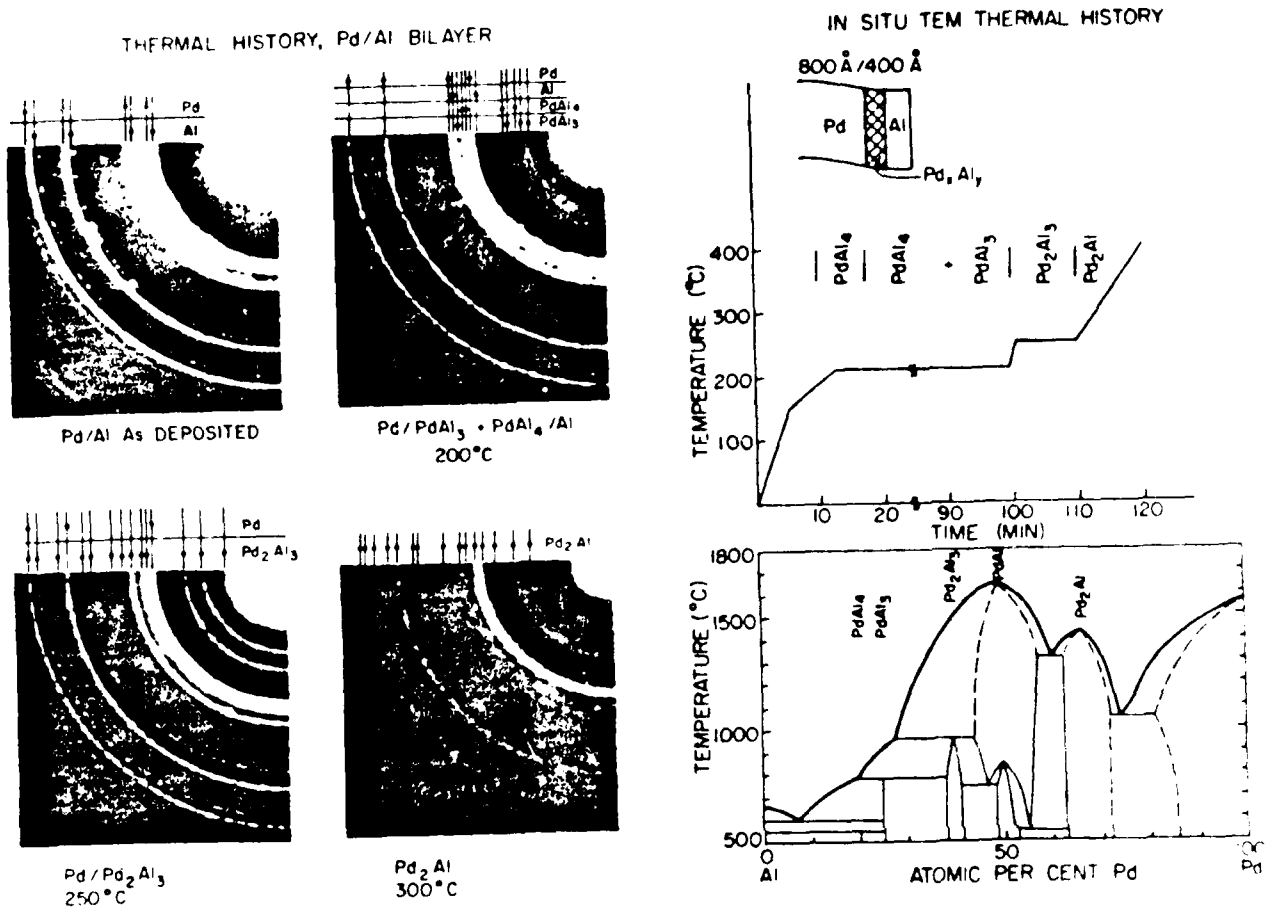


Fig. 6. Pd/Al bilayer thermal history. (a) Electron diffraction patterns obtained from in situ TEM thermal studies on Pd/Al bilayers. (b) Pd/Al phase diagram along with a thermal history curve showing the phase sequence found from the in situ thermal TEM studies. The first compound found to form thermally was PdAl₄.

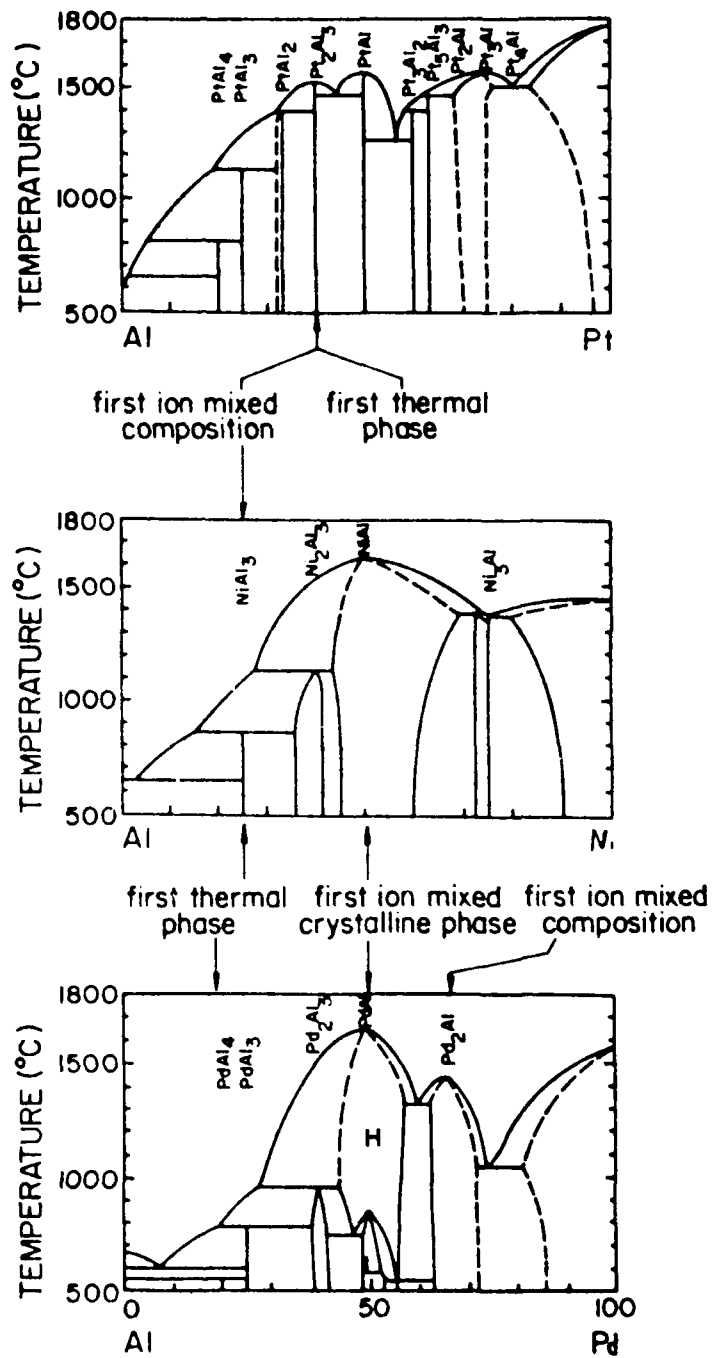


Fig. 7. Pt/Al, Ni/Al and Pd/Al phase diagrams along with the results obtained from bilayer reaction experiments.



"Ion-Beam Induced Changes in Alloy Composition"

L. E. Rehn and H. Wiedersich
Materials Science & Technology Division
Argonne National Laboratory
Argonne, Illinois 60439

AD P 00 1659

In general, point defect fluxes transport alloying components in proportions which differ from the bulk alloy concentration. Hence, even in initially homogeneous alloys, the local concentration will be altered in any region which experiences a net influx or outflow of defects. Because large numbers of point defects are introduced by each implanted ion, preferential transport of certain alloying components by persistent defect fluxes generated during ion bombardment can be highly efficient in modifying near-surface alloy compositions. This nonequilibrium, radiation-induced segregation (RIS) adds a further degree of complexity to the ion-implantation process. In a more positive vein, however, the established existence of strong RIS effects should allow certain materials modifications to be achieved more efficiently, and make possible additional types of modifications which otherwise would not be feasible⁽¹⁾.

Considerable progress has occurred over the last few years in our basic understanding of RIS. A strong correlation has been established between the sign of the lattice mismatch of the alloying components and the direction of segregation. To a great extent, elements which decrease the lattice parameter upon alloying are observed to move in the same direction as the defect

flux, while alloying components which expand the lattice are found to move in the opposite direction. The size-effect correlation lends strong support to the idea that preferential transport by interstitial fluxes generally dominates the segregation process.

Very detailed and systematic studies of RIS have been performed on Ni-Si alloys. Rate constants for the growth of radiation-induced Ni₃Si surface coatings were measured and used to determine the dose, dose-rate and temperature dependences of RIS^(2,3). Relatively simple models account quantitatively for the observed effects in terms of point-defect properties and irradiation parameters. The good quantitative agreement between the models and the experimental results provides a basis for extracting information about more general aspects of ion bombardment at elevated temperatures from the measured growth-rate constants. For example, most radiation-induced microstructural modifications (such as the coating growth) are driven by those defects that escape the parent cascade and can migrate long distances before annihilation. The RIS results show that when normalized to the same deposited damage energy, heavy ion bombardment is much less (< 5%) efficient than light-ion bombardment at producing long-range migrating defects. Thus light-ion bombardments appear advantageous for ion-beam modifications which require long-range defect migration, e.g. modifications by RIS or alloying by radiation-enhanced diffusion. This increased efficiency for production of migrating point defects can be contrasted with the observation discussed by R. S. Averback

at this workshop that heavy-ion bombardment is more efficient for mixing metal-silicide interfaces.

The mean square average diffusion distance for both vacancies and interstitials can be very large at elevated temperatures ($> \mu\text{m}'\text{s}$ in 1s at 500°C). Consequently, defects which escape the implanted region at elevated temperature can produce compositional and microstructural changes to depths which are much larger than the ion range. A particularly dramatic example of this occurs during ion sputtering of Cu-Ni alloys, where significant changes in composition are produced to depths which are three orders of magnitude greater than the implanted layer. Because of the large defect mobilities, and the fact that diffusion processes must compete with the rate of surface recession, the effects of defect production (ballistic mixing), radiation-enhanced diffusion and RIS become separated spatially during ion sputtering at elevated temperatures, and thus can be studied simultaneously in the same alloy⁽⁴⁾.

References

1. L. E. Rehn, in Metastable Materials Formation by Ion Implantation, S. T. Picraux and W. J. Choyke, Eds., (Elsevier Science Publishing Co. Inc., New York, 1982), MRS Symposia Vol. 7, pp. 17-33.
2. R. S. Averback, L. E. Rehn, W. Wagner, H. Wiedersich, and P. R. Okamoto, submitted to Phys. Rev. B15.
3. P. R. Okamoto, L. E. Rehn, and R. S. Averback, J. Nucl. Mater. 108&109, 319-330 (1982).

4. L. E. Rehn, N. Q. Lam, and H. Wiedersich, to be published.

Ion-Beam Induced Changes
in Alloy Composition
(Role of defect fluxes)

Homogeneous Alloy (200-600°C) → Demixes

Nonequilibrium Effects:

(like ion-beam mixing, they offer higher efficiency, greater flexibility but may produce unwanted effects)

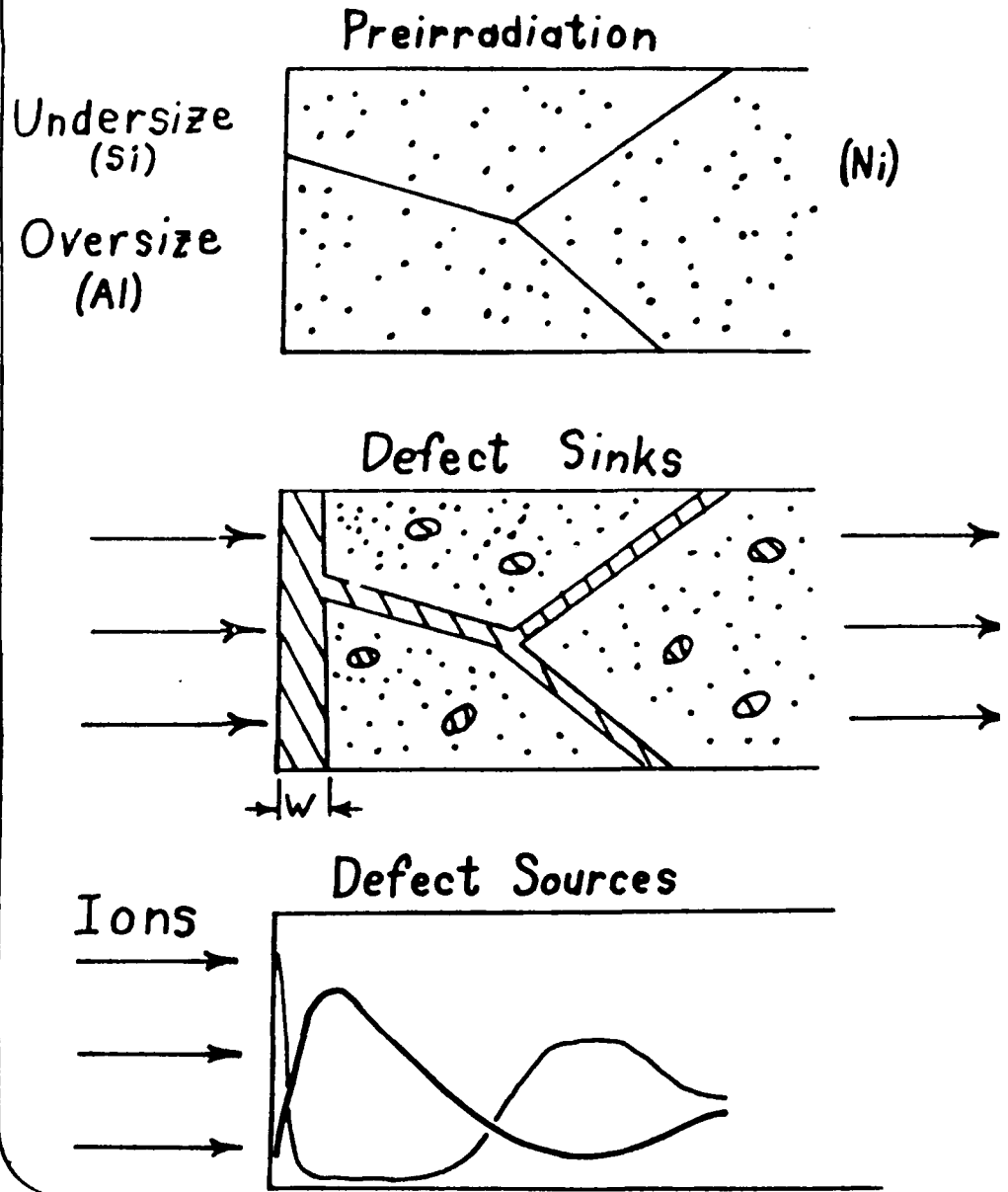
- a. can be quite large
- b. can be understood in simple terms

Talk → 2 parts

- I. Radiation-Induced Segregation-Ni(Si)
- II. Sputtering of Cu-Ni Alloys

H. Wiedersich, R. S. Averback, P. R. Okamoto

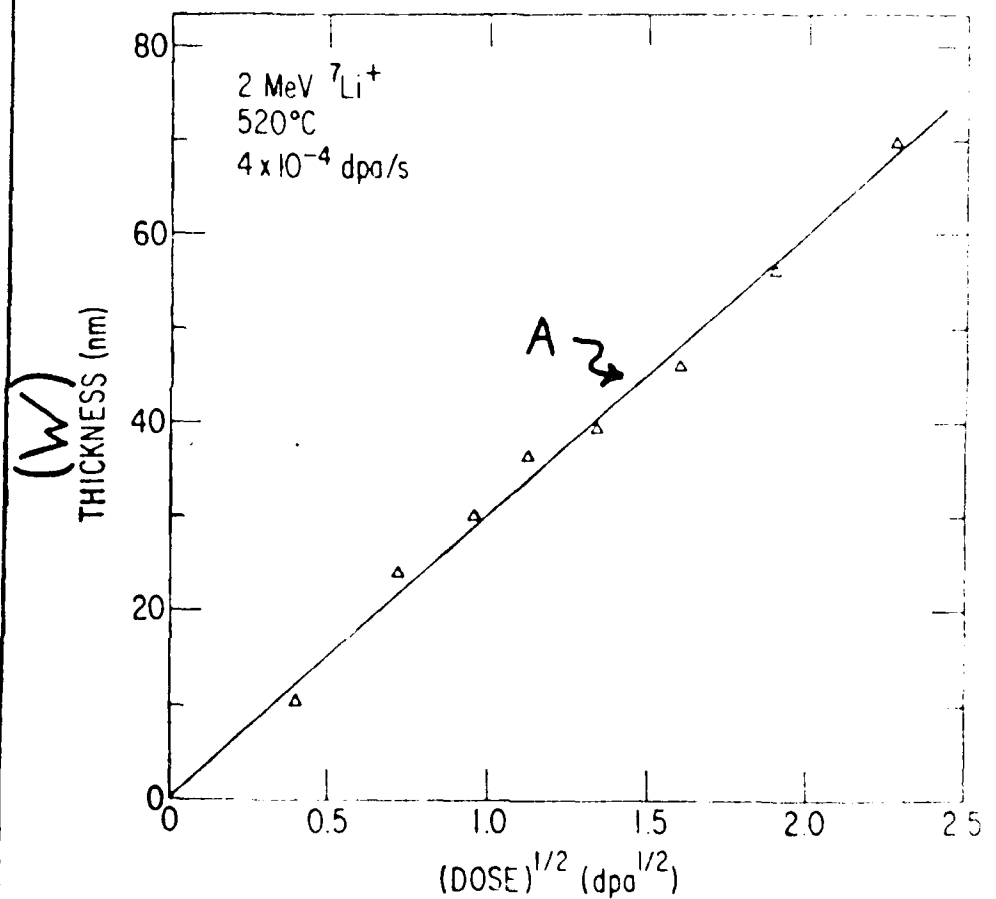
1.) Radiation-Induced Segregation



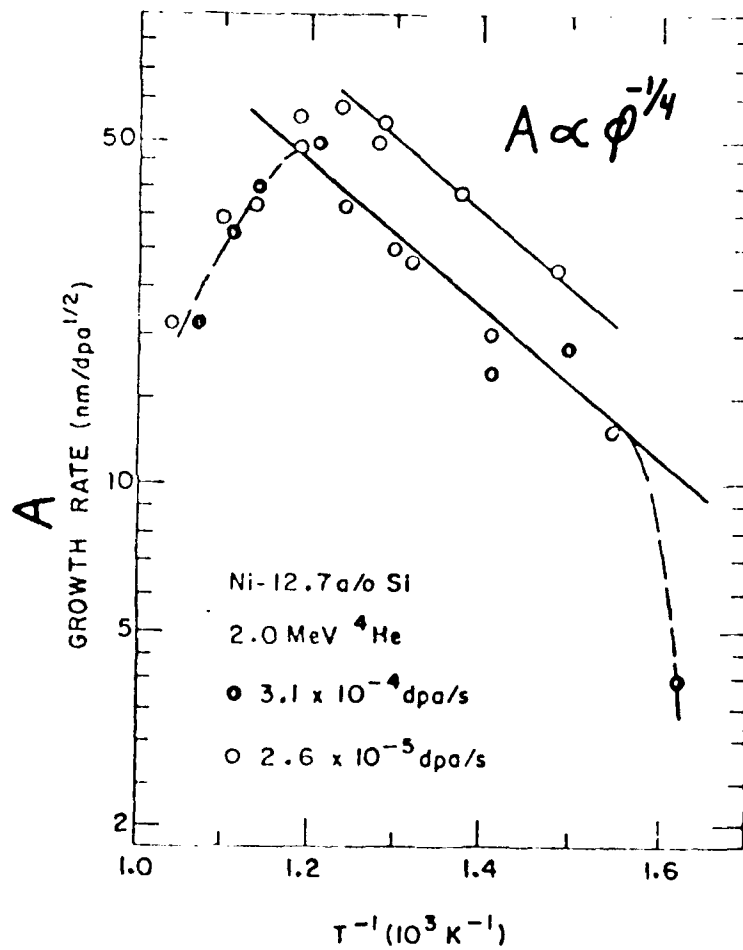
Rutherford Backscattering

$$\text{Thickness} = A (\phi t)^{1/2}$$

$A \Rightarrow$ Growth Rate Constant

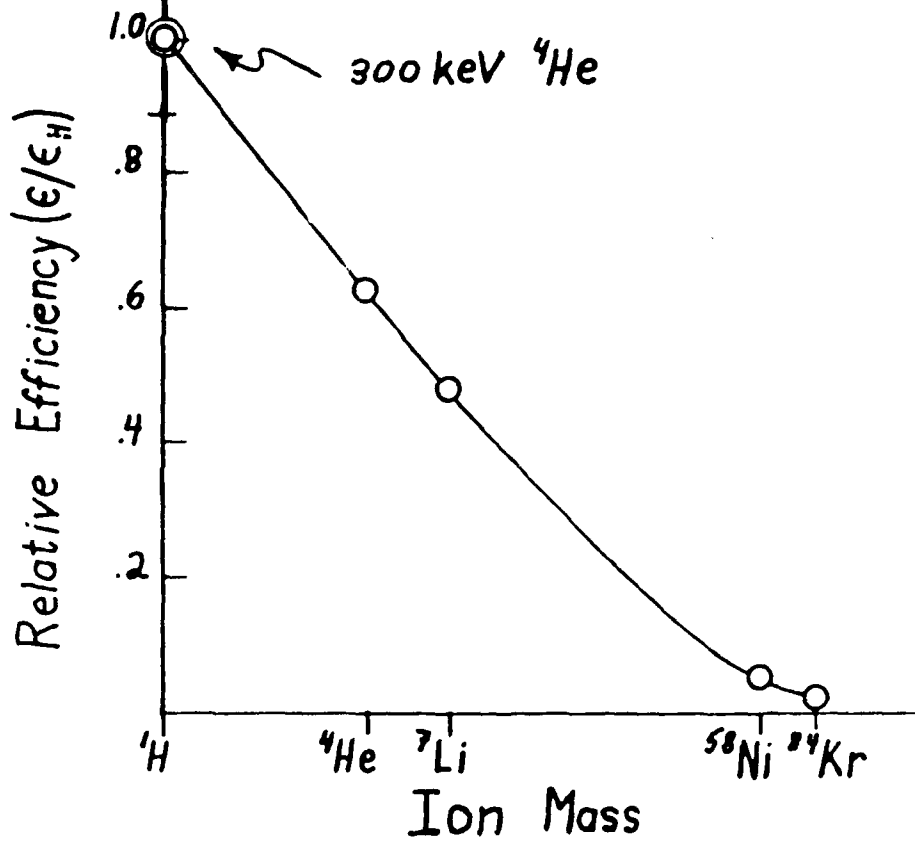


Dose-Rate Dependence



\therefore Can determine production efficiency
for long-range migrating defects!

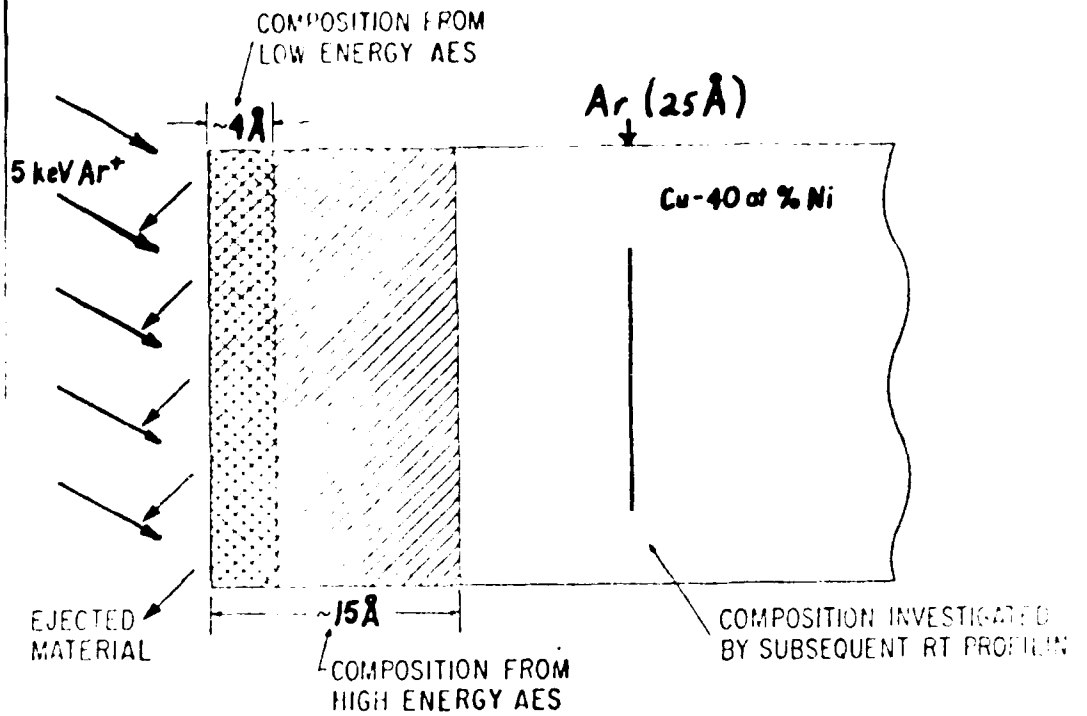
Production of Migrating Defects



Light ions (Low Energies) are advantageous
for RED/RIS Modifications

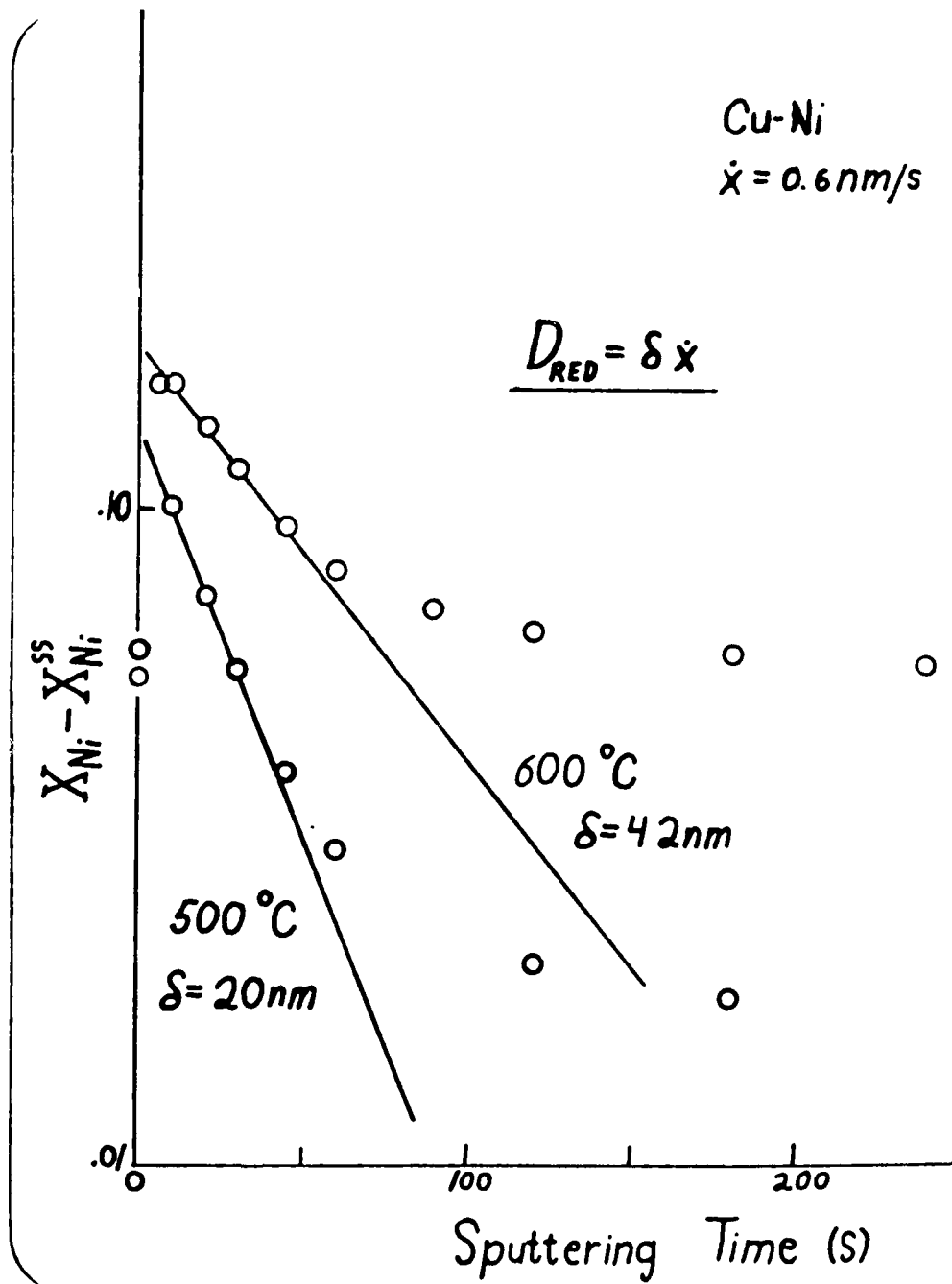
NB: Opposite to metal-silicide mixing (low-T)
R.S. Averbach

II. Sputter-Induced Changes

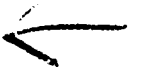
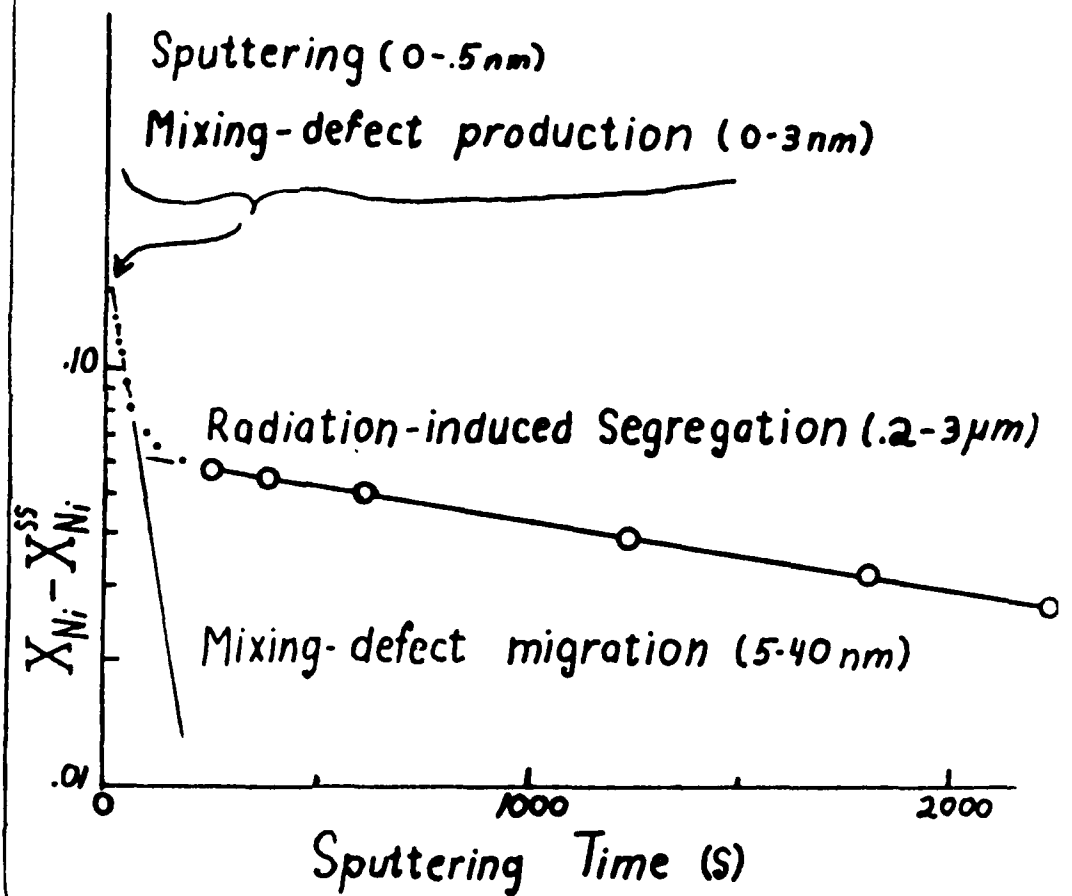


$$\bar{x} = \sqrt{4D_v t} \quad \text{for } H_v^m = 1 \text{ eV}; t = 1 \text{ s}$$

	300°C	500°C
\bar{x}	.2 μm	2.7 μm



Spatial Dependence of Dominant Effect
(At Steady State)



↖

"High Energy Heavy Ion Induced Enhanced Adhesion"

Marcus H. Mendenhall
California Institute of Technology
Pasadena, California 91125

DESCRIPTION

↘ Interfaces bombarded with ions in the electronic stopping regime ($E > 100$ keV/amu) can be bonded together quite strongly. Metal-metal, metal-semiconductor, metal-dielectric and dielectric-dielectric combinations have been successfully bonded.



ADVANTAGES OVER LOW ENERGY TECHNIQUES

- 1) The technique is universal: All tested combinations of materials show enhanced adhesion including difficult systems such as Ag on Si.
- 2) Very low beam dose required on many systems: For Au on Ta, 20 MeV Cl requires only $2 \times 10^{13}/\text{cm}^2$ ions. For Au on PTFE, $1 \times 10^{13}/\text{cm}^2$ of 1 MeV protons is sufficient.
- 3) Low damage to conductive materials - High energy heavy ion beams do not significantly sputter or disrupt metals. This allows thin optical films, for example, to be processed without major changes in optical properties.
- 4) Long Beam Range - Beam particles are implanted about 10 μm into the target, allowing fairly thick films to be bonded.

AD P 0 0 1 6 6 0

- 5) Very shallow mixing depth: No mixing has been seen at the 2 nm level on bonded systems. Any mixing occurring is expected to have much shorter range than this since ions in the electronic stopping power regime do not produce many high energy recoil particles.

DISADVANTAGE OVER LOW ENERGY TECHNIQUES

- 1) High energy ion beams require very large accelerators which are expensive and produce high radiation levels, requiring substantial shielding.

Table 1
Material Combinations Tested
for
High Energy Heavy Ion Induced
Enhanced Adhesion

Table 1 lists the various substrate, film and beam combinations we have tested for enhanced adhesion. In the dose column, numbers preceded by \approx or \leq have been measured using movable slits to define the beam shape, so the actual dose is not well known. Numbers preceded by $<$ have been tested at the dose shown, and show adhesion, but lower doses have not been tried so the threshold may be much lower. Numbers without any prefix represent values measured as described in §4.3 and should be reliable to $\sqrt{2}$. All numbers represent the dose required to pass the "Scotch Tape" test.

Substrate	Film	Beam	Dose (#/cm ²)	Comments
Si, n-type 10 Ω-cm	Au	20 MeV Cl	≈5×10 ¹⁴	Residual adhesion is very good. Unirradiated samples often pass tape test.
	Ag	20 MeV Cl	≈2×10 ¹⁵	Very low residual adhesion except when sample not rinsed in methanol after HF dip. Then, residual adhesion is near the tape threshold.
Ta	Au	107 MeV Kr	5×10 ¹²	*
	Au	87 MeV Ar	2.8×10 ¹³	*
	Au	27 MeV Ar	2×10 ¹³	*
	Au	20 MeV Cl	2.5×10 ¹³	
	Au	7.2 MeV Cl	4.5×10 ¹³	
	Au	3.2 MeV Cl	9×10 ¹³	
	Au	12 MeV F	7×10 ¹³	
	Au	3.7 MeV F	1.3×10 ¹⁴	
	Au	35 MeV O	1×10 ¹⁴	*
	Au	1 MeV He	6×10 ¹⁵	
	Au	1 MeV H	3×10 ¹⁶	Peak adhesion is very weak. Very little material is left after the tape test, but there seems to be a real threshold for none vs. what little remains.
	Ag	20 MeV Cl	≤1×10 ¹⁴	

* Berkeley runs, listed doses adjusted down from measured value by 0.1 to bring 27 MeV Ar point into line with CIT data.

Table 1
(cont'd)

Substrate	Film	Beam	Dose (#/cm ²)	Comments
	Au	107 MeV Kr	1.5×10^{13}	•
	Au	20 MeV Cl	5×10^{14}	
Fused SiO ₂	Au	12 MeV F	$> 5 \times 10^{10}$	No adhesion observed with 12 MeV F beam.
	Au	27 MeV Ar	$\approx 3 \times 10^{14}$	
	Ag	20 MeV Cl	$< 2 \times 10^{14}$	
InP p-type .001 Ω -cm	Au	20 MeV Cl	$< 5 \times 10^{14}$	
GaAs, heavily doped	Au	20 MeV Cl	$\leq 1 \times 10^{14}$	
W	Au	20 MeV Cl	$< 1 \times 10^{14}$	
Teflon®	Au	1 MeV H	$\approx 3 \times 10^{13}$	Higher doses burn substrate
Polytetrafluoroethylene	Au	1 MeV He	$\leq 1 \times 10^{14}$	
Topaz	Au	20 MeV Cl	$\approx 5 \times 10^{15}$	
Al ₂ SiO ₅ (OH,F) ₂				
Al ₂ O ₃	Pd	20 MeV Cl	$< 1 \times 10^{15}$	
	Ag	20 MeV Cl	$\leq 1 \times 10^{15}$	
Alumina/Silica/ Magnesia Glass-Ceramic	Cu	20 MeV Cl	$\leq 3 \times 10^{15}$	
Ferrite	Au	20 MeV Cl	$\approx 1 \times 10^{15}$	
I-Carbon (See §2.1.4)	Ag	20 MeV Cl	$\approx 1 \times 10^{15}$	These films seem to decompose under irradiation. The adhesion was at best weak, and where the metal peeled, the I-carbon had turned dark brown underneath. I suspect that the films were reverting to graphite (as diamond is wont to do)

Fig. 18 Comparison of Ag edges on Ag/Si stack target

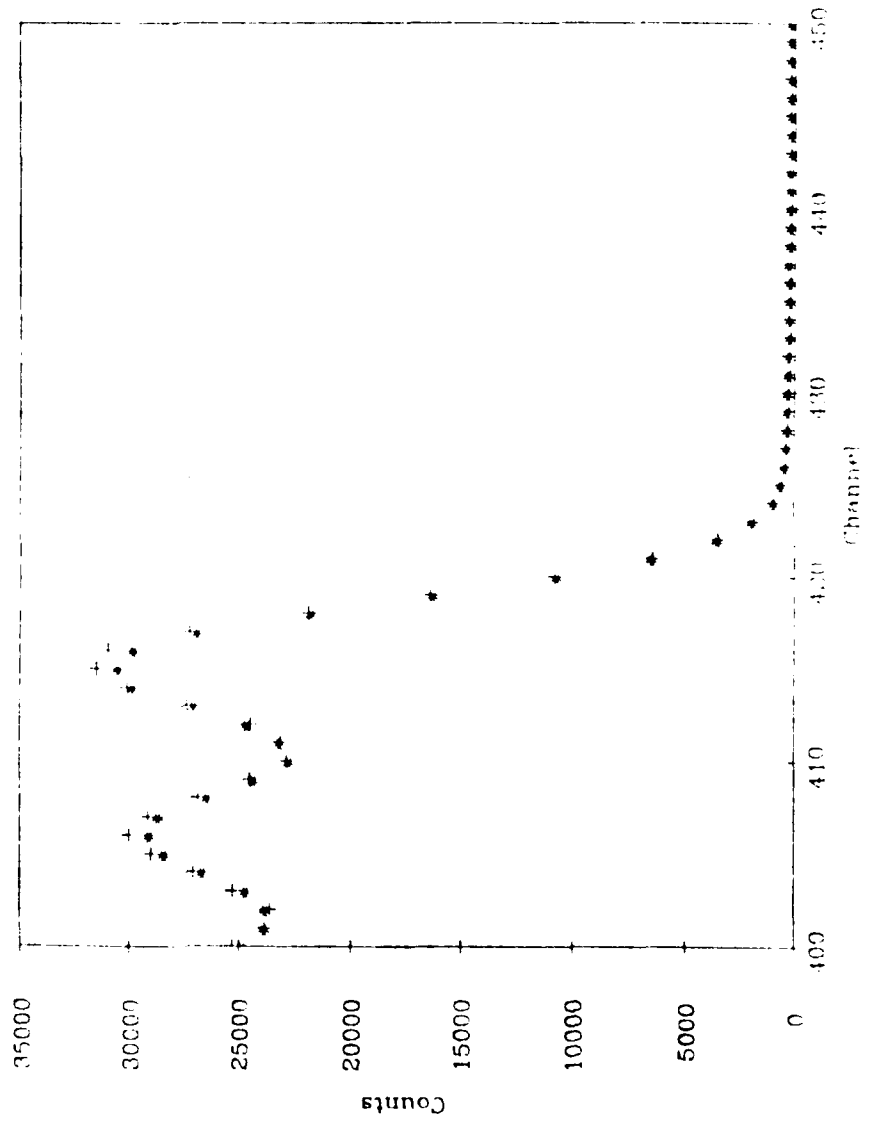


Figure 18
Expanded View of Ag Edge
on
Backscattering Spectrum
from
Multilayer Ag/Si Target
(sec §4.1.2)

This spectrum is an expansion and comparison of the high edge of the silver peak from an irradiated and unirradiated part of the target. The curve plotted with the symbol + is from the irradiated area. The curve plotted with the symbol * is from the unirradiated area. The + curve is not raw data; it has been translated along the x-axis by 1.7 channels to the right and interpolated back to integral channel numbers to remove the effects of the slight carbon buildup on the target. Note how well the edges agree; there is no visible evidence for any broadening that might be caused by mixing.

The + curve is 3-Mar-1983 run 7, interpolated

The * curve is 3-Mar-1983 run 10

Fig. 21 Beam Dose vs. dE/dx for Au on Ta

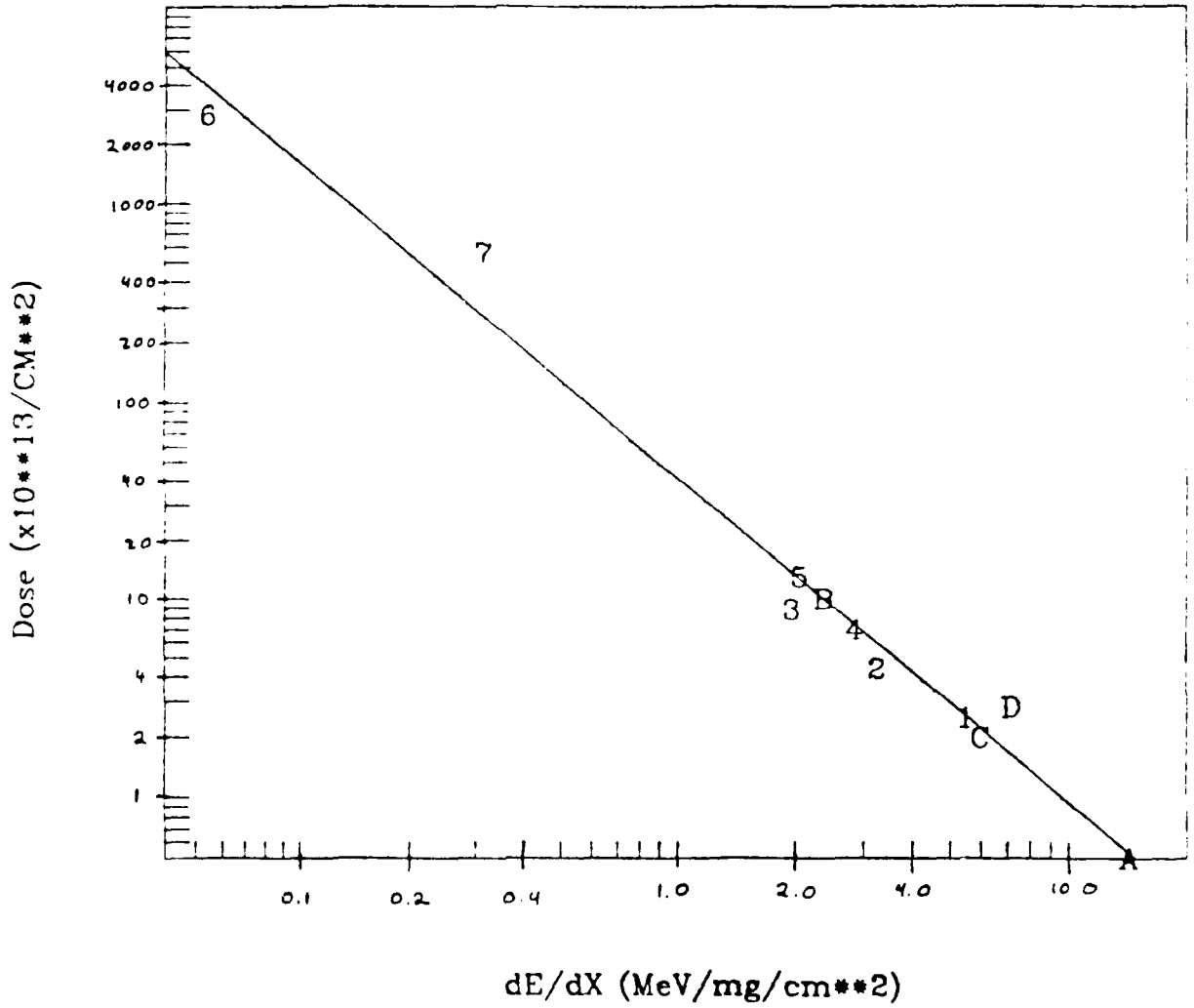


Figure 21
 Plot of Beam Dose Required to Pass Tape Test
 vs.
 dE/dx for the Ion Beam
 on Au on Ta Targets
 (see §4.3)

This plot shows the dependence of beam dose required to produce sufficient adhesion to pass the "Scotch Tape" test on the energy loss of the beam. The points plotted are

- 1 20 MeV Cl
- 2 7.2 MeV Cl
- 3 3.2 MeV Cl
- 4 12 MeV F
- 5 3.7 MeV F
- 6 1 MeV H
- 7 1 MeV He
- A 107 MeV Kr *
- B 35 MeV O *
- C 27 MeV Ar *
- D 87 MeV Ar *

and the line plotted is $Dose = 4.2 \times 10^{14} (dE/dx)^{-1.65}$. The point for protons has substantial uncertainties, since the peak adhesion for protons was very weak. However, the rest of the points should be reliable to within $\sqrt{2}$.

All points marked * above were run on the LBL 88" Cyclotron. As is described in §4.3, they have been adjusted downwards by a factor of 2 so that the 27 MeV Ar point lies on the curve from data obtained at Caltech. If the adjustment is omitted, the slope of the curve does not change significantly (since all the LBL points are internally consistent with this slope), but the multiplier for the doses increases by 15%.

III. Surface Modification-Ion Implantation and Mixing

"Ion Mixing of Cr Layers on Steel:
Effect of Impurities During Ion Mixing"

K. S. Grabowski and R. J. Colton
Naval Research Laboratory
Washington, D. C. 20375

W. K. Chan and C. R. Clayton
State University of New York
Stony Brook, New York 11974

AD P 001661

Ion bombardment under normal vacuum conditions is commonly known to deposit carbon on the target surface. It has been observed that such effects during ion mixing of Cr layers on bearing steels may encourage pitting corrosion of an ion mixed surface. Xe^+ was found to incorporate O, and Cr^+ was found to incorporate C during ion mixing of Cr films deposited on AISI 52100 steel.

To help identify the source of these contaminants and define implantation conditions sufficient to eliminate them, experimental work was undertaken using a UHV target chamber, a controlled partial pressure of ^{13}CO , and varied ion beam currents differing by about an order of magnitude.

SIMS analyses for ^{13}C incorporation following Cr^+ mixing of Cr films on AISI-M50 steel have been performed. They indicated that a relative impingement rate of gas molecules to Cr^+ ions of approximately less than 1 is necessary to prevent the incorporation of C from the vacuum during implantation.

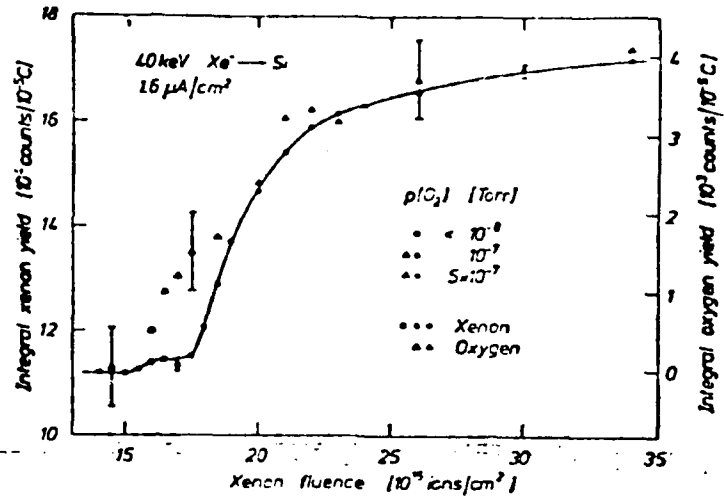
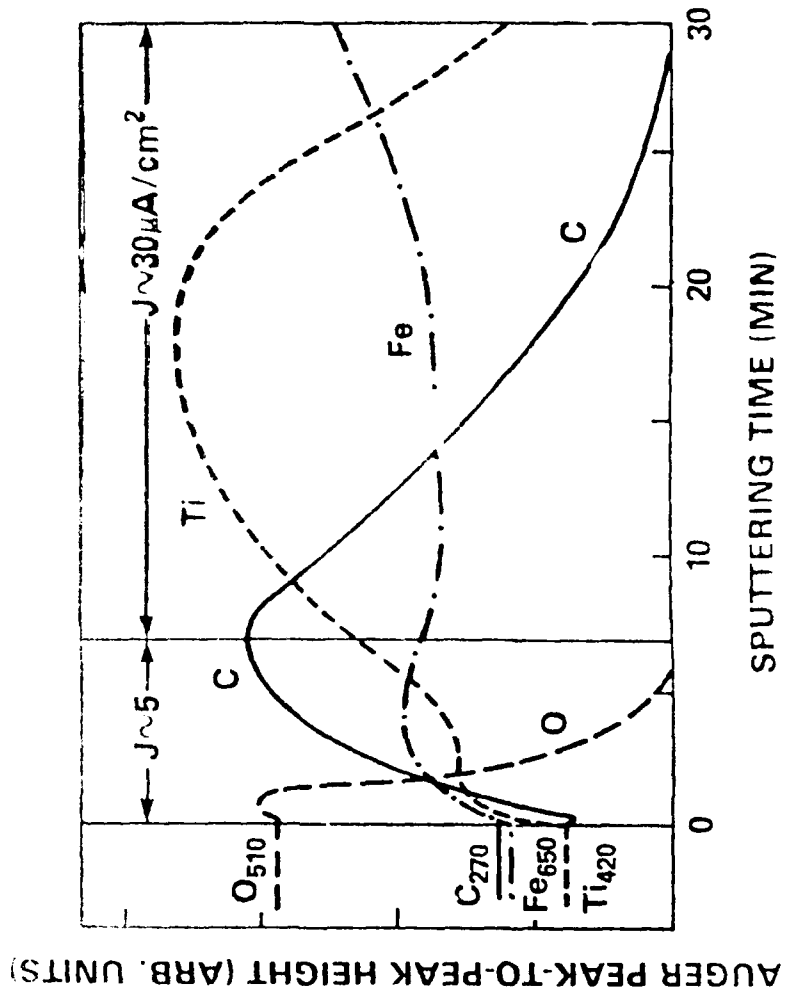


Fig. 6. Fluence dependence of oxygen recoil implantation and oxygen enhanced xenon collection in silicon.

from K. Wittmaack and P. Blank,
Ion Implantation in Semiconductors,
 Boulder (1976), p. 363.

AUGER DEPTH PROFILE OF 304 STEEL
 IMPLANTED WITH Ti ($5 \times 10^{17}/\text{cm}^2$ AT 190 keV)
 IN PRESENCE OF ^{13}CO GAS ($p \sim 4 \times 10^{-6}$ Torr)



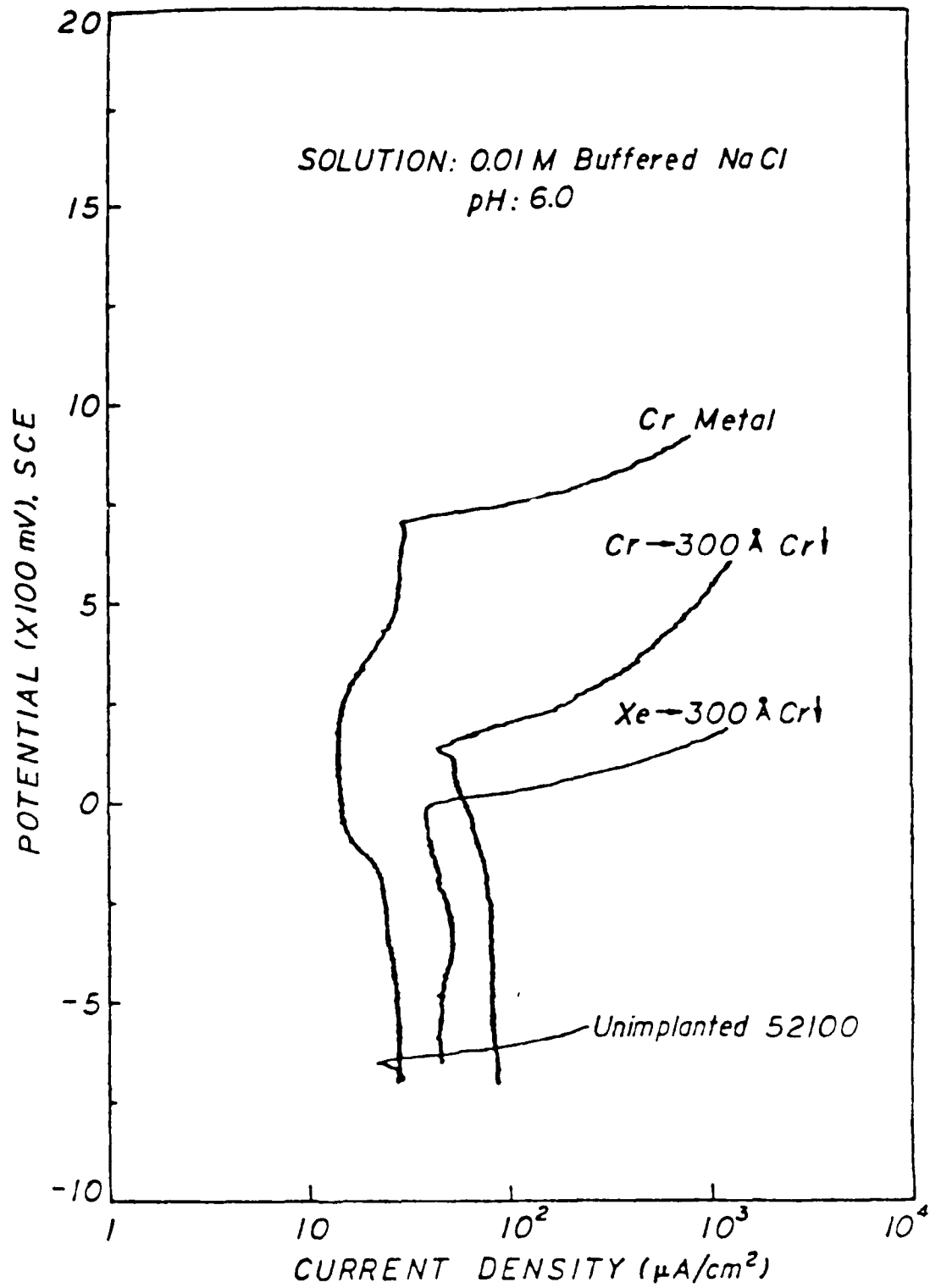


Fig. 10 Anodic polarization curves of intermix 52100 bearing steel in 0.01 M NaCl solution buffered at pH=6 with cathodic pretreatment

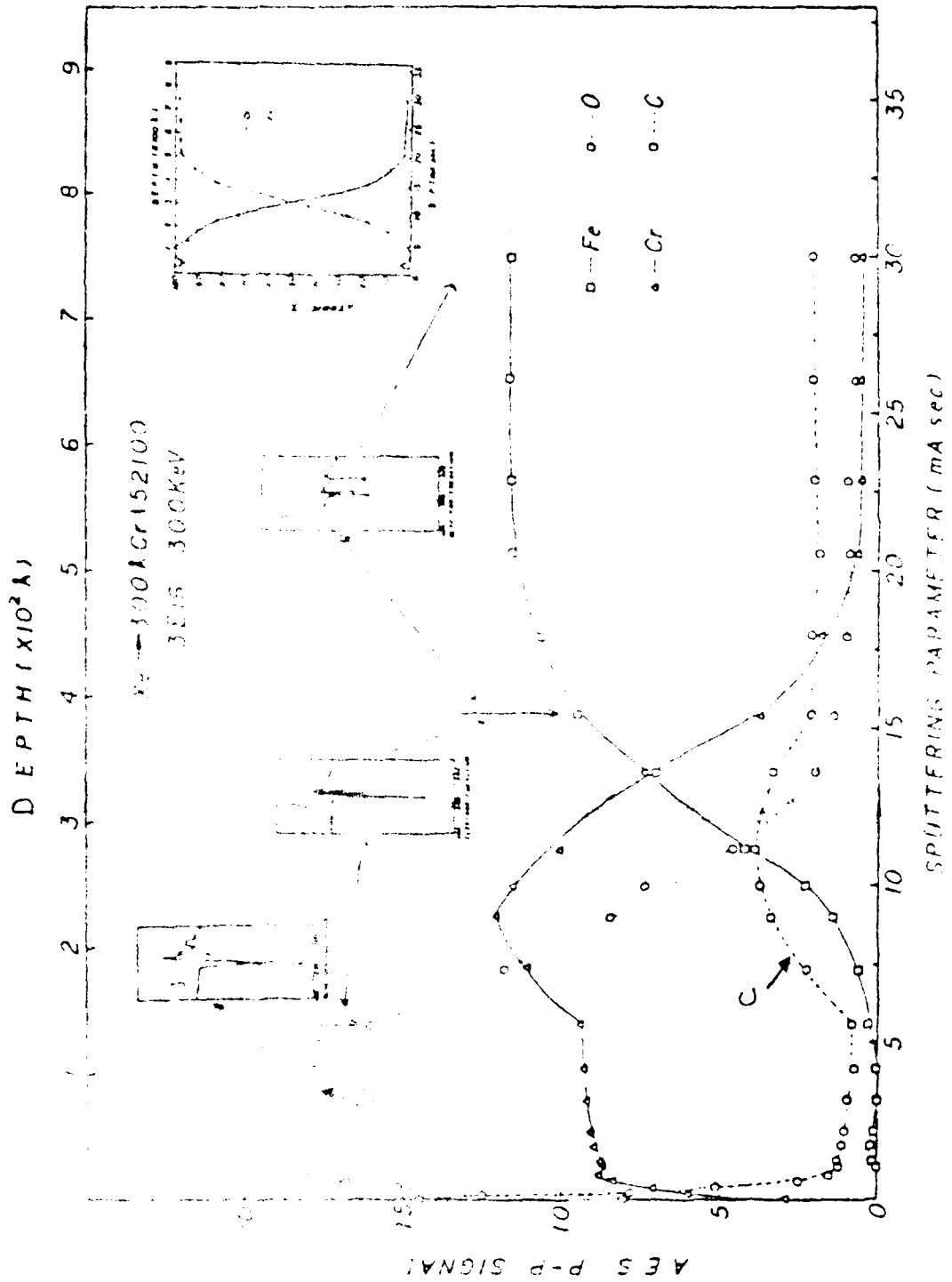


Fig. 5 Auger depth profile of Fe, Cr, and C in X₂ intercalated with 52100

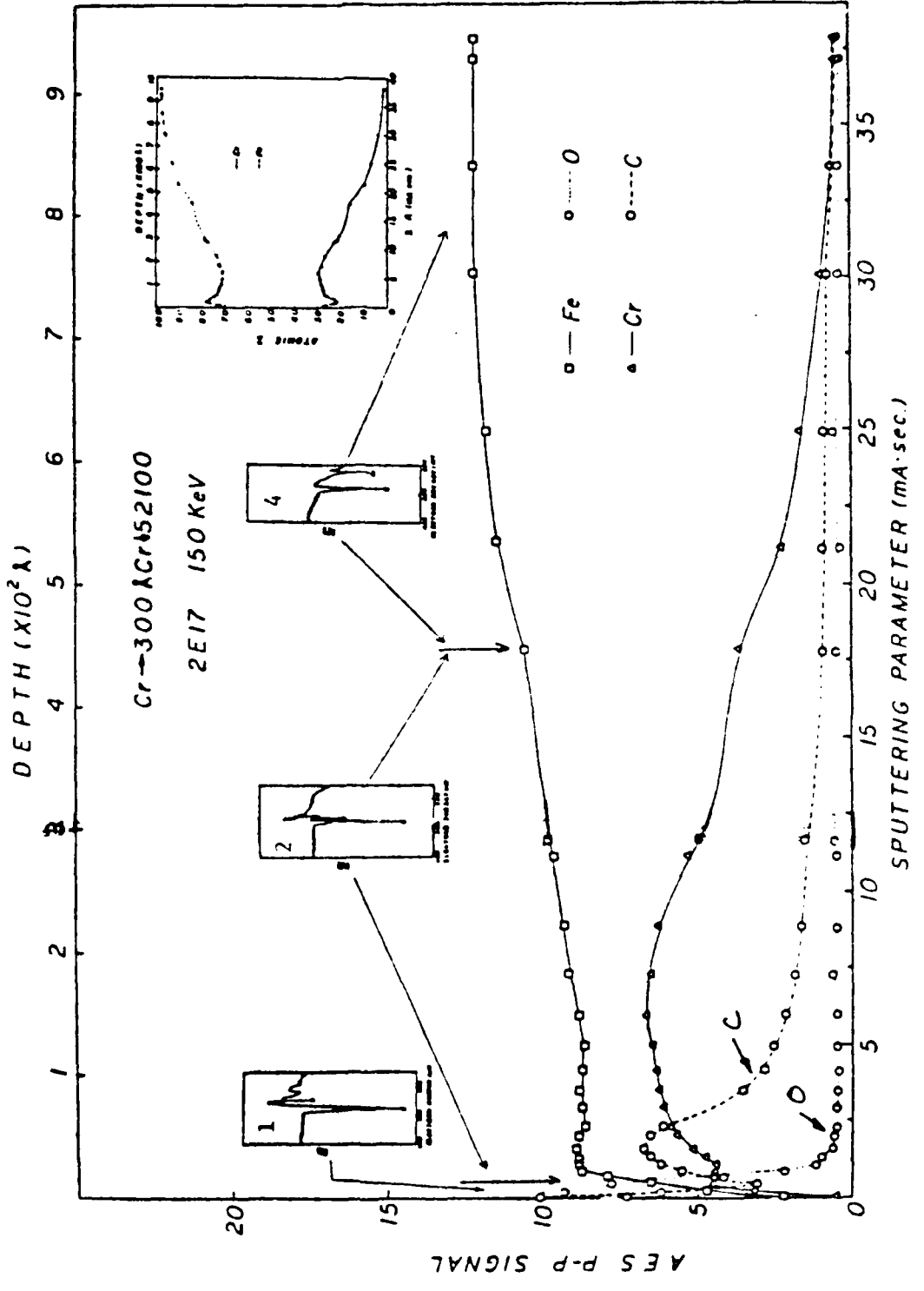


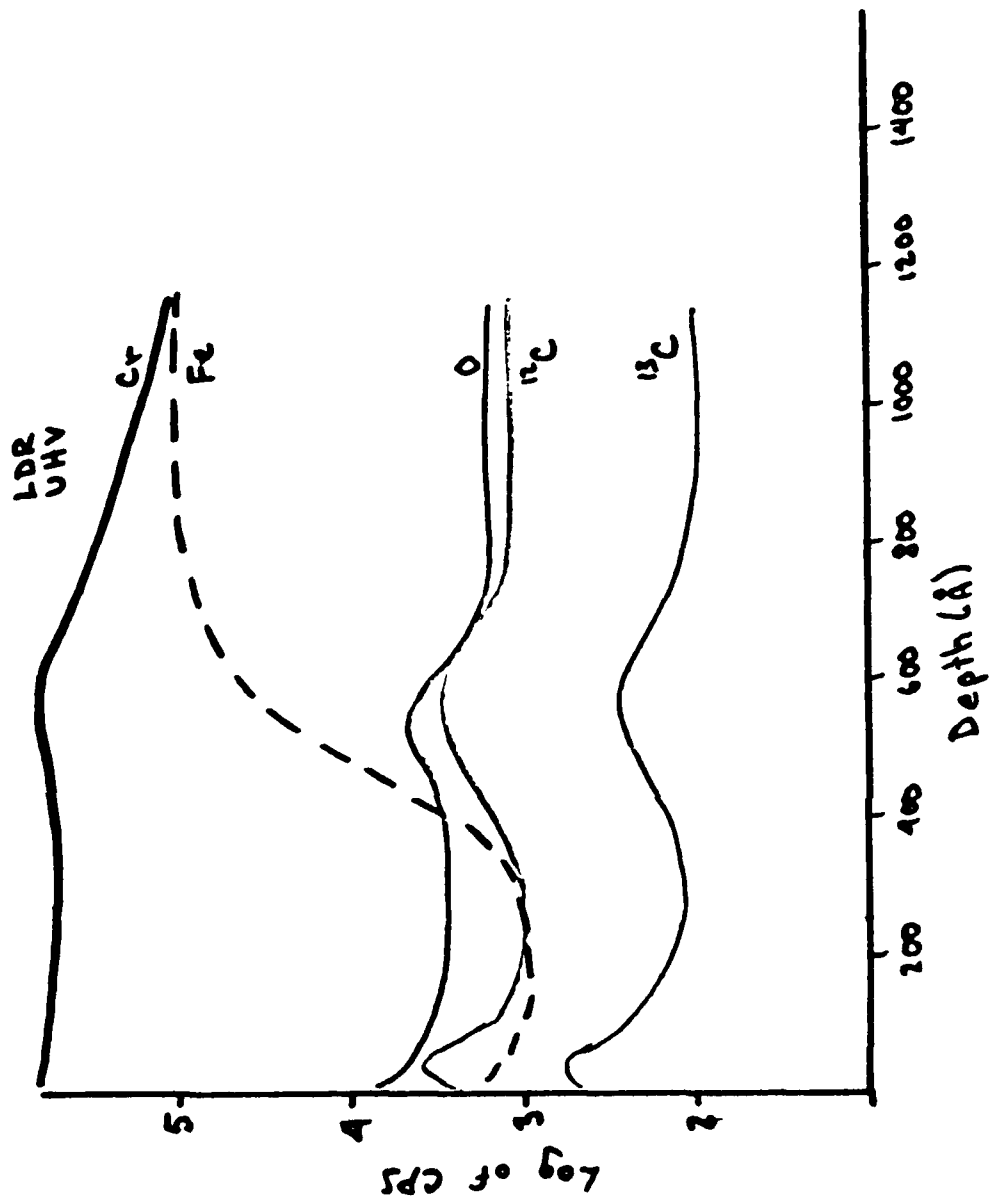
Fig. 4 Auger depth profile of Fe, Cr, O, C in Cr intermix with 52100

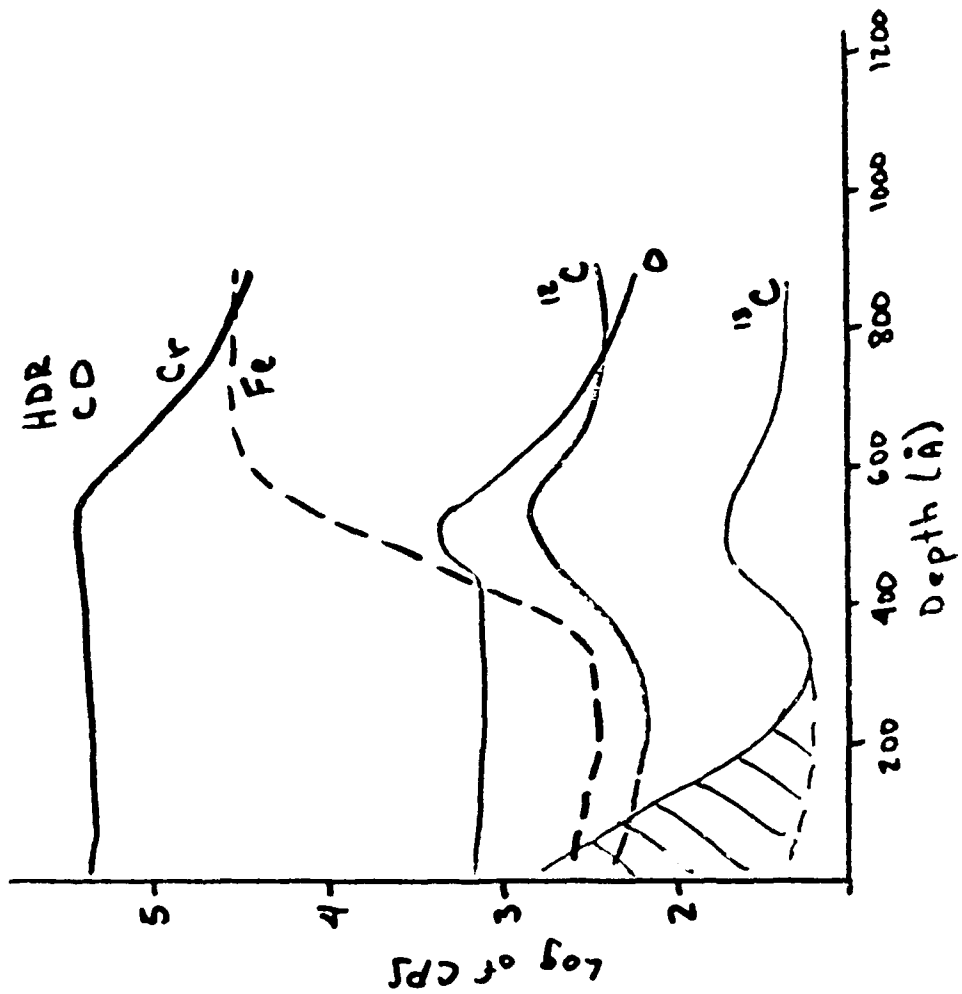
CO IMPLANTATION CONDITIONS

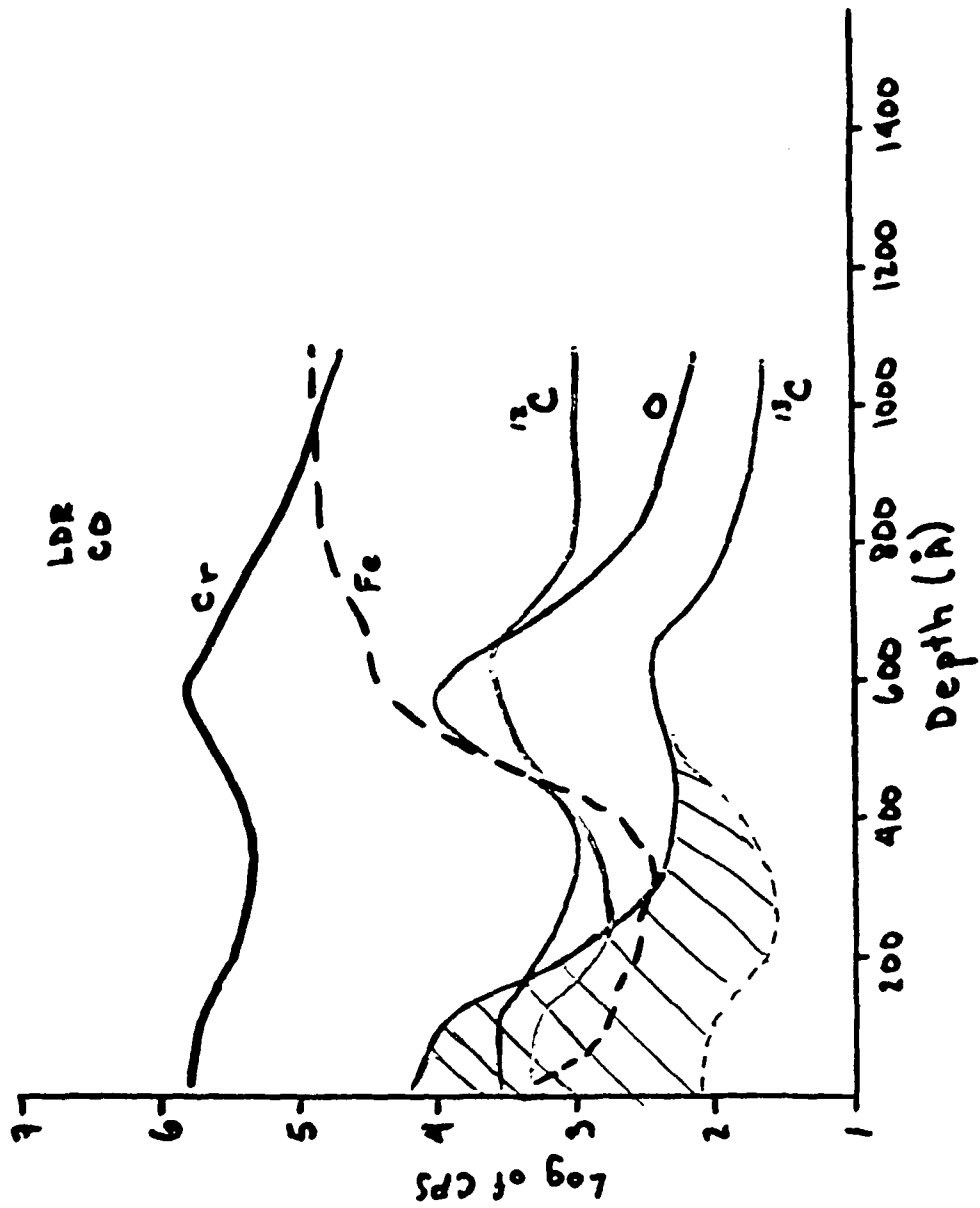
Sample	Time (hr)	Temp (°C)	Pressure (torr)	Depth (μm)
HDR-UHV	70	~50	<30 (est.)	<0.2 (Est.)
LDR-UHV	5.3	3	< 2.2	<0.3
HDR-CO	60	100	110	1.1
LDR-CO	4.9	100	110	14

80 nm Cr films on 316L MS steel
 2 F17 Cr¹⁺/cm² at 100 eV

Following SIMS profiles show Cr, Fe, O, ¹²C and ¹³C depth distributions in Cr¹⁺ implanted Cr films. LDR UHV, HDR-CO, and LDR-CO samples are shown.







AD P 00 1662

"Mechanical Properties and Microstructure of Fe Alloys
Implanted With Ti and C"

D. M. Follstaedt
Sandia National Laboratories*
Albuquerque, New Mexico 87185

Iron-based alloys implanted with Ti and C are of increasing interest because of their favorable surface properties (1-3). Similar improved surface properties are found for alloys into which only Ti was deliberately implanted, but which also acquired C at the surface during the implantation (3-6). Most notable of these properties are reduced friction coefficients and wear depths relative to values for the unimplanted surface. Friction is typically reduced by 50% and wear by up to 90% in unlubricated pin-on-disc tests when the discs are implanted. Moreover, these results are obtained on a wide range of steels (Knoop hardnesses from 180 to 789) with both hard and soft pin materials (440C and 304 stainless steels, respectively). Tests at other laboratories on 52100 bearing steel show reduced wear and reduced friction during lubricated testing as well (3,7).

It is of further interest to compare the mechanical test results with Ti and C implantations to those with N implantation, which is more commonly used. Studies of the latter treatment demonstrate reduced wear on mild steels, but results are mixed on 304 stainless steel and transformation-hardened steels. For instance, Type 52100 shows no reduction in wear (3,7). Furthermore,

N implantation in most instances does not reduce friction^(3,7,8).

Thus surfaces alloyed with Ti and C appear very promising for reducing wear, because of their applicability to many steels, and also for reducing friction. While these effects have been demonstrated on ion-implanted surfaces, alloys with the same properties might be obtainable by other methods, such as sputter or vapor deposition or ion beam mixing of deposited layers. The deposited layers offer the potential for thicker surface alloys, which could extend the beneficial effects to greater wear depths.

Recent transmission electron microscopic (TEM) examinations of f.c.c. 304 implanted with Ti and C show that the surface alloys is amorphous⁽⁹⁾. Furthermore, wear tracks on discs produced by light pin loads and showing reduced wear were observed to have a nearly continuous amorphous layer across the track⁽¹⁰⁾. Wear tracks due to heavier pin loads do not show reduced wear; no amorphous layer and greatly reduced Ti contents were found in these tracks. We have also run pin-on-disc tests with devitrified 304 (Ti,C); these tests showed no reduction in friction, thus demonstrating that the amorphous phase is required for this property⁽⁹⁾. Thus all evidence to date indicates that reduced friction and wear are the direct result of the amorphous phase with Ti and C. The observed amorphization of b.c.c. Fe^(5,6), f.c.c. 304⁽⁹⁾ and b.c.t. (martensite) 52100⁽⁴⁾ suggests that a similar amorphous layer is formed on all the steels.

* This work was performed at Sandia National Laboratories and supported by the U.S. Department of Energy under contract #DE-AC04-76DP00789.

References

1. L. E. Pope, F. G. Yost, D. M. Follstaedt, J. A. Knapp, and S. T. Picraux, in Wear of Materials, 1983, (ASME, 1983).
2. F. G. Yost, L. E. Pope, D. M. Follstaedt, J. A. Knapp, and S. T. Picraux, in Metastable Materials Formation by Ion Implantation, S. T. Picraux and W. J. Choyke, Eds., (North-Holland, New York, 1982), p. 261.
3. C. A. Carosella, I. L. Singer, R. C. Bowers, and C. R. Gossett, in Wear of Materials, 1983, (ASME, 1983), p. 103.
4. I. L. Singer, C. A. Carosella, and J. R. Reed, J. Nucl. Inst. and Meth. 182/183, 923 (1981).
5. J. A. Knapp, D. M. Follstaedt, and S. T. Picraux, in Ion Implantation Metallurgy, C. M. Preece and J. K. Hirvonen, Eds., (The Metallurgical Soc. of AIME, Warrendale, PA, 1980), p. 152.
6. D. M. Follstaedt, J. A. Knapp, and S. T. Picraux, Appl. Phys. Lett., 37, 380 (1980).
7. T. E. Fischer, M. J. Luton, J. M. Williams, C. W. White, and B. R. Appleton, presented at the ASME/ASLE Lubrication Conference in Washington, D.C., October 5-7, 1982.
8. F. G. Yost, S. T. Picraux, D. M. Follstaedt, L. E. Pope, and J. A. Knapp, Proc. Conf. on Metallurgical Coatings, April 18-22, 1983, San Diego, CA; to appear in THIN SOLID FILMS.
9. D. M. Follstaedt, L. E. Pope, J. A. Knapp, S. T. Picraux, and F. G. Yost, Proc. Conf. on Metallurgical Coatings, April 18-22, 1983, San Diego, CA.; to appear in THIN SOLID FILMS.
10. D. M. Follstaedt, F. G. Yost, L. E. Pope, J. A. Knapp, and S. T. Picraux, submitted to Appl. Phys. Lett.

Ti AND C IMPLANTED STEELS

<u>STEEL</u>	<u>TEST CONDITIONS</u>	<u>FLUENCE</u>	<u>REDUCED FRICTION</u>	<u>REDUCED WEAR</u>
FE 304 15-5 PH NITRONIC 60 440C	[UNLUBRICATED PIN-ON-DISC (440C AND 304 PINS)]	[2×10^{17} Ti/cm ² (180-90 KEV) 2×10^{17} C/cm ² (30 KEV) (~20 AT.% Ti, f OVER ~70 NM)]	~ 30% 35% ~ 50% ≤ 50% ~ 60%	~ 50% ≤ 90% ≤ 95% ~ 50% ~ 50%
52100	UNLUBRICATED BALL-ON-DISC	[4.6×10^{17} Ti/cm ² (190 KEV) (~25 AT.% Ti, 5-15 AT.% C)]	40-50%	MUCH LESS WEAR SCAR
52100	HEXADECANE, BALL-ON-DISC		NO "STICK- SLIP"	GREATLY REDUCED ~ 80% ~ 80%
52100 } 304 }	ABRASIVE WEAR BY DIAMOND PARTICLES			~ 80%
52100	LUBRICATED, BALL-ON- CYLINDER	[2×10^{17} Ti/cm ² (150 KEV)]		~ 80%
52100	BALL-ON-CYLINDER - UNLUBRICATED - HEXADECANE - LUBRICATED	[4×10^{17} Ti/cm ² (300-100 KEV)]	~ 50% ~ 50% UNCHANGED	REDUCED REDUCED POSSIBLY REDUCED

+ SANDIA NATIONAL LABORATORIES

• NAVAL RESEARCH LABORATORY

† EXXON RESEARCH AND ENGINEERING COMPANY/OAK RIDGE NATIONAL LABORATORY

WEAR AND FRICTION SUMMARY

N IMPLANTATION

- OFTEN REDUCED SLIDING WEAR (BUT NOT 52100)
- USUALLY NO REDUCTION IN FRICTION

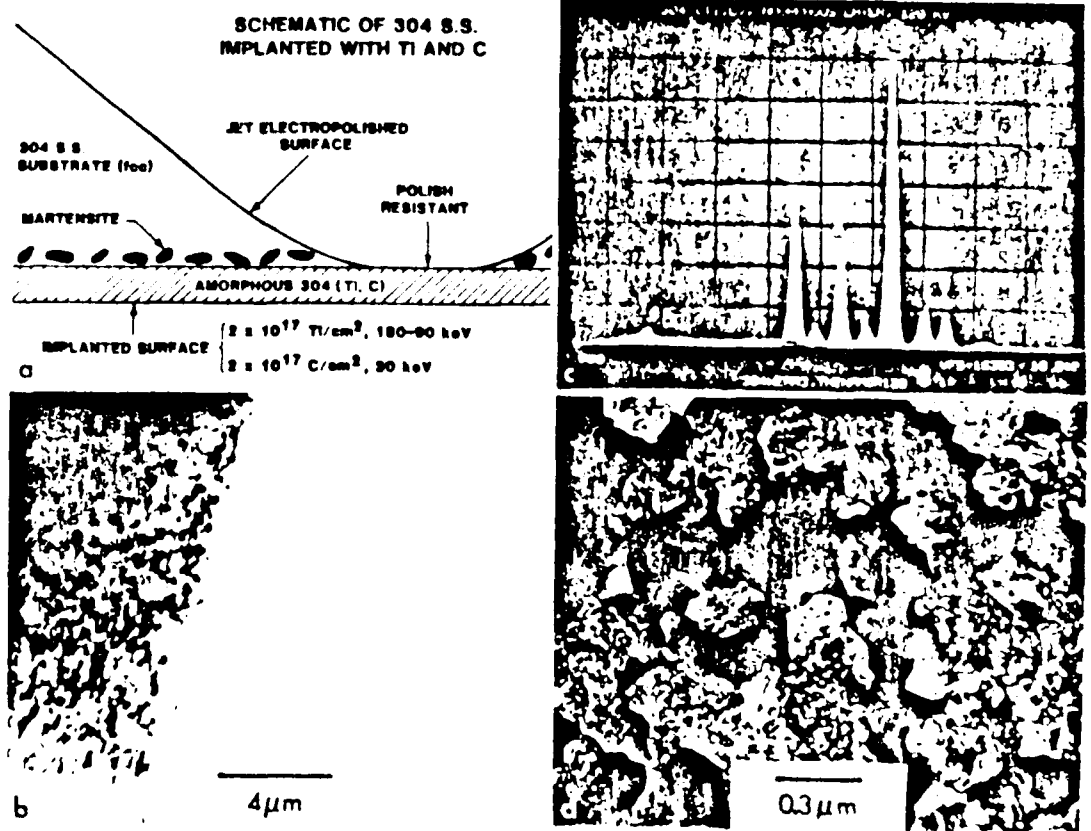
Ti + C IMPLANTATION

- UNLUBRICATED REDUCED WEAR IN WIDE RANGE OF STEELS (KNOOP HARDNESSES 180 - 789)
- UNLUBRICATED REDUCED WEAR WITH BOTH HARD (440C) AND SOFT PINS (304)
- REDUCED ABRASIVE WEAR
- REDUCED LUBRICATED WEAR (52100)
- REDUCED UNLUBRICATED FRICTION (ALL STEELS)
- REDUCED FRICTION IN HEXADECANE

Ti + C SURFACE ALLOYS LOOK PROMISING, BUT

- Ti IS RELATIVELY MORE DIFFICULT TO IMPLANT THAN N
 - THIN IMPLANTED LAYERS ($\sim 0.1 \mu\text{m}$); Ti DIFFUSION INWARD NOT EXPECTED.
- ION BEAM MIXING MIGHT BE USEFUL IN PRODUCING THICKER LAYERS WITH LOW ION FLUENCES OF READILY IMPLANTED SPECIES.

Figure 1. a) Schematic cross section of the microstructure observed by TEM in 304(Ti,C). b) Bright field TEM micrograph showing amorphous layer (light area) and thicker (darker) area which includes the crystalline substrate. c) EDS spectrum



from the amorphous layer. d) Dark field TEM micrograph in which bcc particles in the substrate are illuminated.

THERMAL EVOLUTION OF AMORPHOUS 304 S.S. IMPLANTED WITH Ti AND C

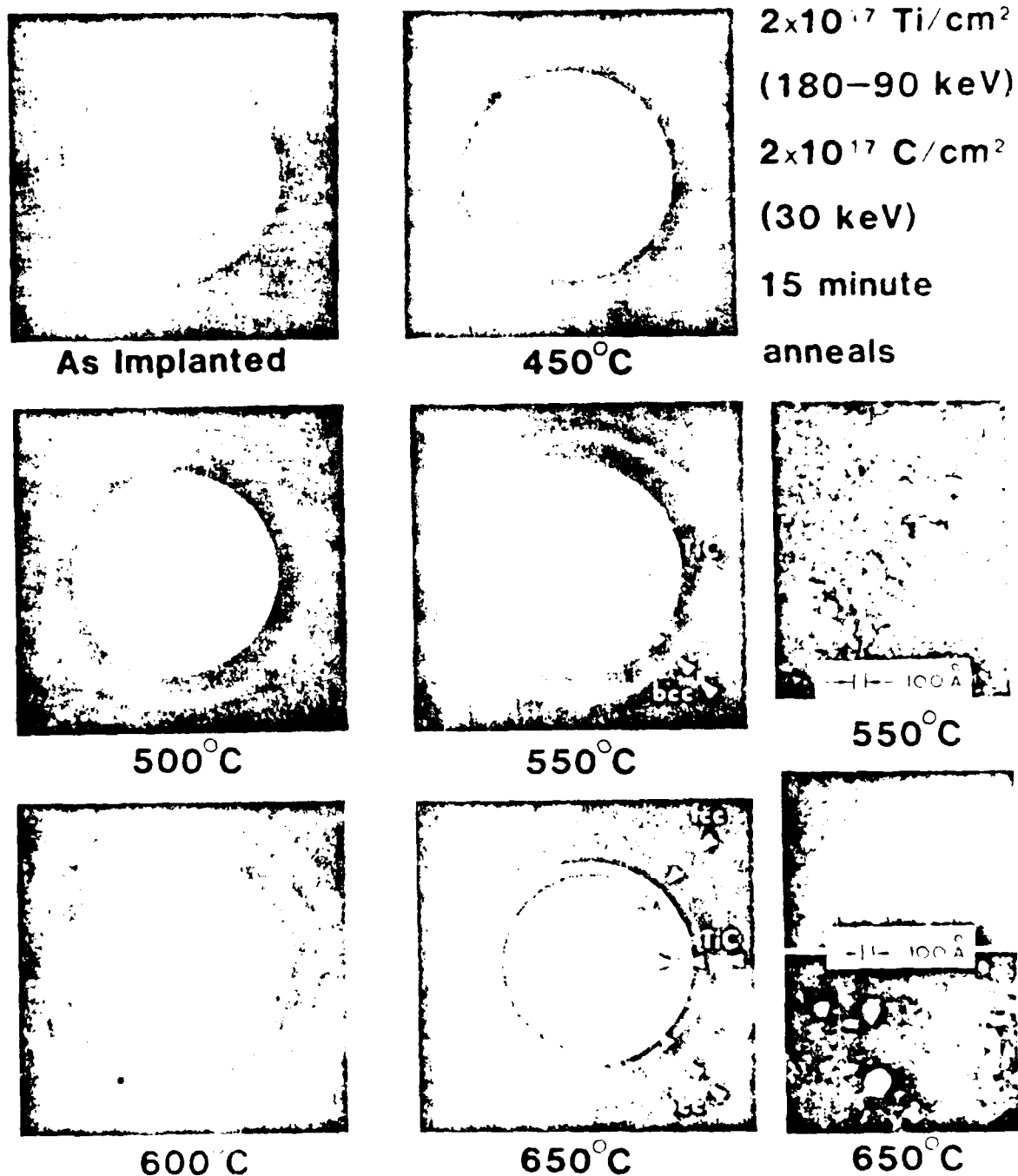


Figure 2. Electron diffraction patterns and dark field micrographs showing the thermal evolution of amorphous 304(Ti,C). Pictures were taken near the end of 1/4 hr. anneals at successively higher temperature.

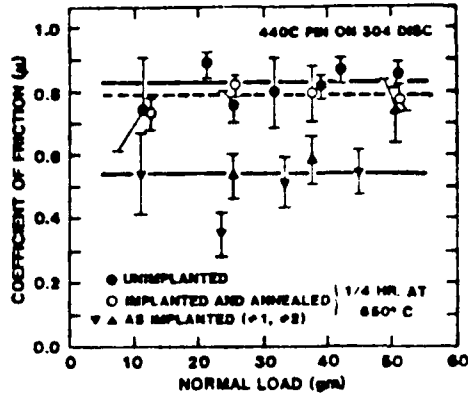


Fig. 3 Coefficient of friction values plotted versus pin load for 304 stainless steel. (Measured by L. E. Pope.)

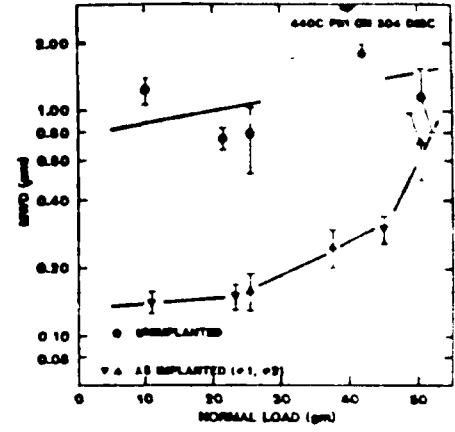
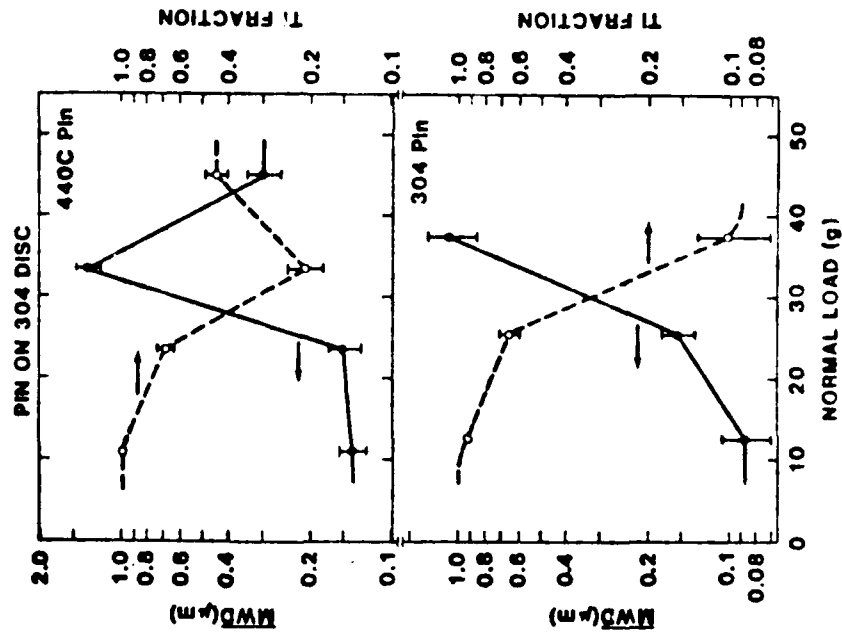


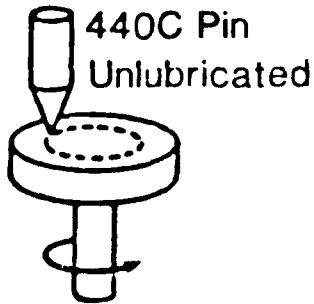
Fig. 4 Maximum wear depths after 1000 cycles plotted versus pin load for 304 stainless steel. (Measured by F. G. Yost.)



Wear depth and remaining Ti fraction for wear tracks made with 304 and 440C pins with loads ≤ 50 g on a 304 disc implanted with Ti and C.

MICROSTRUCTURE OF WEAR TRACKS IN 304 S.S. IMPLANTED WITH Ti AND C

23.6 gm Pin Load, Wear Depth $\leq 0.15 \mu\text{m}$



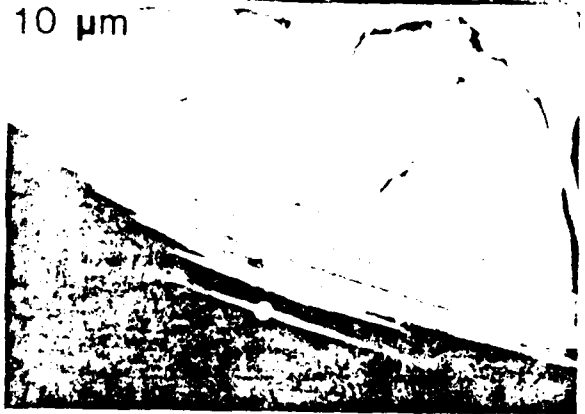
304 Disc
Implanted With
 $2 \times 10^{17} \text{ Ti/cm}^2$,
180-90 keV
and
 $2 \times 10^{17} \text{ C/cm}^2$,
30 keV
(~20 at % Ti and C)

● WEAR TRACK
IS A NEARLY
CONTINUOUS
AMORPHOUS
LAYER

SEM



TEM

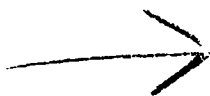


TED



a) SEM and b) TEM micrographs from the same area of the wear track made with a 440C pin and 23.6 g load. c) and d) Electron diffraction patterns from the areas indicated in b).

AD P 00 1663



"High Dose Ion Implantation And
Corrosion Behavior of Ferrous Metals"

B. D. Sartwell* and N. S. Wheeler
Bureau of Mines, 4900 LaSalle Road
Avondale, Md. 20782

G. K. Hubler and E. McCafferty
Naval Research Laboratory
Washington, D. C. 20375

C. R. Clayton
State University of New York
Stony Brook, New York 11794

There are two possible approaches to applying ion implantation to the modification of the corrosion behavior of metals and alloys. The first approach is to use ion implantation to produce metastable or amorphous corrosion-resistant surface alloys that are inaccessible by conventional metallurgical techniques, and to apply them to specific applications where corrosion is a severe problem. Secondly, and of a more fundamental nature, ion implantation can be used to introduce controlled amounts of various elements into the surface of a metal as part of a research effort to identify the mechanisms responsible for certain forms of general and localized corrosion. The technique of alloying to produce more corrosion resistant materials is widely used and the choice of a particular alloying element is usually based on the fact that it will enhance the formation of a passive film or will reduce the rate of the various cathodic processes that occur on the metal's surface. It is also possible to

7

reduce the overall corrosion rate by introducing an element that displays rapid cathodic kinetics, but it is essential that the original material passivate in the corrosive environment that is being considered.

Aqueous corrosion proceeds through an electrochemical mechanism and there are various types of electrochemical techniques used to evaluate the corrosion resistance of alloys. Linear polarization and Tafel region extrapolation have been used to evaluate binary Fe-Pb and Fe-Ti surface alloys formed by ion implantation. The instantaneous corrosion rate of the Fe-Pb alloys in 0.1 N H_2SO_4 was approximately 3 to 4 times lower than that of pure iron. The reason for this is a decrease in the hydrogen exchange current density caused by the presence of the lead, which is a poison for the hydrogen evolution reaction. The corrosion rate of the Fe-Ti alloys was approximately two times higher than that of iron. Auger analysis of the Fe-Ti alloy before exposure to the acid solution indicated that TiC was in the region about 4.3 to 34 nm from the surface. SEM analysis following the electrochemical tests revealed the presence of square flat-bottomed pits, a morphology which is usually associated with inclusion etch pits. Thus, it is proposed that the square pits may have been formed as TiC precipitates were etched from the sample surface.

The implantation of zirconium into iron reduces the corrosion rate by an order of magnitude by enhancing the rate of passivation in a 1 N H_2SO_4 solution. The corrosion rate is still considerably higher, however, than that observed for an

amorphous $\text{Fe}_{90}\text{Zr}_{10}$ coating even though the near-surface concentration of Zr in the implanted sample was estimated to be 20 to 30 atomic percent.

The implantation of Ti into 52100 steel results in the formation of an amorphous Ti-Fe-C surface, which provides modest improvements in corrosion resistance in 1 N H_2SO_4 and 0.1 N NaCl. The anodic current density in both solutions is about 10% that of unimplanted 52100 steel, up to an anodic overpotential of about 800 mV. Pitting, which is initiated at low overpotentials, leads to undermining of the implanted layer and its eventual peeling off at higher potentials. Detailed optical and surface analytical studies show that the pitting initiates at surface flaws, which are most likely surface carbides or oxide inclusions. Galvanic action between free Ti beneath the pitted amorphous film and Fe in the bulk steel thus leads to undermining of the amorphous layer.

The effect of the implantation of various ions on the pitting corrosion resistance of 52100 steel in a 0.01M NaCl solution has been investigated. Molybdenum implantation provided very little improvements; however, a combination of both chromium and molybdenum significantly increased the breakdown potential for initiation of pitting corrosion. Finally, tantalum implantation proved to be the most effective in protecting the surface of the 52100 from pitting corrosion.

* Present Address: Naval Research Laboratory, Code 6675, Washington, D.C. 20375

TABLE 1. - Corrosion rates, expressed in mils/year, in 0.1 N H₂SO₄ for several different metals and ion-implanted alloys using two different test methods, Tafel extrapolation and three-point linear polarization

Test method	Fe	Fe-Pb	Pb	Fe-Ti	Ti
Tafel extrapolation..	50±2	12±2	0.42±0.19	96±22	0.69±0.04
Linear polarization...	32±0	16±10	(<u>1</u>)	55±47	0.98±0.52

¹Could not measure corrosion rate due to cathodic Tafel slope being indeterminate.

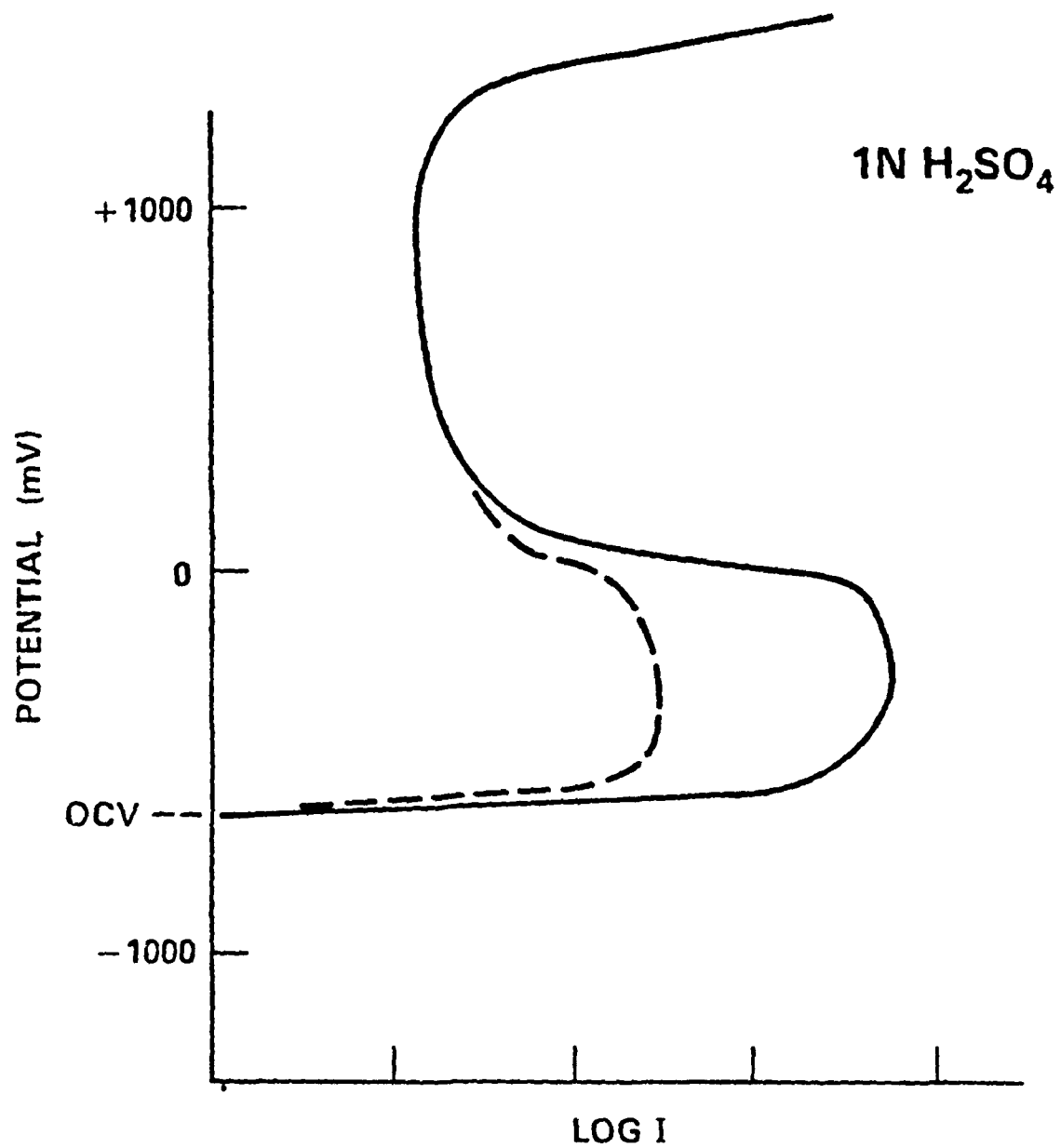


FIGURE 1. Idealized potentiodynamic polarization scan (current vs. voltage characteristic) for a ferrous alloy in 1N H₂SO₄ at room temperature. The dashed line indicates an improvement in the passivity of the surface and therefore improved corrosion resistance.

FIGURE 2

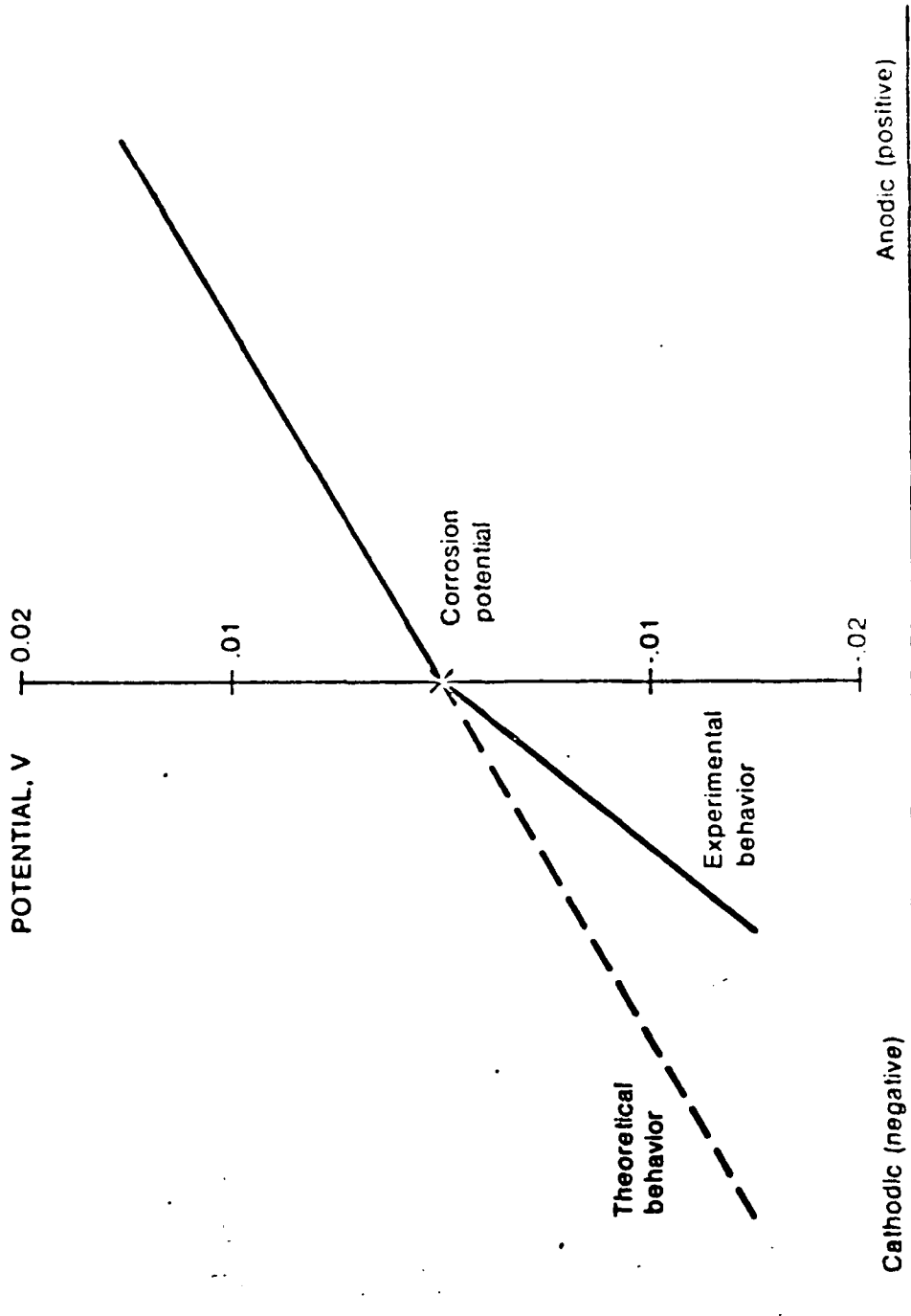


Figure--Caption

FIGURE 2 . Two electrochemical methods used for determining corrosion rates were Tafel region extrapolation and three-point linear polarization. The former determines the corrosion rate graphically whereas the latter requires calculations based on experimental data. When the logarithm of the absolute value of the measured current density is plotted against the sample potential, the resulting curve generally has two linear portions (Tafel regions), one on the anodic and one on the cathodic side of the SSOC (steady-state open-circuit) potential. Extrapolation of the Tafel regions gives a point of intersection, the coordinates of which are the corrosion potential E_c and the corrosion current density I_c , or corrosion rate.

The basis for linear polarization, or polarization resistance, lies in the assumption that potential varies linearly with current density for a range of ± 20 mV from E_c , as illustrated in this figure. The slope of this line can be related to the Tafel region slopes (found from $\log I$ vs. E curves) to give I_c . Some metal/environment systems display linear E vs. I curves, but most are nonlinear as shown by the solid line. The three-point linear polarization method was devised to provide a means for determining the slope of the E vs. I curve in the nonlinear case.

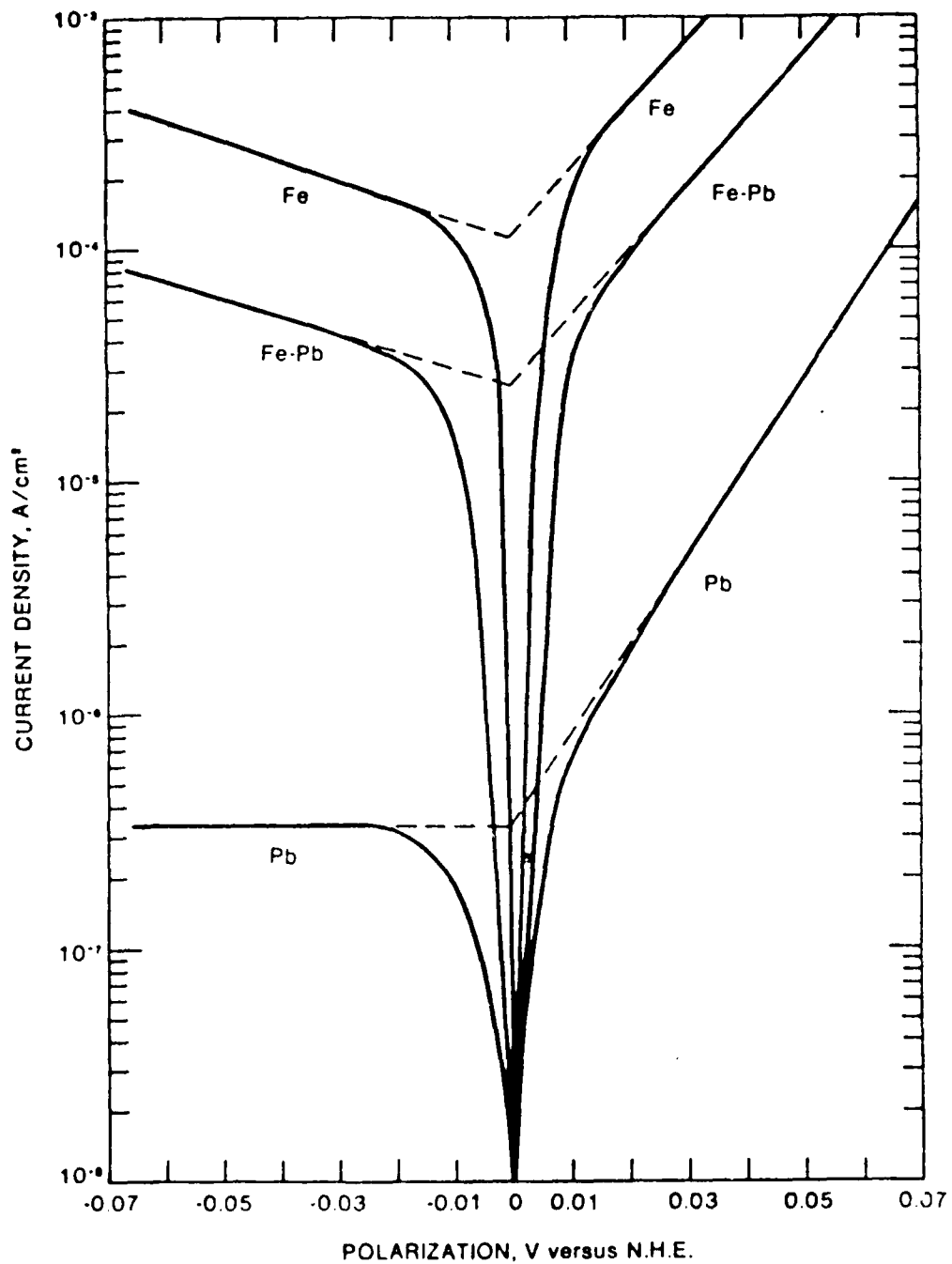


FIGURE 3. Current density as a function of sample potential for Fe, Fe-Pb, and Fe implanted with 30 keV Pb^{+} such that the final retained dose was 1.0×10^{16} atoms/cm². The potential is shown as volts from the steady-state open-circuit potential. The dashed lines represent the extrapolation from the Tafel region of each curve.

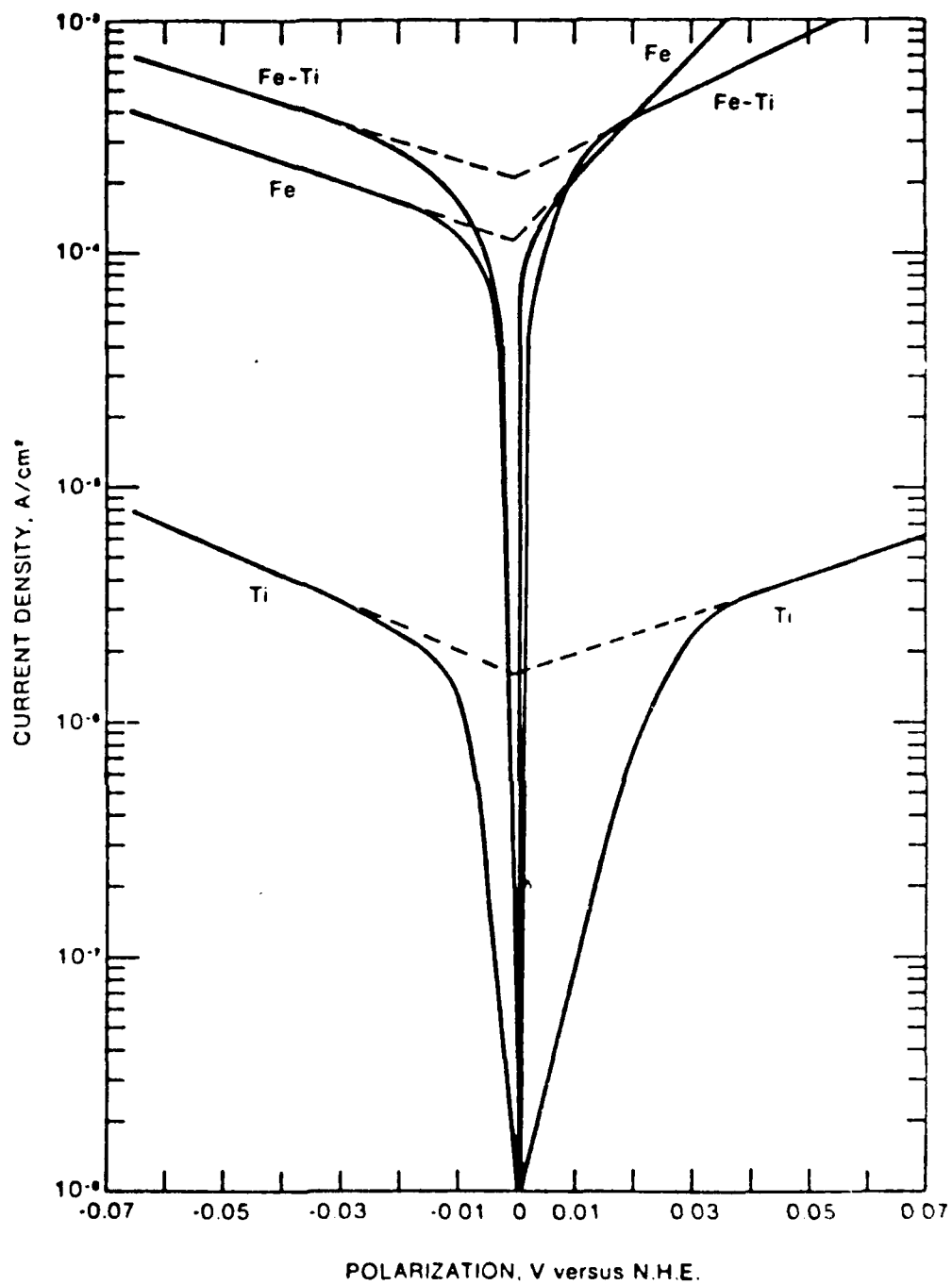
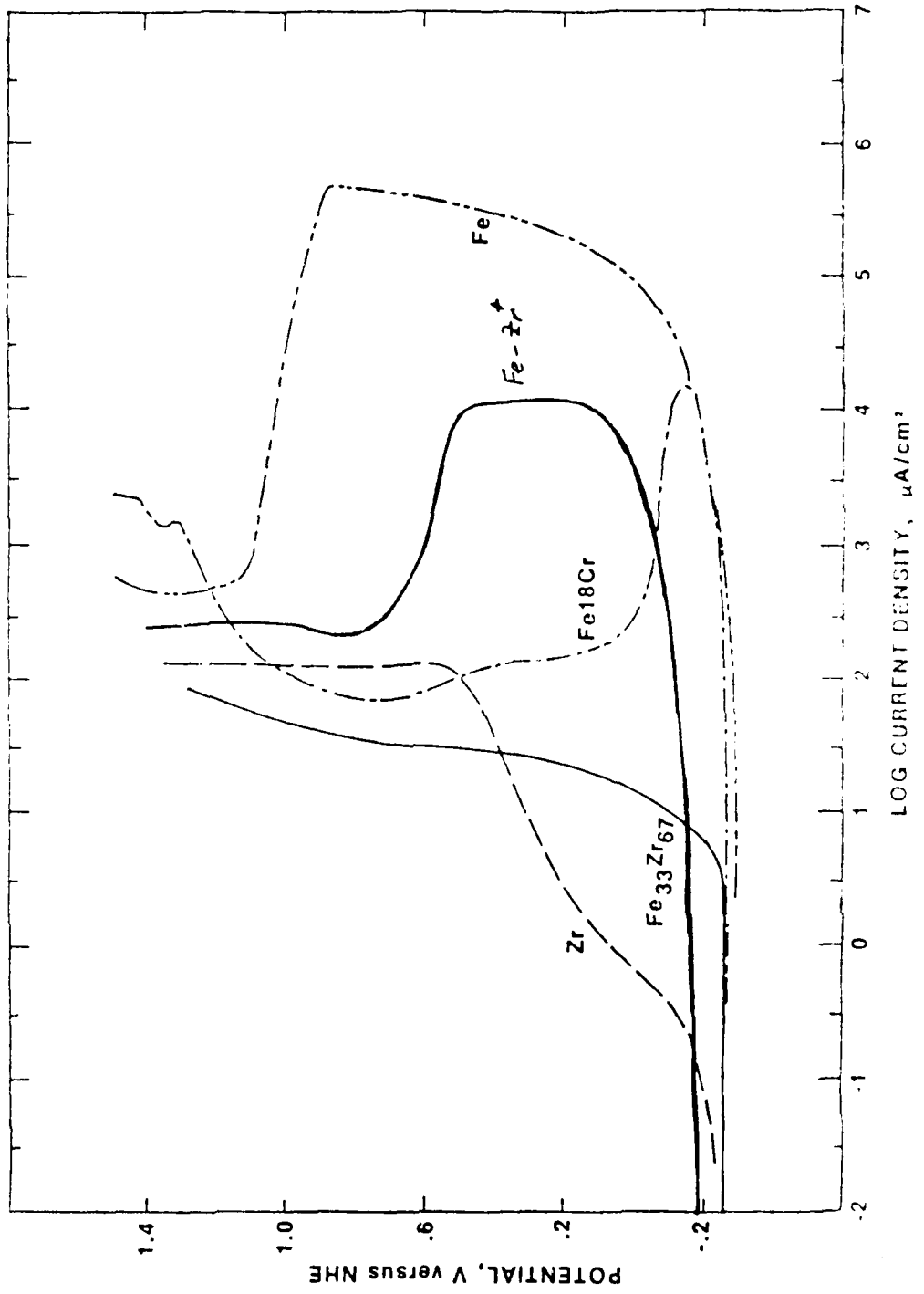


FIGURE 4 . Current density as a function of sample potential for Fe, Ti, and Fe implanted with 50 keV Ti⁺ to a total retained dose of 7×10^{16} atoms/cm², with the potential shown as volts from the SSOC potential.

FIGURE 5. Polarization curves in deaerated 1M H₂SO₄ obtained at a rate of 500 V/hour for Fe, Fe₁₈Cr, Cr, an Fe₃₃Zr₆₇ amorphous coating, and Fe implanted with a dose of 2×10^{17} ions/cm².



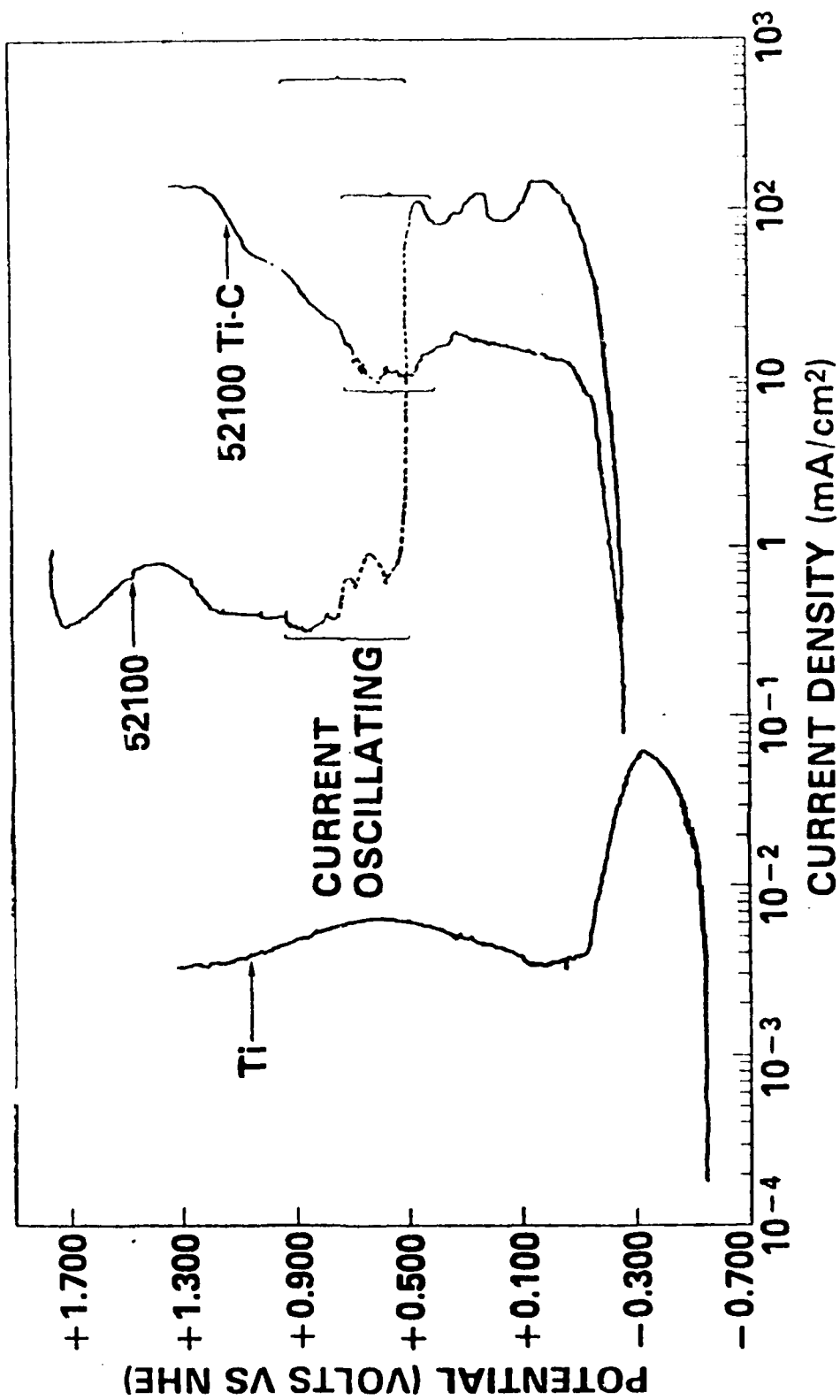


FIGURE 6. Anodic polarization curves of titanium in 0.1M NaCl solution at 100°C, and Ti-10% TiC at 100°C and 200°C. The scan rate was 10 mV/min.

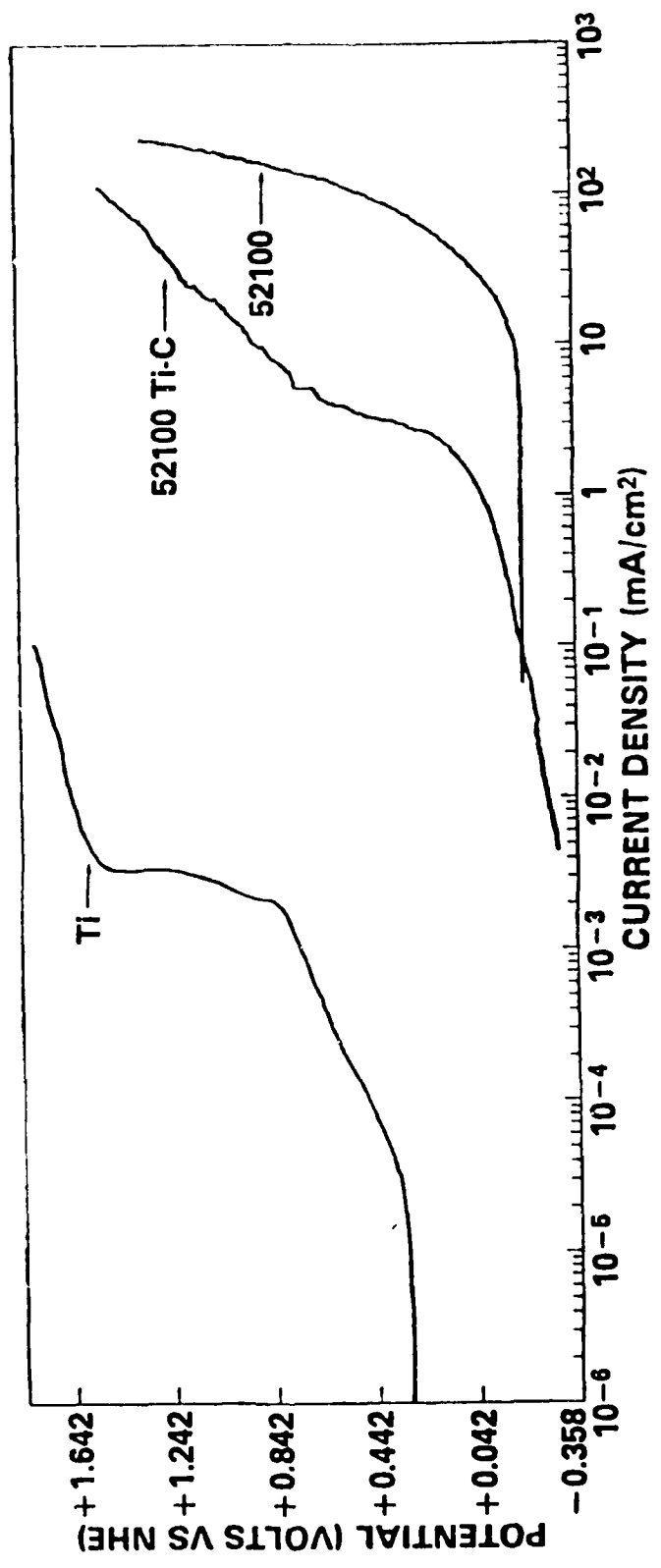


FIGURE 7 . Anodic potential-density polarization curves for unimplanted 52100 steel and Ti-implanted 52100 steel (4.5×10^{17} ions/cm² at 190 keV) in 0.1 M NaCl solution.

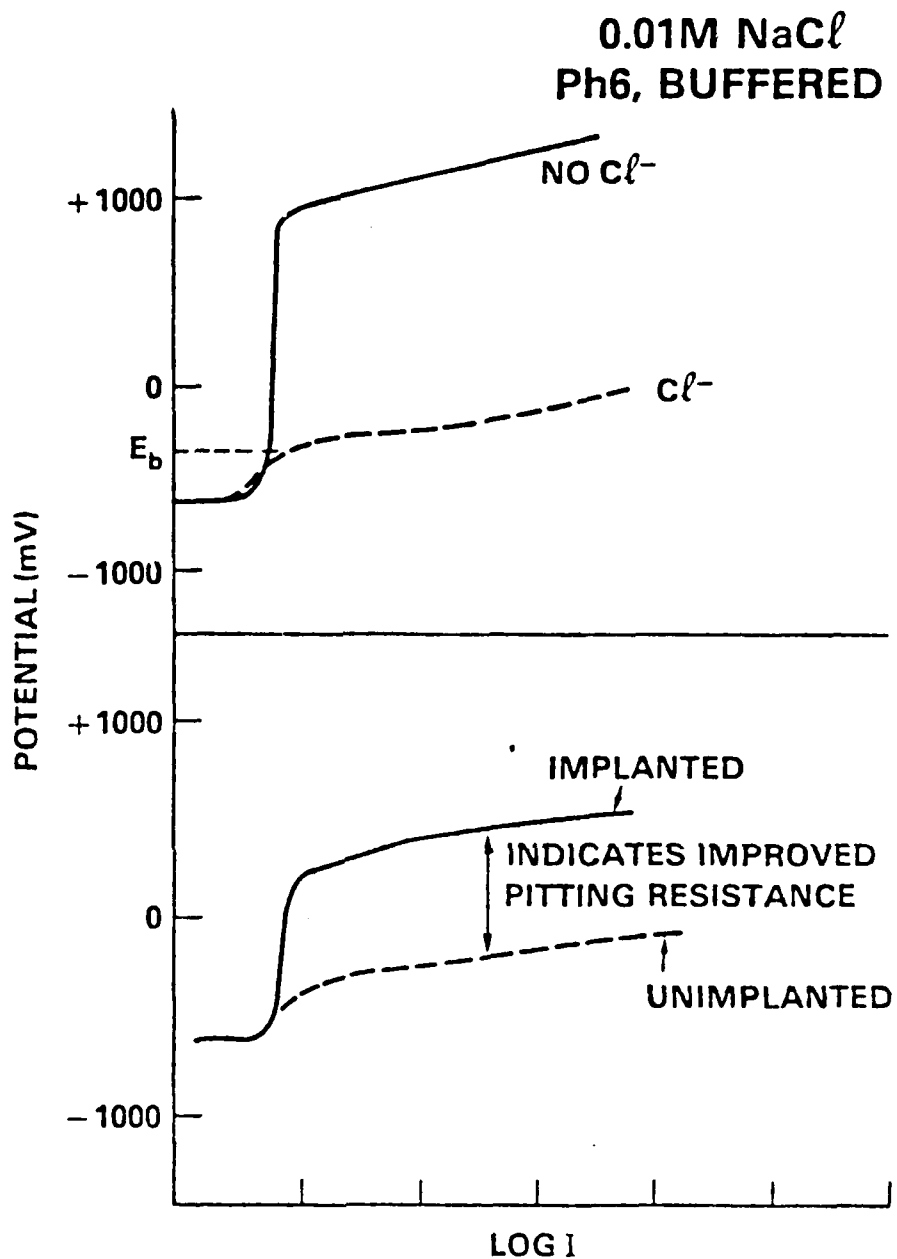
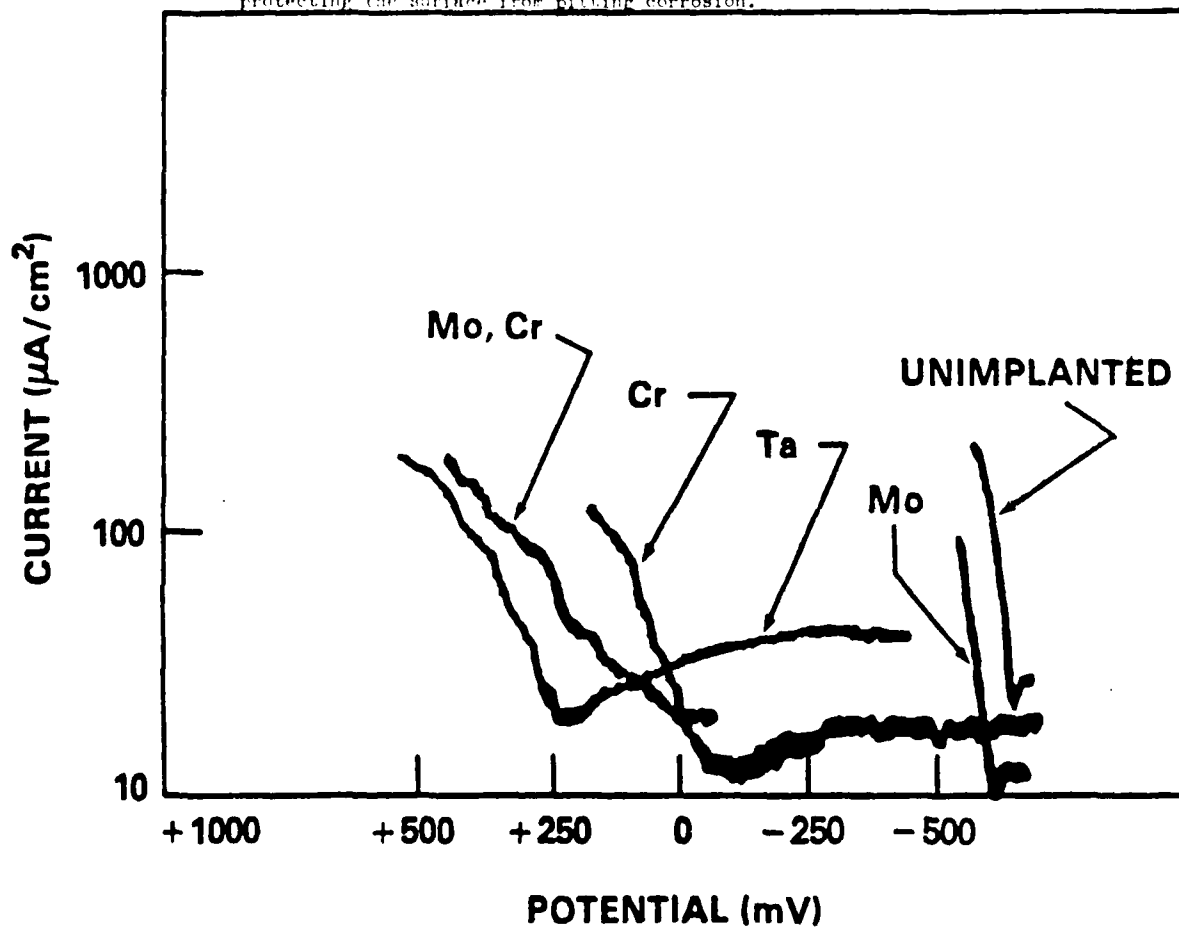


FIGURE 8 . Idealized potentiodynamic polarization scans (current vs. voltage characteristic) for a ferrous alloy in a buffered pH 6 solution at room temperature. The upper set of curves demonstrate the effect of adding Cl^- ions to the solution. E_b defines the pitting potential where a sharp increase in current results when pits form on the surface. The lower set of curves demonstrate the desired result of ion implantation, i.e., force the pitting potential toward higher values.

FIGURE 9 . Potentiodynamic anodic polarization data produced in buffer solution of pH6 containing 0.01M NaCl for 52100 steel, and for 52100 steel implanted with molybdenum (3.5×10^{16} ions/cm²), chromium (2×10^{17} ions/cm² at 150 keV), chromium plus molybdenum (2×10^{17} Cr/cm² at 150 keV, 3.5×10^{16} Mo/cm² at 100 keV), and tantalum (1×10^{17} ions/cm² at 150 keV). The curves indicate that tantalum was most effective in protecting the surface from pitting corrosion.



"Ion Beam-Enhanced Deposition and
Ionized Cluster Beam Deposition"

J. K. Hirvonen
Zymet, Inc.
Danvers, Massachusetts 01923

A. ION BEAM-ENHANCED DEPOSITION

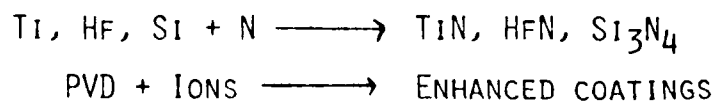
(SEE, PRANEVICIUS, WEISSMANTAL, COLLIGON, CUOMO, OTHERS?)

1. MAJOR FEATURES.

- TRANSCENDS ADVANTAGES OF CONVENTIONAL COATING PROCESSES AND ION IMPLANTATION.
- ALREADY DEMONSTRATED:
 - "DIAMOND-LIKE" CARBON (I-C) QUASI-AMORPHOUS
 - CUBIC BORON NITRIDE
 - H-C-SI
- ADVANTAGES:
 - NO LIMIT TO COATING THICKNESS
 - CONTROLLABLE STOICHIOMETRY
 - SUPERIOR ADHESION
 - HIGH-DENSITY COATINGS
 - LOW-TEMPERATURE PROCESS

2. APPLICATION TO WEAR- AND CORROSION-RESISTANT COATINGS.

EXAMPLES:



AD P 0 0 1 6 6 4

THE ION BEAM:

- PROVIDES CHEMICAL DOPING , AND
- PROMOTES NUCLEATION AND KINETICS OF FILM GROWTH TO HIGH-TEMPERATURE REGIME WHILE SUBSTRATE REMAINS AT LOW TEMPERATURE

3. VARIABLES TO BE STUDIED.

- OPTIMUM FLUXES OF IONS AND DEPOSITED ATOMS
- CHARACTERIZATION OF MICROSTRUCTURE
- EFFECT OF ION SPECIES AND ENERGY ON THIN-FILM STRUCTURE (100 EV - 10 KEV)
- MECHANICAL INTEGRITY OF COATING

B. IONIZED CLUSTER BEAM DEPOSITION

(SEE, T. TAKAGI, 19TH UNIVERSITY CONFERENCE ON CERAMIC SCIENCE, NOVEMBER 8-10, 1982, JANE S. MCKIMMON CENTER, NORTH CAROLINA STATE UNIVERSITY, NORTH CAROLINA)

1. MAJOR FEATURES.

- ABILITY TO ADJUST AVERAGE ENERGY PER DEPOSITION ATOM OVER 0.01 - 100⁺ EV RANGE
- EFFECTIVE CONVERSION OF CLUSTER KINETIC ENERGY TO ADATOM SURFACE ENERGY DUE TO SNOWBALL EFFECT
- INHERENT CLEANSING ACTION BY SPUTTERING AND MICRO-SCALE HEATING
- ENHANCED REACTIVE PROCESSES DUE TO IONIC CHARGE PRESENCE

2. TECHNICAL PROSPECTS.

- BULK MATERIAL PROPERTIES
- CONTROL OF MORPHOLOGY
- SELECTION OF GROWTH STRUCTURE
- HIGH TEMPERATURE EQUIVALENT PROCESSES AT LOW TEMPERATURE
- PROCESS CLEANLINESS
- EFFICIENT REACTIVE FORMATION
- CONVENIENT DOPING
- QUANTITATIVE PARAMETERS
- AUTOMATION
- CLOSED-LOOP CONTROL
- MATERIAL USE EFFICIENCY
- CURRENTLY R&D APPLICATIONS
- SCALE UP CAPABILITY
- VERSATILITY

Figure Captions

Figure 1 Ion beam-enhanced deposition.

Figure 2 Ionized cluster beam deposition.

Figure 3 Cluster impact phenomena.

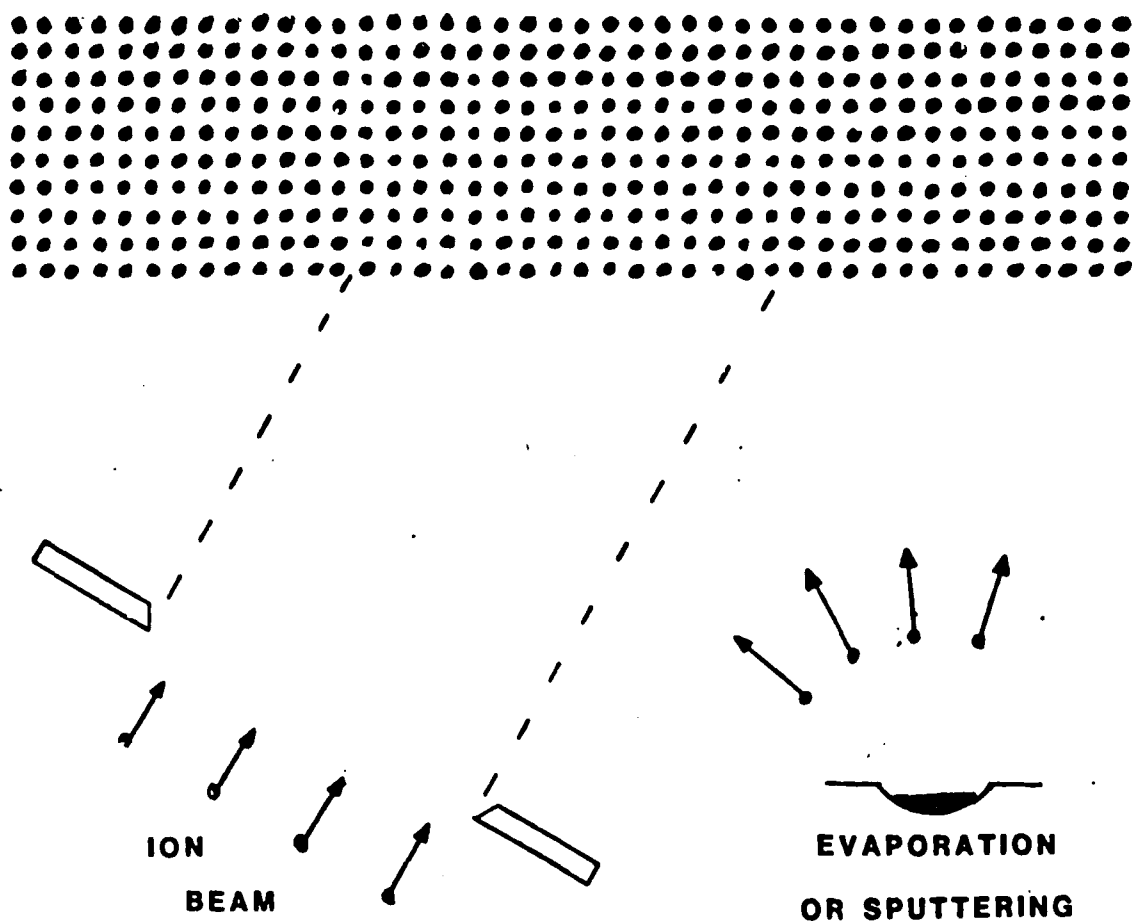


Fig.1

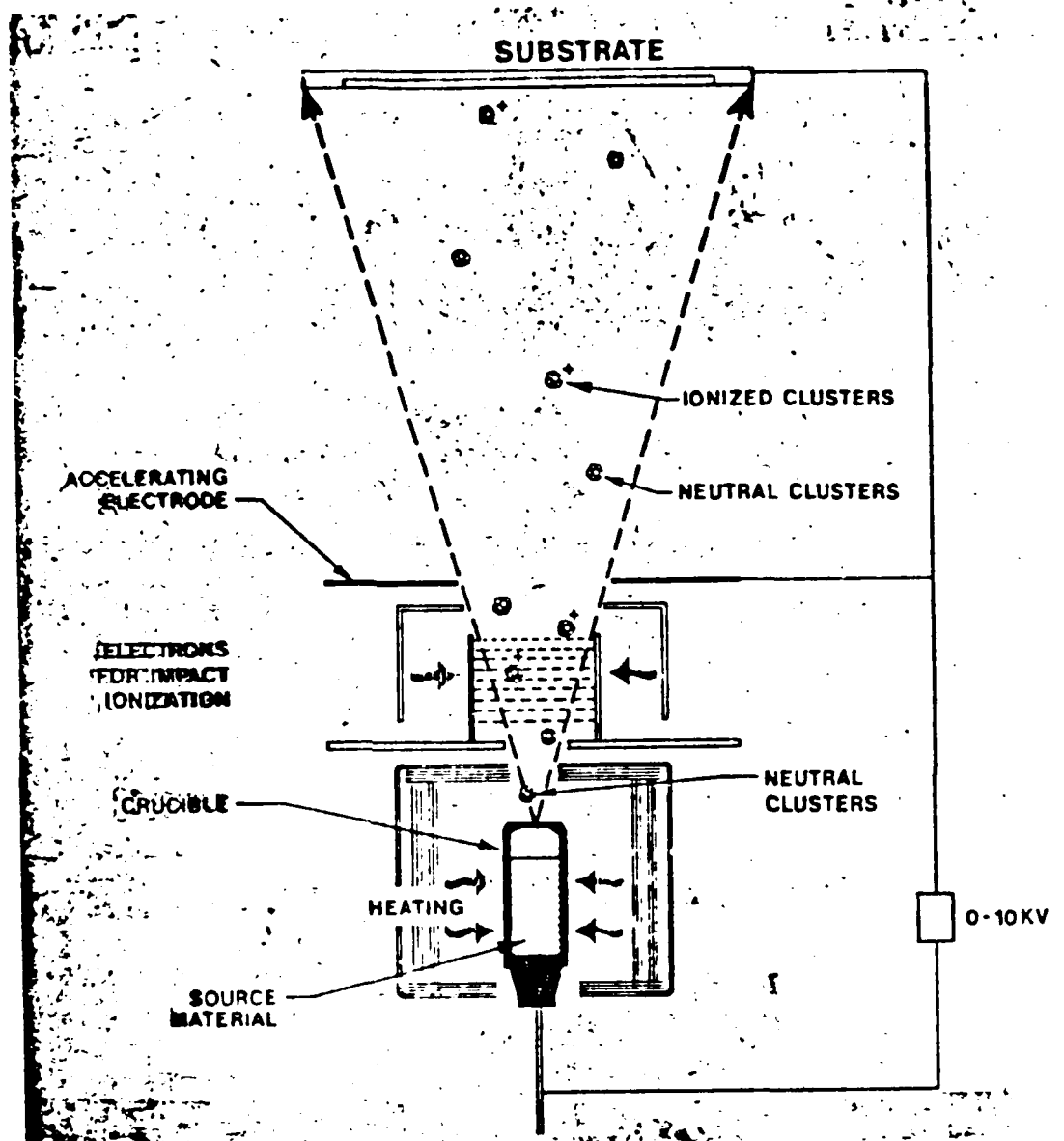


Fig. 2

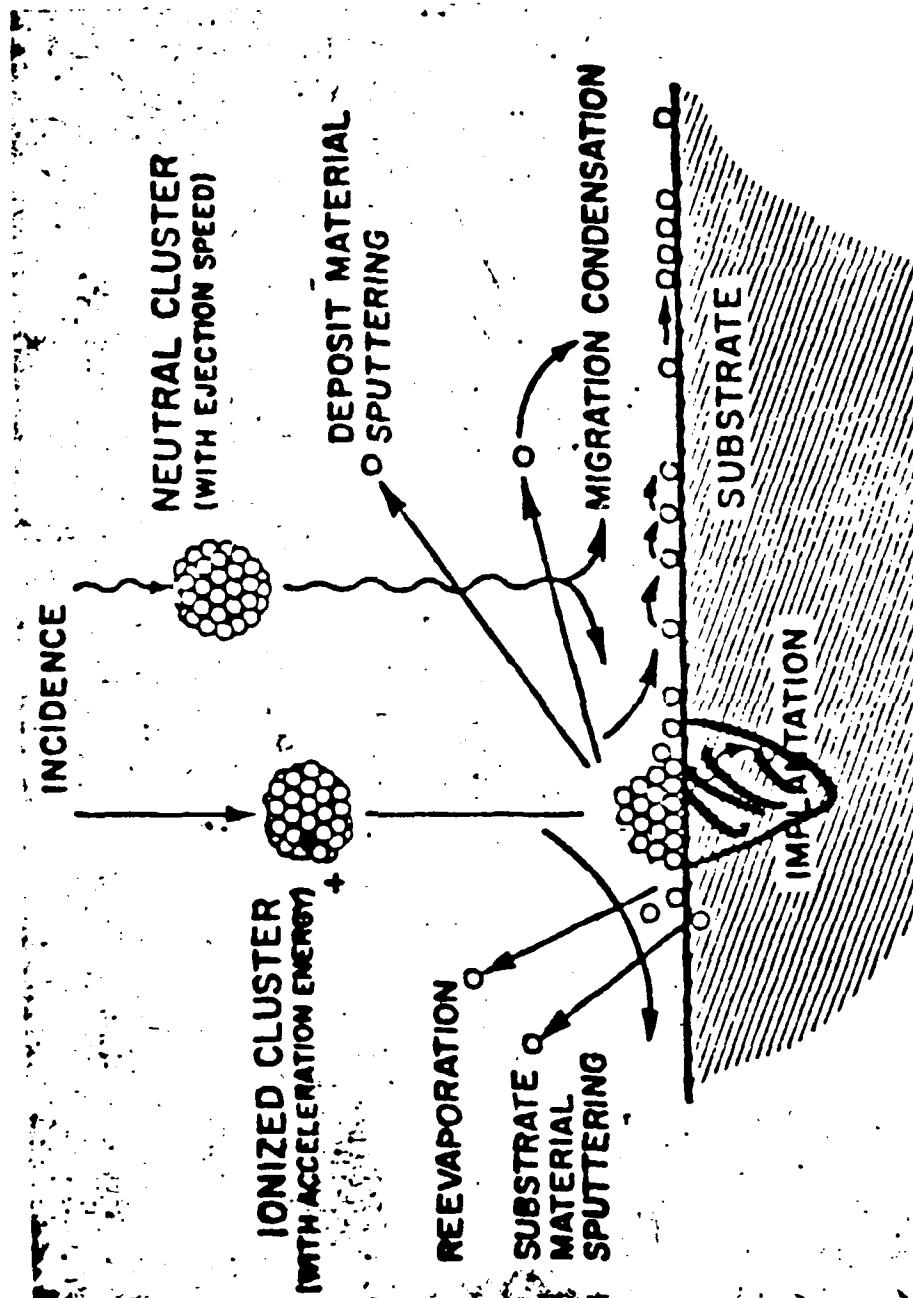
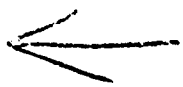
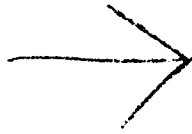


Fig. 3



"Ion Beam Mixing Research At Westinghouse"



R. Kossowsky and R. R. Jensen
Research and Development Center
Westinghouse
Pittsburgh, Pennsylvania 15235

The program on ion implantation and ion beam mixing has concentrated on three areas of major applications: improvement of wear properties, specifically cemented carbide tools; oxidation resistance for gas turbine applications; and bonding of metal to ceramics.

The first slide lists the major species we have been experimenting with ("Recoil Implantation Areas").

To allow a routine of recoil implantation, the pertinent parameters should be known. Our simple minded view of recoil is shown in the next two vu-graphs ("Coating - Substrate" and "Solution"). We assume a modified diffusional mixing where a balance has to be obtained among the various processes, i.e. - rate of surface recession by sputtering (V) and the forward motion of the mixed ion by an effective diffusivity, D , and is defined as the sputtering efficiency, α is the dose and Ω - the atomic volume. The "Solution" page shows that the problem is reduced to solution in terms of one parameter - $\alpha\sqrt{D}$, where W is the thickness of the deposited film.

The next three graphs ("Recoil Implantation Concentration Profiles" for Cr, Mo, Cr) show typical calculated recoil profiles

AD P 0 0 1 6 6 5

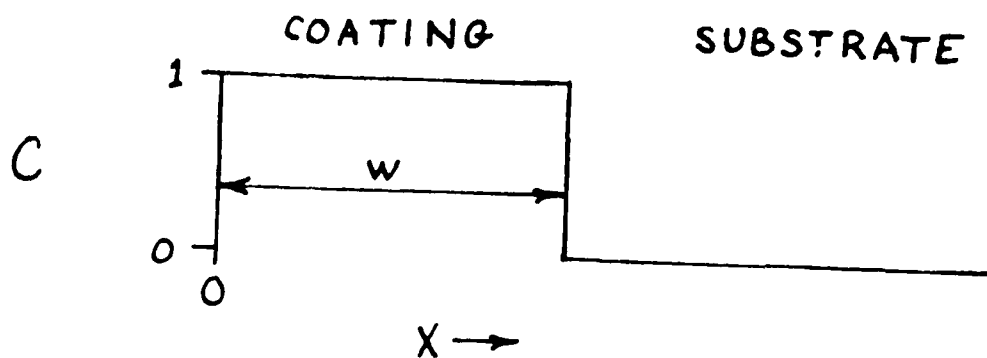
for Cr recoiled with three different gases, with the parameter α decreasing, respectively from 0.58 to 0.28. This demonstrates that the best mixing of Cr is to be obtained with N gas.

The last set of slides ("Metal-Glass Bonding", "Au on SiO₂ - evaporation, sputter deposited, and flat faced pins glued on implanted and unimplanted Au films") show a progression of an experimental program to bond Au to glass. The glass is significantly weakened by the process of recoil.

The last slide ("Recoil Implantation of Carbon ...") shows an expected result re-incorporation of carbon into the matrix of steel during N implantation due to ambient residual carbon on the surface.

RECOIL IMPLANTATION AREAS

<u>Species Implanted</u>	<u>Substrate</u>
B	steel
Y	Ni-Cr-Al alloys
Cr	Cu
Ti	WC
Cr	WC
Hf	WC
Ni	SiO ₂
Ni	Si ₃ N ₄
Au	SiO ₂



$$\frac{\partial C}{\partial t} - V \frac{\partial C}{\partial x} = D \frac{\partial^2 C}{\partial x^2}$$

$$\text{I.C. } C(x, 0) = \begin{cases} 1 & 0 \leq x \leq w \\ 0 & x > w \end{cases}$$

$$\text{B.C. } \left. \frac{\partial C(x, t)}{\partial x} \right|_{x=0} = 0$$

WHERE

$$V = S\phi\Omega$$

$$D = \frac{1}{2} K \langle R^2 \rangle$$

SOLUTION

$$C(x,t) = \frac{1}{2} \left[\operatorname{erfc} \left(\frac{x+vt-w}{2\sqrt{Dt}} \right) - e^{\frac{wv}{D}} \operatorname{erfc} \left(\frac{x+vt+w}{2\sqrt{Dt}} \right) \right]$$

LET

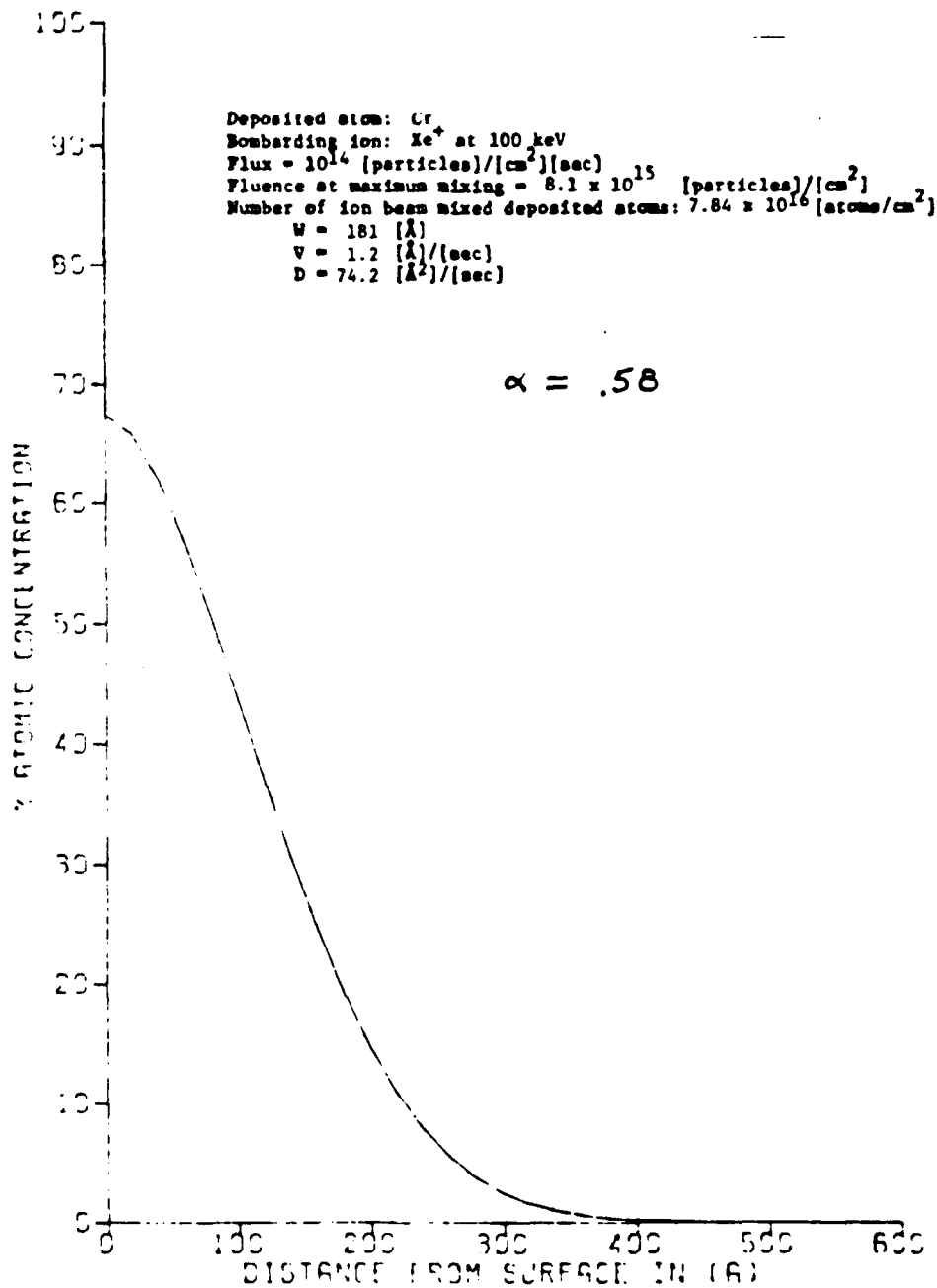
$$x' = \frac{x}{w}$$

$$t' = \frac{vt}{w}$$

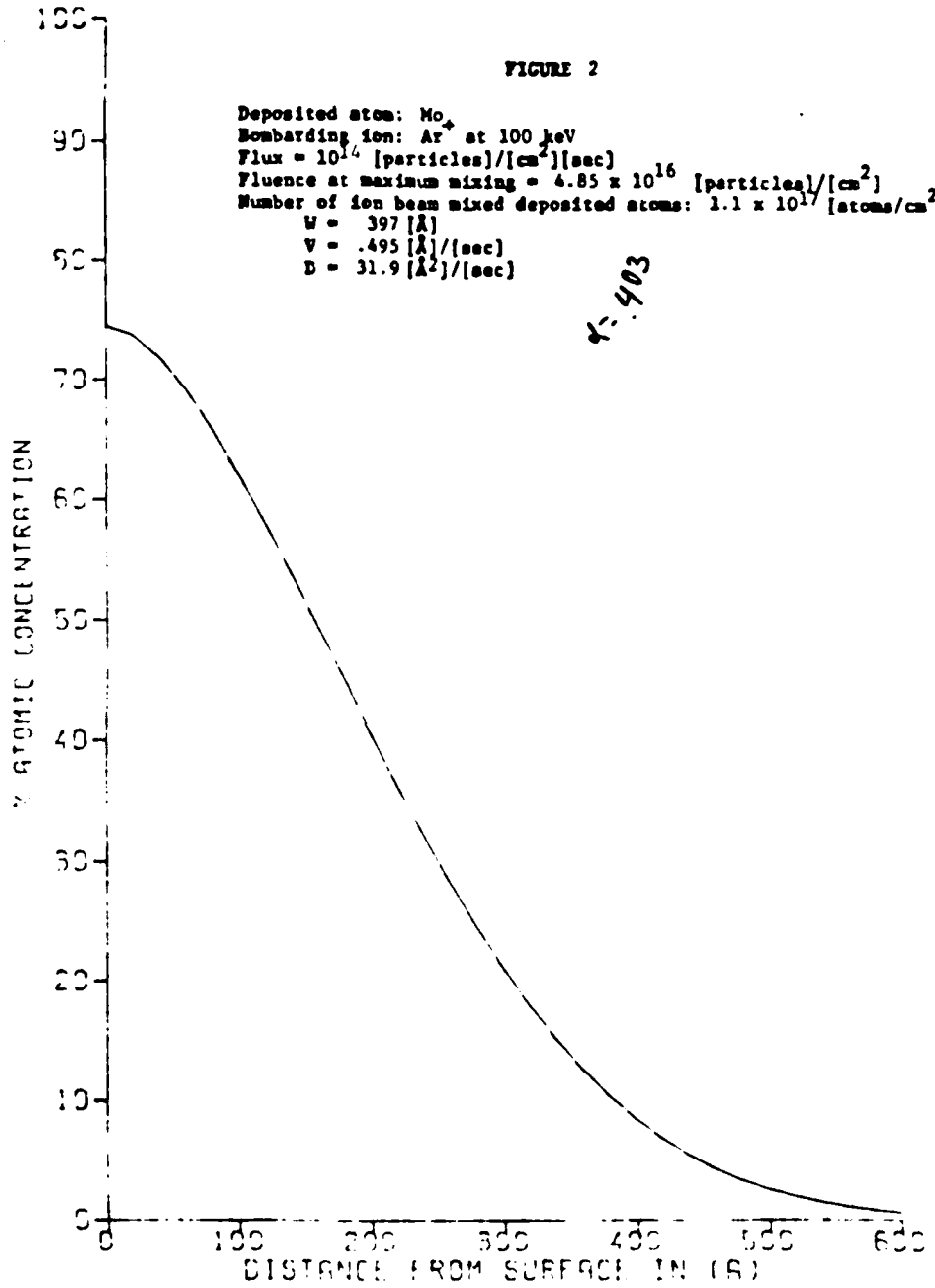
$$\alpha = \sqrt{\frac{D}{vw}}$$

$$C(x',t') = \frac{1}{2} \left[\operatorname{erfc} \left(\frac{x'+t'-1}{2\alpha\sqrt{t'}} \right) - e^{1/\alpha^2} \operatorname{erfc} \left(\frac{x'+t'+1}{2\alpha\sqrt{t'}} \right) \right]$$

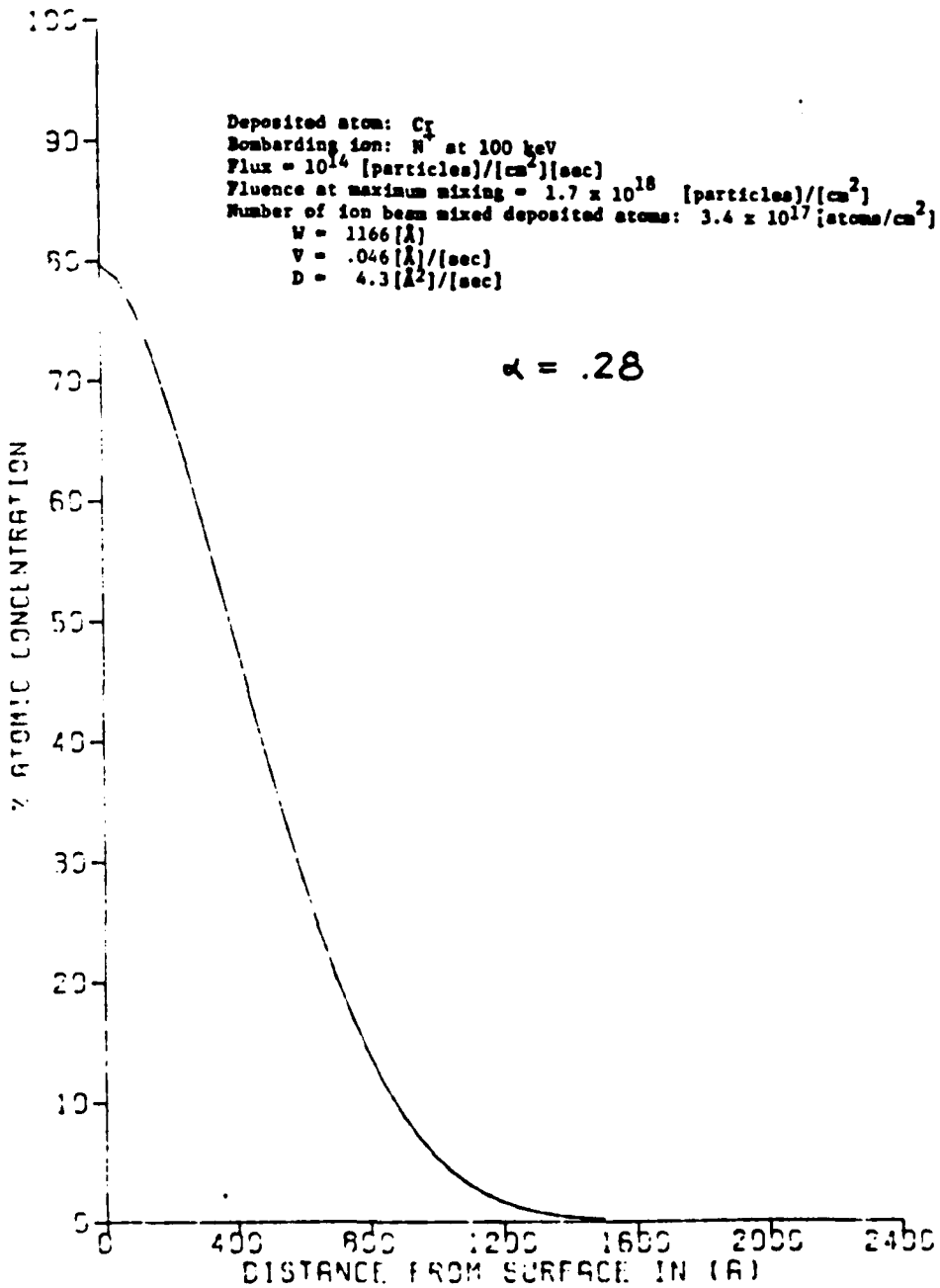
RECOIL IMPLANTATION CONCENTRATION PROFILES



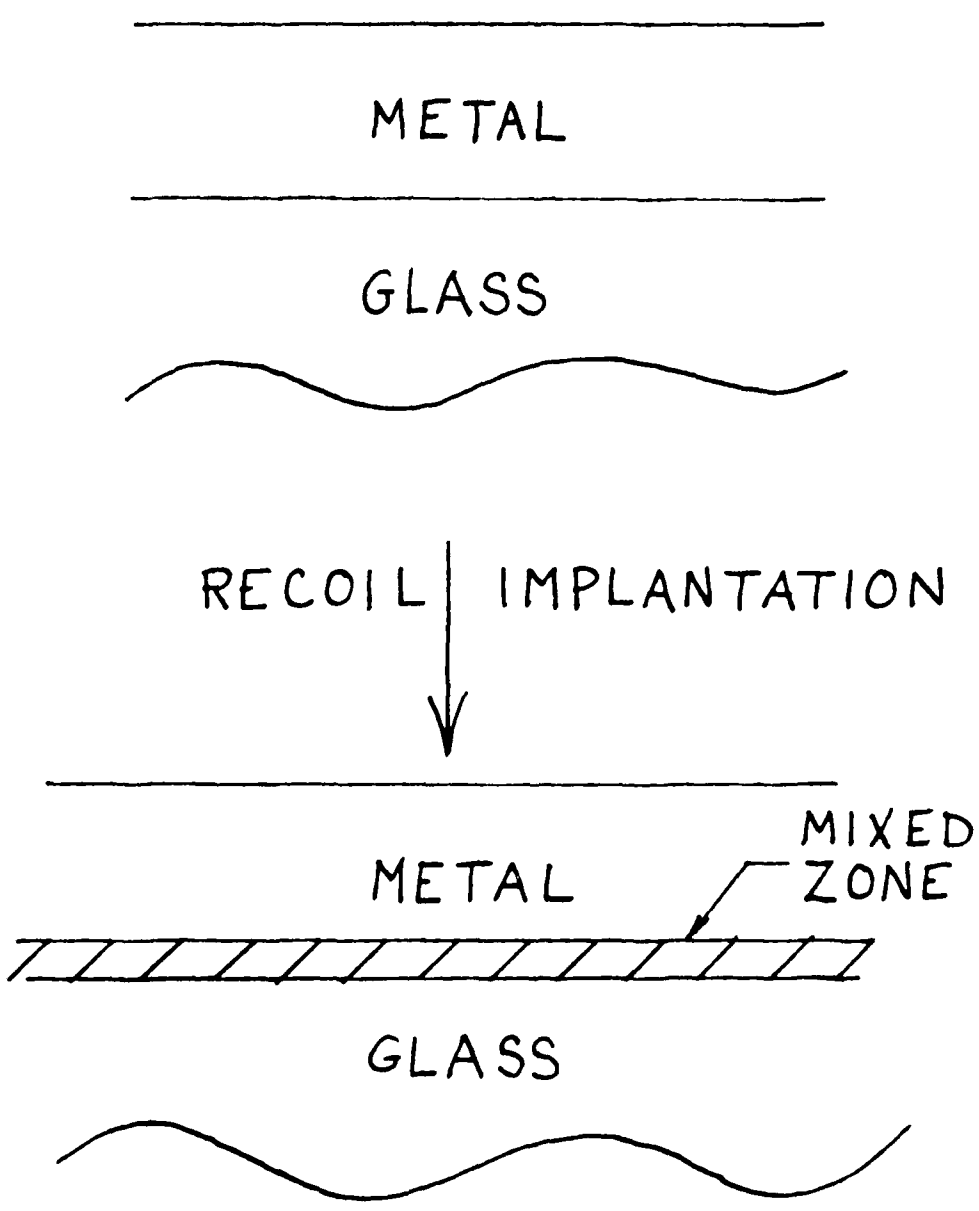
RECOIL IMPLANTATION CONCENTRATION PROFILES



RECOIL IMPLANTATION CONCENTRATION PROFILES



METAL - GLASS BONDING



Au on SiO₂

Experiment:

- 500 Å Au evaporated onto SiO₂
- Ar⁺ ion implanted to 1×10^{16} ions/cm²
- α⁺ 100 keV

Results:

- Unimplanted Au film easily removed by single adhesive tape test
- After implantation, Au film adherent, unaffected by multiple tape tests
- Au film sputtered nonuniformly during implantation due to poor initial adherence of film

Au on SiO₂

Experiment:

- 500 Å Au sputter deposited on SiO₂
- SiO₂ precleaned in-situ by sputter etching
- Ar⁺ ion implanted to 1×10^{16} ions/cm² at 100 keV

Results:

Both implanted and unimplanted Au films strongly adherent. Impossible to remove either film with any type of tape.

Au on SiO₂

Experiment:

- Flat faced pins glued on implanted and unimplanted sputtered Au films.
- Pins pulled in tension to test adherence of films

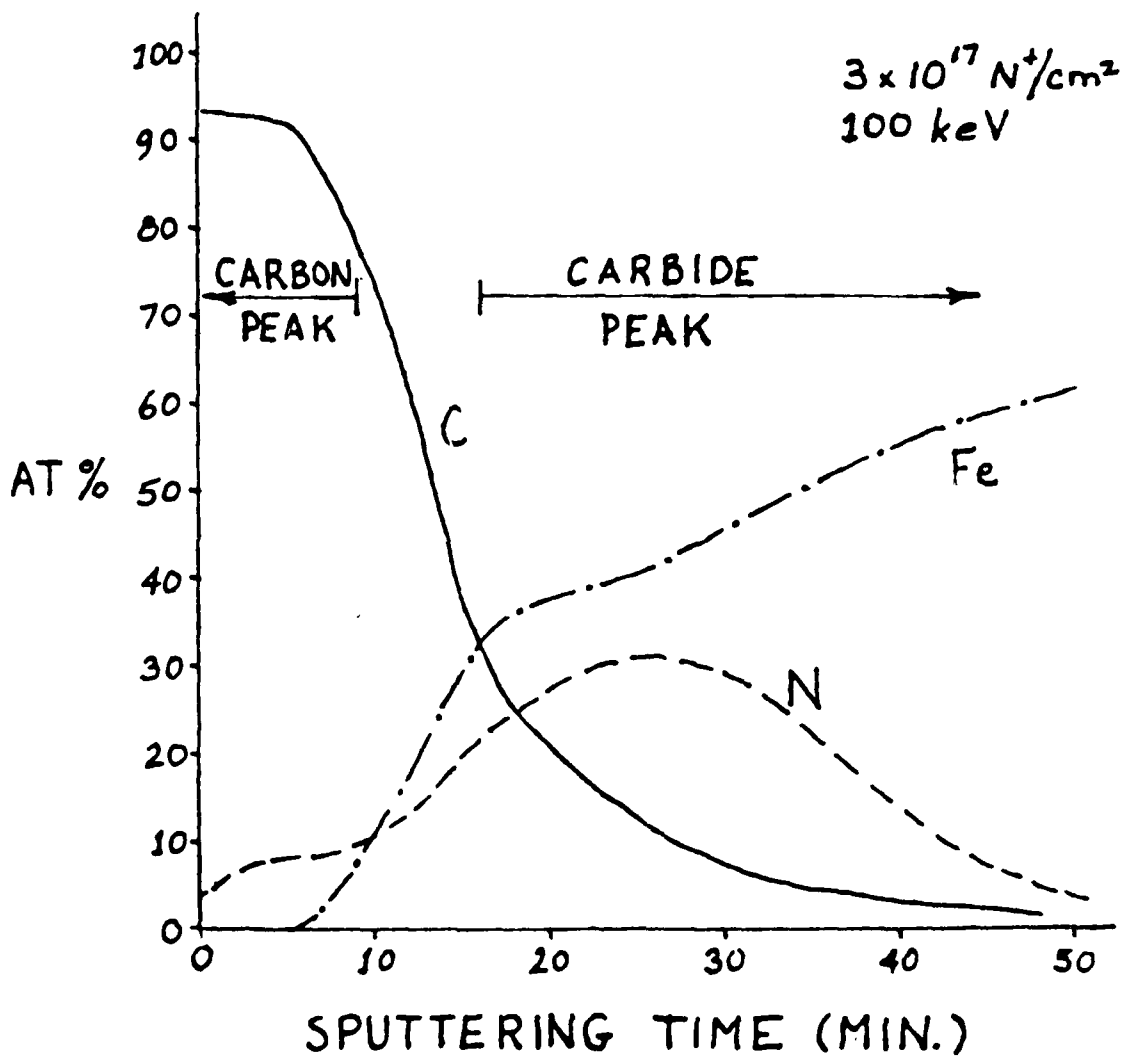
Results:

Failure Stress
(Average of five tests)

<u>Unimplanted</u>	<u>Implanted</u>
814 ± 142 psi	308 ± 88 psi
Glue failure	Glass fracture

In both cases, film not removed from SiO₂.

RECOIL IMPLANTATION OF CARBON INTO 304 SS BY N⁺





REPORT DOCUMENTATION PAGE		READ INSTRUCTIONS BEFORE COMPLETING FORM
1 REPORT NUMBER	2 GOVT ACCESSION NO. A131469	3 RECIPIENT'S CATALOG NUMBER
4 TITLE (and Subtitle) PROCEEDINGS OF THE WORKSHOP ON ION MIXING AND SURFACE LAYER ALLOYING		5 TYPE OF REPORT & PERIOD COVERED Final - April 14 to 16, 1983
7 AUTHOR(s) Marc-A. Nicolet and S. Thomas Picraux		6 PERFORMING ORG. REPORT NUMBER
8 CONTRACT OR GRANT NUMBER N00014-83-G-0057		9 PERFORMING ORGANIZATION NAME AND ADDRESS Dr. Marc-A. Nicolet California Institute of Technology, 116-81 Pasadena, California 91125
10 PROGRAM ELEMENT PROJECT NUMBER AREA & WORK UNIT NUMBERS Code 410		11 CONTROLLING OFFICE NAME AND ADDRESS Leader Electronics Division Office of Naval Research 800 N. Quincy Street, Arlington, VA. 22217
12 REPORT DATE May 6, 1983		13 NUMBER OF PAGES 173
14 MONITORING AGENCY NAME & ADDRESS (if different from Controlling Office) Office of Naval Research Detachment Pasadena 1030 East Green Street Pasadena, California 91106		15 SECURITY CLASS. (of this report)
16 DISTRIBUTION STATEMENT (of this Report)		15a DECLASSIFICATION/DOWNGRADING SCHEDULE
17 DISTRIBUTION STATEMENT (of the abstract entered in Block 20, if different from Report)		
18 SUPPLEMENTARY NOTES Prepared in cooperation with S. Thomas Picraux, Division 1111, Sandia National Laboratories, Albuquerque, New Mexico 87185		
19 KEY WORDS (Continue on reverse side if necessary and identify by block number) ion mixing, ballistic mixing, irradiation, implantation		
20 ABSTRACT (Continue on reverse side if necessary and identify by block number) Summaries are presented of all prepared contributions to the workshop. They cover the basic mechanisms of ion mixing, its relation to high-dose implantation, and areas of potential applica- tions. In addition, we outline the major conclusions of the work- shop and give a tentative scheme of nomenclature for the mechanisms of ion mixing.		

DD FORM 1473 1 JAN 73 EDITION OF 1 NOV 65 IS OBSOLETE

(Intentionally left blank)

Distribution:

3141 L. J. Erickson (5)
3151 W. L. Garner (3)
3154-3 C. Dalin (25)
(for DOE/TiC)
1110 P. S. Peercy
1100 F. L. Vook
1111 S. T. Picraux (60)
1111 G. W. Arnold
1111 K. L. Brower
1111 B. L. Doyle
1111 J. A. Knapp
1111 H. J. Stein
1112 S. M. Myers
1112 C. I. H. Ashby
1112 D. K. Brice
1112 D. M. Follstaedt
1112 C. E. Land
1112 W. R. Wampler

Dr. Robert S. Averback
Materials Science and
Technology Division
Argonne National Laboratory
Argonne, IL 60439

Mr. Thomas Banwell
Electrical Engineering
Department, 116-81
California Institute of Technology
Pasadena, CA 91125

Dr. Adam Barcz
Electrical Engineering
Department, 116-81
California Institute of Technology
Pasadena, CA 91125

Dr. Kenneth S. Grabowski
Naval Research Laboratory
Washington, DC 20375

Dr. James K. Hirvonen
Zymet, Inc.
Liberty Square
Danvers, MA 01923

Prof. William L. Johnson
Applied Physics Department, 138-78
California Institute of Technology
Pasadena, CA 91125

Distribution continued

Dr. Harald Jorch
Chalk River Nuclear Laboratories
Chalk River, Ontario
Canada KOJ 1J0

Dr. Adam Kossowsky
Manager, Physical Metallurgy
Research and Development Center
Westinghouse
1310 Beulah Road
Pittsburgh, PA 15235

Prof. S. S. Lau
Department of Electrical Engineering
and Computer Sciences
C-104
University of California, San Diego
La Jolla, CA 92093

Dr. Sam Matteson
Texas Instruments, Inc.
M.S. - 147
PO Box 225936
Dallas, TX 75265

Mr. Marcus Mendenhall
Physics Department, 301-38
California Institute of Technology
Pasadena, CA 91125

Mr. Mike Nastasi
Materials Science Department
Cornell University
Ithaca, NY 14853

Prof. Marc-A. Nicolet
Electrical Engineering
Department, 116-81
California Institute of Technology
Pasadena, CA 91125

Dr. Bruce M. Paine
Electrical Engineering
Department, 116-81
California Institute of Technology
Pasadena, CA 91125

Distribution continued

Dr. Lynn E. Rehn
Materials Science and
Technology Division
Argonne National Laboratory
Argonne, IL 60439

Dr. B. David Sartwell
Naval Research Laboratory
Washington, DC 20375

Dr. Uri Shreter
Electrical Engineering
Department, 116-81
California Institute of Technology
Pasadena, CA 91125

END

DATE
FILMED

9 - 83

DTIC